Control of the Space Shuttle Angle-of-Attack during Reentry

by

Farid Ganji

M.S. Mechanical Engineering, 1994
Sharif University of Technology, Iran

B.S. Mechanical Engineering, 1990
Ferdowsi University of Mashhad, Iran

Submitted to the Department of Mechanical Engineering
in Partial Fulfillment of the Requirements for the Degree of
Master of Science in Mechanical Engineering

at the

Massachusetts Institute of Technology

February 2002

Signature of Author.....
Department of Mechanical Engineering
September 10, 2001

Certified by.....
Rudrapatna V. Ramnath
Senior Lecturer
Department of Aeronautics and Astronautics
Thesis Supervisor

Accepted by.....
Ain A. Sonin
Chairman, Department Committee on Graduate Students
Department of Mechanical Engineering

Control of the Space Shuttle Angle-of-Attack during Reentry

by

Farid Ganji

Submitted to the Department of Mechanical Engineering
on September 10, 2001
in Partial Fulfillment of the Requirements for the Degree of
Master of Science in Mechanical Engineering

ABSTRACT

In this study, different approaches to the control of the space shuttle angle-of-attack unwanted oscillations during reentry are presented. The space shuttle glides over a prescribed trajectory that is optimal in that it minimizes the weight of the thermal protection system. The angle-of-attack oscillations are governed by a unified equation that results from the transformation of the equations of motion by means of a change of variable from time to a non-dimensional distance parameter along the trajectory. The original unified equation is modified to be applicable for control purposes and using a generic hypersonic simulation model. The dynamic response obtained by using the generic model shows good agreement with that of the actual space shuttle model. In traversing the earth's atmosphere during reentry, the coefficients of the unified equation vary due to changes in the air density, velocity of the vehicle, flight path angle, nominal angle-of-attack, and aerodynamic characteristics of the space shuttle. The transient response is stable but highly-oscillatory and long-lasting with increasing frequency where it is shown that the die-out time is much longer in the upper atmosphere than that of the lower altitudes. As such, the need for providing the space shuttle orbiter with an angle-of-attack controller is readily justified.

Three different controllers using nonlinear, optimal, and adaptive control methods are developed and simulated. The performance of each controller is analyzed along the upper and lower portions of the trajectory. In both altitude ranges, the controllers eliminate the oscillations and considerably reduce the die-out time. In reducing the time required to achieve the control tasks, the maximum available deflection of the elevator is a major constraint.

The feedback-linearization nonlinear approach proves to be a useful and simple control strategy. Because of its simplicity, the nonlinear controller is employed to characterize the controlled response and calibrate the optimal and adaptive controllers.

In the optimal control approach, a numerical exact solution as well as an analytical approximate solution is developed. The analytical approximate solution is developed through linearizing the Riccati matrix equation and applying the asymptotic multiple time-scales method. The resulting solution for the linearized Riccati matrix is a combination of the elementary harmonic and hyperbolic functions. It is shown that the application of the analytical approximate solution

considerably reduces the optimal controller computation time. The coefficients and the forcing term in the unified equation vary slowly compared to the highly-oscillatory response of the shuttle to the atmospheric disturbances, regardless of the altitude. It is shown that for the controlled response however, the assumption of slow variations is valid as long as the distance traversed during the control period is small compared to the total distance along the trajectory. Accordingly, it is shown that while the optimal controller using the asymptotic solution performs excellently for lower altitudes, the asymptotic approximation is not applicable in the high-altitude portion of the trajectory.

The parameters appearing in the unified equation are complicated functions of the prescribed trajectory variables and the aerodynamic characteristics of the space shuttle during reentry. As opposed to the nonlinear and optimal controllers, the adaptive controller achieves the control task through a parameter estimation process without using any a priori knowledge of the system parameters. The adaptive controller, as formulated in this study, performs excellently in both upper and lower portions of the trajectory regardless of the level of variations of the aerodynamic and trajectory parameters during the course of control action. It is seen that at lower altitudes, the parameter estimates and the true parameters have the same orders of magnitude which is quite noticeable.

Thesis Supervisor: Rudrapatna V. Ramnath

Title: Senior Lecturer, Department of Aeronautics and Astronautics

CONTENTS

To my beloved family

ACKNOWLEDGMENTS

I am very grateful that Prof. Ramnath agreed to be my thesis supervisor and provided me with direction and advice during the course of our relationship. I also thank him for choosing a challenging and fascinating thesis topic. I am very appreciative of his supportive efforts and proud of the work that we have done together, and I offer my sincerest thanks to him.

I do not know how to begin to express my gratitude to Prof. Mary Boyce, because it is difficult to quantify the many ways in which she contributed to my development as a graduate student at MIT. She provided me with continual funding, and especially the opportunity to work on a TA project, which allowed me to make a lasting contribution to MIT through the creation of learning-aid desktop experiments that have been and will be used by the institute undergraduates. More importantly, she provided continuous support, guidance, and most significantly, friendship. Her advice and sincere concern was very important during my research and studies. She is an outstanding mentor and friend who I will not soon forget. I thank her wholeheartedly.

I would like to deeply thank Prof. Sanjay Sarma for believing in me and for his strong and unconditional support, and sincere advice throughout my studies at MIT. I am eternally grateful for his friendship, guidance, and confidence in my abilities.

I am also appreciative to Prof. Lallit Anand that admitted me to the institute and provided me with a wonderful opportunity to contribute to and become enriched by the MIT environment.

I would also like to express my sincerest thanks and appreciation to Ms. Leslie Regan for her endless patience, courtesy and assistance throughout my studies at MIT and even before coming to the institute. She always answered my questions and responded to my requests in a professional and thoughtful manner. Although that she is responsible for responding to a large number of students, she always made me feel that she was giving me full consideration, respect and attention.

NOMENCLATURE

A = coefficient matrix
B = coefficient vector
$\bar{c}$ = mean aerodynamic chord of the generic model
C_{ij} = coefficients of characteristic Eqs. (4.79)
C_{ijk} = complex characteristic coefficients
C_D = drag coefficient
C_L = lift coefficient
C_m = pitching moment coefficient
$C_{D_0}, C_{L_0}, C_{m_0}$ = nominal aerodynamic coefficients
$C_{D_\alpha}, C_{L_\alpha}, C_{m_\alpha}$ = aerodynamic stability derivatives
$C_{m_{\dot{\alpha}}}, C_{m_q}$ = aerodynamic stability derivatives
$C_{m_{\delta_e}}$ = elevator effectiveness
D = drag force
D_{ijk} = substitute characteristic coefficients
e = base of the natural logarithm
E = Lyapunov function
f = non-dimensional induced disturbance
F = linear dependence factor
g = acceleration due to gravity
g_s = acceleration due to gravity at sea level
G = universal gravitational constant
h = altitude
H = constant scaling altitude, Eq. (1.5). Hamiltonian, Eq. (4.12)
i = $\sqrt{-1}$
I = identity matrix
I_x, I_y, I_z = principal moments of inertia
J = performance measure
k = components of the Riccati matrix
K = Riccati matrix
L = lift force, Eq. (1.9). Reference length of the space shuttle, Eq. (1.26)
m = mass of the space shuttle
m, c, k, d, n = true parameters
$\hat{m}, \hat{c}, \hat{k}, \hat{d}, \hat{n}$ = estimated parameters
$\tilde{m}, \tilde{c}, \tilde{k}, \tilde{d}, \tilde{n}$ = parameter estimation errors
M = transformation matrix
M_{δ_e} = elevator control torque
$\tilde{M}_{\delta_e}$ = elevator disturbance control torque

N = transformation matrix

p_1, p_2 = components of the co-state vector

P = co-state vector, Eq. (4.10). Vector of true parameter, Eq. (5.8)

P^* = optimal co-state vector

$\hat{P}$ = vector of parameter estimates

$\tilde{P}$ = vector of parameter estimation errors

q = angular velocity in pitch about the space shuttle center of mass

$\overline{q}$ = dynamic pressure

Q = state penalty gain matrix

r = radial distance from the Earth center to the space shuttle center of mass

R = control penalty gain

R_e = Earth radius

R_{air} = gas constant of air

s = root of characteristic Eqs. (4.80). Sliding variable, Eq. (5.15)

s_k = complex characteristic roots

S = reference area

t = time

T_{iso} = absolute temperature of the isothermal atmosphere

u = control variable

u^* = optimal control variable

V = Nominal Velocity

X = state vector

X^* = optimal state vector

Y_m = linear parameterization row vector

z = root of characteristic Eqs. (4.81)

α = perturbation angle-of-attack

$\overline{\alpha}$ = total angle-of-attack

α_0 = nominal angle-of-attack

β = ratio of the generic model mean chord to the shuttle reference length

γ = flight path angle

Γ = transformation vector, Eq. (4.102). Adaptation gain matrix, Eq. (5.20).

δ = non-dimensional atmospheric mass density

δ_e = elevator angle

$\tilde{\delta}_e$ = elevator disturbance control deflection

ε = measure of slowness of variations

η = slow non-dimensional distance variable

λ = characteristic value

λ_{ij} = characteristic functions

Λ = linearized Riccati matrix

μ = elevator control coefficient

θ = pitch angle

θ_0 = nominal pitch angle
ν = ratio of moments of inertia
ξ = non-dimensional distance variable
ξ_0 = initial non-dimensional distance
ξ_f = final non-dimensional distance
ρ = atmospheric mass density
ρ_s = atmospheric mass density at sea level
σ = inverse non-dimensional pitching moment of inertia
τ_0, τ_1 = time scales
ϕ = angular range
ϕ_{ij} = components of the transition matrix
Φ = transition matrix
ω_0, ω_1 = stiffness and damping coefficients in the unified Eq. (1.38)
Ω_0, Ω_1 = coefficient matrices, Eq. (4.46)

Subscripts

0 = nominal value
r = radial component
ϕ = tangential component
Re = real part
Im = imaginary part
x, y, z = stability axes

INTRODUCTION

This thesis is concerned with the development of different solutions to the control of the space shuttle angle-of-attack oscillations caused mainly by the atmospheric disturbances during reentry. The motivation for doing this investigation stems from the fact that as opposed to the dynamics and stability analysis of the space shuttle during reentry that has been investigated a great deal in the literature such as those done by Vinh and Laitone in [12] and by Ramnath and Sinha in [9], the control aspect of the problem has not been particularly worked on. More specifically, developing an approximate but closed-form solution to the optimal control of the space shuttle angle-of-attack during reentry (Chap. 4) is a novel approach being presented in this thesis. Also, the adaptive controller developed and designed in this thesis (Chap. 5) has its own peculiarities as an application of the adaptive control theory to the reentry problem.

In this investigation., it is assumed that the Earth is spherical, the atmosphere is isothermal, and the shuttle vehicle does not roll. The space shuttle orbiter glides over a prescribed reentry trajectory that is optimal in that it minimizes the weight of the thermal protection system. A realistic generic hypersonic aerodynamic model taken from [3] is used for the computer simulations. The model is a geometrically-simplified hypersonic delta-wing aircraft that has similar aerodynamic characteristics to that of the space shuttle.

Subject to certain conditions, the nonlinear equations of motion and the corresponding kinematic relations are transformed by a change-of-variable, corresponding to the number of scale lengths traversed by the vehicle along the trajectory of the center of mass, to get a unified equation of motion describing the variations of the space shuttle angle-of-attack during reentry [12]. The so called unified equation is a linear second-order inhomogeneous ordinary differential equation with time-varying coefficients.

The coefficients and the forcing term in the unified equation are functions of the prescribed trajectory variables and the aerodynamic characteristics of the space shuttle during reentry. As has been discussed by Ramnath and Sinha in [9], these functions vary slowly along the trajectory as compared to the highly-oscillatory transient response of the space shuttle to angle-of-attack perturbations regardless of the duration of the response. However, it will be shown that for the case of the controlled response, the assumption of slow variation of these parameters is valid as long as the distance traversed during the control period is small compared to the total distance along the reentry trajectory. This is due to the fact that the controlled response is an over-damped non-oscillatory response where its fastness is inversely proportional to the duration of the control action. In fact, the time constant of the controlled response is nearly equal to the duration of control action. It is shown that for the high-altitude portion of the reentry trajectory, the assumption of slow variations is not valid since the space shuttle travels about a quarter of the entire trajectory during the optimal control period.

In this study, three different control approaches are investigated and applied to the unified angle-of-attack equation. In the case of the optimal controller, the control law and the corresponding controlled response of the space shuttle are obtained using both numerical and analytical solutions.

Practically, the space shuttle orbiter is classified as a long-range hypervelocity vehicle designed for atmospheric as well as extra-atmospheric flights [11]. A typical long-range trajectory with atmospheric and extra-atmospheric portions is illustrated in Fig. 1. The flight is assumed to take place in the plane containing the great circle arc, between the launch point and the landing point. The entire flight is thought of in two phases as described below.

(a) The powered phase in which sufficient kinetic energy provided by the propulsion system is imparted to the vehicle to bring it, under proper guidance, to a prescribed position and velocity in space. The trajectory followed is the arc AB in Fig. 1. The point B is referred to as the burnout position. The powered phase is generally short in terms of both duration and length compared to those of the entire trajectory.

(b) The unpowered phase in which the vehicle travels to its destination under the influence of the gravity and aerodynamic forces. The trajectory followed is the arc BC. For long-range flights like that of the space shuttle orbiter, the total energy imparted to the vehicle at the burnout position B is sufficiently high, with a proper orientation of the burnout velocity, the trajectory followed will have a long portion entirely outside the dense layer of the atmosphere. This portion of the trajectory which is a Keplerian conic is represented by the arc BE in Fig. 1. This is one of the most interesting features in hypersonic flight. For long-range operation, hypervelocity vehicles reduce the cost in fuel consumption since the range $X_B - X_E$ can be made infinite with finite energy input. This basic idea led to the concept of present-day shuttle vehicles where, after the powered phase, the subsequent trajectory is entirely flown outside the atmosphere for several days and the required mission is accomplished without additional energy input. When it comes time to return to the Earth, a rocket may be fired to deflect the trajectory such that it intersects the atmosphere of the Earth at a certain point E called the entry position (Fig. 1). This point E is assumed to be at the top of the sensible atmosphere. The subsequent trajectory is called the reentry trajectory. This portion of the trajectory is illustrated by the arc EC in Fig. 1. In this study, we shall be concerned with the reentry portion of the space shuttle flight.

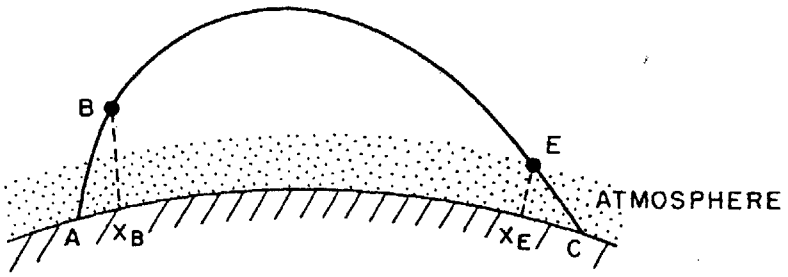

Fig. 1 Typical complete trajectory of long-range hypervelocity vehicles, taken from [11]

In Chapter 1, the longitudinal dynamic equations of motion of the space shuttle orbiter during atmospheric reentry glide are derived, following by the derivation of the unified perturbation

angle-of-attack equation describing the angle-of-attack oscillations about its prescribed trajectory values. It is assumed that the planet is spherical, the atmosphere is isothermal, and the shuttle vehicle experiences lift and does not roll.

The oscillations of the space shuttle angle-of-attack during reentry have been shown by Vinh and Laitone in [12] to be governed by a second-order inhomogeneous linear differential equation with variable coefficients. This so called unified equation results from the transformation of the nonlinear equations of motion by using a change of independent variable from time to a non-dimensional distance parameter along the trajectory. In this study, the original unified equation is modified to be applicable for control purposes and using the abovementioned generic hypersonic model. In traversing the earth's atmosphere during reentry, variations in the coefficients of the unified equation are due to changes in air density, velocity of the vehicle, flight path angle, nominal angle-of-attack, and the aerodynamic characteristics of the space shuttle vehicle. However, the aerodynamic stability and control derivatives of the shuttle as a hypersonic vehicle vary only due to variations of the nominal angle-of-attack and velocity along the prescribed trajectory. Of these two variable parameters, the nominal angle-of-attack is the dominant one.

In Chapter 2, the dynamic response of the space shuttle to the angle-of-attack perturbations, while traveling along the prescribed optimal reentry trajectory, is discussed. In order to simulate the space shuttle aerodynamic characteristics, a realistic generic hypersonic-aircraft computer-simulation aerodynamic model was used for all the simulations in this thesis. The model is a geometrically-simplified hypersonic delta-wing aircraft that has similar aerodynamic characteristics to those of the space shuttle. The trajectory model that was used in the simulations is an optimal reentry trajectory, designed to minimize the weight of the thermal-protection system (TPS) of the space shuttle SSV 049 [4]. The simulation results in this chapter, for the dynamic response of the shuttle vehicle using the generic aerodynamic model, show good agreement with those of the actual space shuttle model reported in [9].

In Chapter 3, in order to suppress the undesired angle-of-attack oscillations, the nonlinear control method of feedback linearization is implemented [10]. Because of its simplicity, the feedback linearization is used to characterize the controlled response of the shuttle to the angle-of-attack perturbations. The feedback-linearization nonlinear controller, subject to the maximum available elevator-angle constraint, offers realistic estimations for the duration and the corresponding rate of decay of the controlled response that will be helpful to design the controllers discussed in the subsequent chapters. The feedback linearization is easy to implement since as will be seen, we only needed to specify the desired time for control action and check if the maximum demanded elevator angle is available.

In Chapter 4, in order to control the perturbations of the space shuttle angle-of-attack during reentry, an optimal control approach is applied to the state space representation of the unified equation. The underlying scheme is the linear quadratic regulator (LQR) formulation that forms a boundary value problem with the specified initial and final conditions for the state vector [6]. Due to the zero final conditions for the state vector as a special case, the formulation and the corresponding Riccati equation are different from those of the conventional linear regulator methodology. The Riccati equation for this special case is called the Riccati equation of the Lyapunov type [5]. Subsequently, a fully numerical solution is discussed followed by

development of a completely-analytical solution for the control of the space shuttle angle-of-attack perturbations during reentry.

The numerical solution, that is considered to be exact, is obtained by numerically integrating the Riccati equation backwards, and subsequently, solving the co-state differential equation using forward numerical integration. The analytical solution is developed basically to eliminate the backward and forward numerical integrations from the optimal control solution. The motivation for developing an approximate analytical solution is primarily to reduce the computation time that an optimal controller needs to suppress the unwanted oscillations of the space shuttle during reentry. The fact is that while numerical integration schemes require small stepsize to give acceptable results, the accuracy of analytical solutions is not affected by the evaluation stepsize. In the case of approximate analytical solutions however, there must be a balance between the accuracy of the method versus the computation time. The other reason for developing an asymptotic solution is to gain better mathematical insight into the optimal control approach.

In order to develop an asymptotic analytical solution, first the Riccati matrix equation is linearized by using a rigorous mathematical transformation, and subsequently, an asymptotic analytical solution describing the variations of the linearized Riccati matrix is derived. The asymptotic solution is developed by using the multiple time-scales technique. The analytical solutions to the components of the linearized Riccati matrix appear to be a combination of simple harmonic and hyperbolic functions. In the third step, the co-state first-order matrix differential equation is solved analytically, by using a novel matrix transformation. Eventually, the optimal control law and the corresponding state-vector history are determined by using the solutions for the linearized Riccati matrix and the co-state vector. The performance of the presented asymptotic method is evaluated by comparing the corresponding simulation results and computation time to those of the numerical exact solution.

In Chapter 5, in order to suppress the undesired angle-of-attack oscillations, an adaptive control technique is applied to the unified equation, i.e. the original 2^{nd}-order nonlinear differential equation with variable coefficients for the angle-of-attack perturbations.

The adaptive controller is developed and designed by using the modified adaptive control methodology [10]. The main advantage of the adaptive controllers is that they achieve the control task without using any a priori information about the system parameters and their variations. This fact is of special interest in our problem where the trajectory variables and the aerodynamic characteristics of the space shuttle vary along the reentry trajectory.

The adaptive controller design problem here is to derive a control law for the elevator deflection, and an estimation law for the parameters without using any a priori information about them, such that the space shuttle regains its nominal trajectory angle-of-attack after being perturbed by external or internal disturbances. This means that the deviation of angle-of-attack from its nominal value and all its derivatives with respect to the independent variable or time must vanish at the end of controller action. Thence, the control problem can be categorized as a tracking problem where the desired trajectory is the origin of the state vector space at each instant, or a positioning problem in which the initial position is the disturbed state and the target position is the origin.

CHAPTER 1

LONGITUDINAL DYNAMICS

In this chapter, the longitudinal dynamic equations of motion of the space shuttle orbiter during atmospheric reentry glide are derived, following by the derivation of the unified perturbation angle-of-attack equation describing the angle-of-attack oscillations about its prescribed trajectory values. It is assumed that the planet is spherical, the atmosphere is isothermal, and the shuttle vehicle experiences lift and does not roll. The formulation and treatment are based on the approach as developed by Vinh and Laitone [12], and Ramnath [9].

1.1 AXIS SYSTEM

The stability axes coordinate frame shown in Fig.1.1 will be used to derive the equations of motion of the space shuttle during reentry. As shown in the sketch, the axes emanate from the space shuttle center of mass such that the x-axis is always tangential to the instantaneous flight path and the y-axis passes out the right wing. The z-axis is perpendicular to the other two axes following the orthogonal right-hand rule.

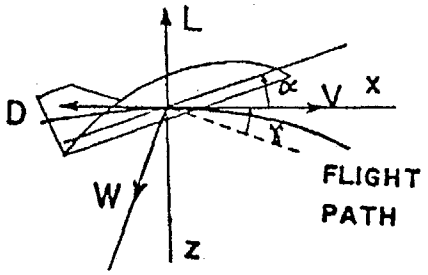

Fig. 1.1 Stability axes, taken from [12]

1.2 ORBITAL AND ATMOSPHERIC PARAMETERS

The gravitational acceleration, g, varies with the altitude and we have

$$g = \frac{GM_e}{r^2} \tag{1.1}$$

where G is the universal gravitational constant, M_e is the mass of the earth, and r is the radial distance between the centers the Earth and the space shuttle center of mass (Fig. 1.2). Of this distance, the radial distance from the sea level to the shuttle center of mass is the altitude denoted by h. Thus, we have

$$r = R_e + h \tag{1.2}$$

where R_e is the average radius of Earth.

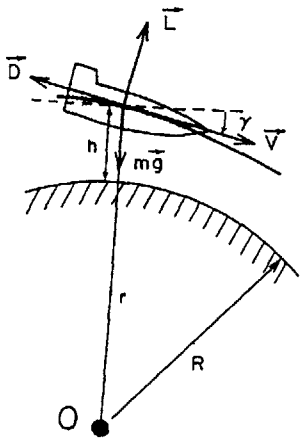

Fig. 1.2 Orbital parameters, taken from [11]

Multiplying and dividing (1.1) by R_e^2, we can write

$$g = g_s \frac{R_e^2}{r^2} \tag{1.3}$$

where g_s is the acceleration due to gravity at sea level.

The air density, ρ, of the isothermal atmosphere is also altitude-dependent. Assuming the air to be a perfect gas and for low orbits like that of the space shuttle, the air density can be calculated with good accuracy by the exponential formula of

$$\rho = \rho_s e^{-h/H} \tag{1.4}$$

where ρ_s is the air density at sea level, and

$$H = \frac{R_{air} T_{iso}}{g_s} \tag{1.5}$$

is a constant scaling altitude. R_{air} is the gas constant for air, T_{iso} is the absolute temperature of the isothermal atmosphere.

1.3 KINEMATIC RELATIONS

The rate of climb or descent of the flight vehicle traveling along its trajectory is related to the total velocity, V, of the vehicle center of mass and the flight path angle, γ, as the following

$$\dot{r} = V \sin\gamma \tag{1.6}$$

where the dot indicates differentiation with respect to time, and this will be the case henceforth. The flight path angle is the slope of the trajectory with respect to the local horizon. It should be noted that in general a constant flight path angle in orbital flights does not mean a straight-line trajectory. In fact, the trajectory curves down towards the planet because γ is measured relative to the local horizon that keeps changing for the aerospace vehicle.

The pitch attitude rate-of-change, is governed by the following relation

$$\dot{\theta} = q + \frac{V}{r}\cos\gamma \tag{1.7}$$

where q is the angular velocity in pitch about the y-axis of the space shuttle, and the second term on the right-hand-side is the absolute value of the angular velocity of the shuttle center of mass around the earth. Note that in (1.7), q can be positive or negative depending on the pitch direction whereas the second term is always positive. It should also be noted that $\dot{\theta}$ represents the variations in pitch attitude relative to the earth local horizon. For instance, in order to keep a constant attitude relative to Earth on a circular orbit ($\gamma = 0$), the shuttle needs to have a steady rotational adjustment of

$$q_{orbit} = -\frac{V_{orbit}}{R_{orbit}}$$

Note that if the space shuttle is inverted when orbiting the earth, i.e. the z-axis is pointing towards the outer space, then the sign changes such that

$$q_{invert} = +\frac{V_{orbit}}{R_{orbit}}$$

1.4 Forces and Moments

Besides the gravity force, the longitudinal aerodynamic forces and moments acting on, and about the center of mass of a gliding vehicle, consist of the drag force D, the lift force L, and the pitching moment M. As sketched in Fig. 1.2, the drag force is in the opposite direction of the vehicle velocity vector or parallel to the wind vector and is defined as positive aft. The lift force is defined as positive up and perpendicular to the wind velocity vector as well as the y-axis (Fig. 1.2). The pitching moment is a combination of the aerodynamic restoring and damping moments as well as the aerodynamic control torques and is positive when the corresponding moment vector points in the positive y-direction. Mathematically, we have

$$D = C_D \bar{q} S \tag{1.8}$$

$$L = C_L \bar{q} S \tag{1.9}$$

$$M = C_m \bar{q} S \bar{c} \tag{1.10}$$

where $\bar{q}$ is the dynamic pressure described by

$$\bar{q} = \frac{1}{2}\rho V^2 \tag{1.11}$$

and C_D, C_L, and C_m are the drag, lift, and pitching moment coefficients, respectively. The aerodynamic coefficients are dimensionless functions of the flight variables and they carry the signs of their associated forces or moments. It should be reminded that C_D is always positive whereas C_L and C_m can be positive or negative, depending on the direction of the lift and pitching moment vectors. The parameter S denotes the reference area and $\bar{c}$ is the wing mean aerodynamic chord of the lifting vehicle.

1.5 Equations of Motion

1.5.1 Drag Equation

The equation of motion along the flight path is as follows

$$-D - mg\sin\gamma = m\dot{V} \tag{1.12}$$

where m is the fuel-burnout reentry mass of the space shuttle. Substituting (1.8) into (1.12), we get

$$\dot{V} = -\frac{\rho S C_D V^2}{2m} - g\sin\gamma \tag{1.13}$$

that is called the drag equation and governs the variations of the shuttle velocity under the effect of the drag force and the gravity.

1.5.2 Lift Equation

The equation of motion normal to the flight path is the following

$$L\cos\gamma - D\sin\gamma - mg = m\ddot{r} - m(V\cos\gamma)^2/r \tag{1.14}$$

Differentiating (1.6) with respect to time gives

$$\ddot{r} = \dot{V}\sin\gamma + V\dot{\gamma}\cos\gamma \tag{1.15}$$

Substituting (1.15) into (1.14) yields

$$L\cos\gamma - D\sin\gamma - mg = m\dot{V}\sin\gamma + mV\dot{\gamma}\cos\gamma - mV^2\cos^2\gamma/r \tag{1.16}$$

However, if we multiply the drag equation (1.12) by $\sin\gamma$, we get

$$-D\sin\gamma - mg\sin^2\gamma = m\dot{V}\sin\gamma$$

Replacing $\sin^2\gamma$ by its cosine equivalent, gives

$$-D\sin\gamma - mg(1-\cos^2\gamma) = m\dot{V}\sin\gamma \tag{1.17}$$

Putting (1.17) into (1.16), we obtain

$$L\cos\gamma = mg\cos^2\gamma + mV\dot{\gamma}\cos\gamma - mV^2\cos^2\gamma/r$$

that leads to

$$V\dot{\gamma} = \frac{L}{m} - (g - \frac{V^2}{r})\cos\gamma$$

and eventually, using (1.9) results in

$$V\dot{\gamma} = \frac{\rho SC_L V^2}{2m} - (g - \frac{V^2}{r})\cos\gamma \tag{1.18}$$

that is called the lift equation and describes the variations in the flight path due to the unbalance of lift and the centrifugal force against the gravity. For circular orbits or flight paths, $\dot{\gamma}$ and γ are both zero, since the gravity minus lift provides the exact amount of centripetal force needed to keep the space vehicle in orbit.

1.5.3 Pitching Moment Equation

The equation of rotational motion about the y-axis of the stability coordinate frame attached to the space shuttle center of mass is as follows

$$M + \frac{3g}{2r}(I_z - I_x)\sin 2\theta = I_y\dot{q} \tag{1.19}$$

where M is the total pitching moment that includes the aerodynamic restoring, damping, and the body flap as well as the elevator-induced control torques. The second term on the left-hand-side is the gravity gradient torque, in which I_x and I_z denote the fuel-burnout rolling and yawing principal moments of inertia, respectively. Similarly, on the right-hand side, I_y denotes the fuel-burnout pitching moment of inertia.

Note that the pitching moment of inertia is the same in both stability and body axes, whereas the rolling and yawing moments of inertia in the stability axes deviate from their principal values in the body axes depending on the angle-of-attack. However, this effect is negligible in our analysis since the rolling and yawing moments of inertia only affect the gravity gradient torque that is inversely proportional to r, and very small compared to the aerodynamic pitching moment. Substituting (1.10) into (1.19) and rearranging leads to

$$\dot{q} = \frac{\rho S \bar{c} C_m V^2}{2I_y} + \frac{3g}{2r}\left(\frac{I_z - I_x}{I_y}\right)\sin 2\theta \tag{1.20}$$

that is called the pitching moment equation and represents the evolution of the pitch angle of the space-flight vehicle, traveling through the atmosphere and gravitational field of a planet. The pitching moment equation is the base equation of motion for pitch and angle-of-attack control purposes.

1.6 AERODYNAMIC COEFFIECIENTS

As pointed out earlier, the aerodynamic coefficients vary as the flight variables change. To this effect, due to the fact that the nominal aerodynamic coefficients and their derivatives along the trajectory are slowly-varying functions of angle-of-attack and Mach number, for small perturbations of angle-of-attack, we can linearize the perturbed aerodynamic coefficients about their nominal trajectory values. When the space shuttle angle-of-attack is perturbed from its nominal value by atmospheric disturbances, we can write

$$\bar{\alpha} = \alpha_0 + \alpha \tag{1.21}$$

where $\bar{\alpha}$, α_0, and α denote the total, nominal, and perturbation angles-of-attack respectively. Accordingly, the total pitch angle of the space shuttle as the complementary kinematic relation will be

$$\theta = \gamma + \bar{\alpha} \tag{1.22}$$

In addition, considering the fact that $\dot{\alpha}_0 << \dot{\alpha}$, using (1.21) we can approximate the pitch attitude rate-of-change in (1.22) and (1.7) as the following

$$\dot{\theta} = \dot{\gamma} + \dot{\alpha} \tag{1.23}$$

As discussed in [12], the perturbed and linearized aerodynamic coefficients can thus be approximated as below

$$C_D = C_{D_0} + C_{D_\alpha}\alpha \tag{1.24}$$

$$C_L = C_{L_0} + C_{L_\alpha}\alpha \tag{1.25}$$

$$C_m = C_{m_0} + C_{m_\alpha}\alpha + C_{m_{\dot{\alpha}}}\left(\frac{L}{V}\right)\dot{\alpha} + C_{m_q}\left(\frac{L}{V}\right)\dot{\theta} + C_{m_{\delta_e}}\delta_e \tag{1.26}$$

where L is the overall length of the space shuttle used as the non-dimensionalizing reference length corresponding to the trajectory model. C_{D_0}, C_{L_0}, and C_{m_0} represent the nominal aerodynamic coefficients along the trajectory and they will be discussed in Sec. 2.3.1. The rest of the coefficients in Eqs. (1.24) through (1.26) are the aerodynamic stability and control derivatives that are described as follows

$$C_{D_\alpha} = \frac{\partial C_D}{\partial \alpha} \quad \text{[per radian]}$$

$$C_{L_\alpha} = \frac{\partial C_L}{\partial \alpha} \quad \text{[per radian]}$$

$$C_{m_\alpha} = \frac{\partial C_m}{\partial \alpha} \quad \text{[per radian]}$$

$$C_{m_{\dot{\alpha}}} = \frac{\partial C_m}{\partial (\frac{L}{V}\dot{\alpha})} \qquad (1.27a\text{-}f)$$

$$C_{m_q} = \frac{\partial C_m}{\partial (\frac{L}{V}\dot{\theta})}$$

$$C_{m_{\delta_e}} = \frac{\partial C_m}{\partial \delta_e} \quad \text{[per radian]}$$

The stability and control derivatives are slowly-varying functions of the angle-of-attack and Mach number and are inputted to the simulations using a generic hypersonic aircraft model data that will be discussed in the next chapter.

In (1.26) and (1.27f), δ_e denotes the required elevator angle to control the angle-of-attack perturbations. It should be reminded that for delta-wing aircrafts including the space shuttle, the term "elevator" refers to the elevator-mode of the elevons. Elevons are the dual-action wing-mounted aerosurfaces that can be actuated in the elevator or the aileron mode. In the space shuttle reentry flights, depending on the speed ranges, the pitching moment required for pitch trim and forcing the shuttle to fly along the prescribed trajectory is provided by the body flap and/or the speedbrakes, rather than the elevons. The body flap is the predominant longitudinal trim device, while the wing-mounted elevons (in the elevator mode) are used for longitudinal stability augmentation and pitching-disturbance control. A sketch of the space shuttle orbiter, showing the relative size and locations of the its aerosurfaces, is presented in Fig. 1.3.

Henceforth, since we are only dealing with the longitudinal control where the elevons function as elevators, we will refer to the elevator-mode of the elevons simply as the elevators.

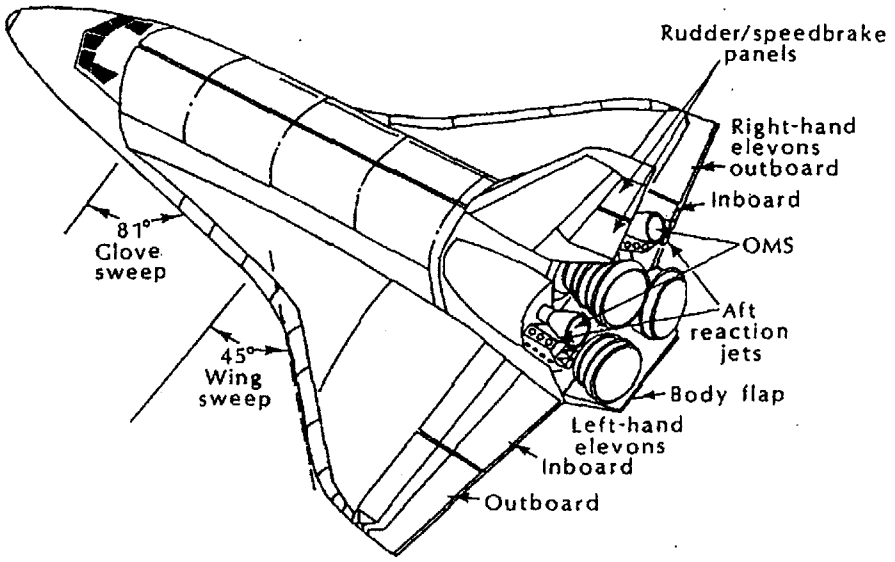

Fig. 1.3 Sketch illustrating the aerosurfaces of the space shuttle orbiter, taken from [11]

Finally, it should be noted that the effect of the trajectory-control body-flap or speedbrake deflections, is accounted for in C_{m_0}, and therefore their deflections and the corresponding aerodynamic effectiveness derivatives do not appear explicitly in the perturbation equations.

1.7 Unified Angle-of-Attack Equation

As derived in the previous section, the following set of coupled nonlinear differential equations, describe the perturbed longitudinal motion of the space shuttle from its prescribed trajectory during reentry.

$$\dot{V} = -\frac{\rho S C_D V^2}{2m} - g \sin\gamma \tag{1.28}$$

$$V\dot{\gamma} = \frac{\rho S C_L V^2}{2m} - (g - \frac{V^2}{r})\cos\gamma \tag{1.29}$$

$$\dot{q} = \frac{\rho S \bar{c} C_m V^2}{2I_y} - \frac{3g}{2r}(\frac{I_x - I_z}{I_y})\sin 2\theta \tag{1.30}$$

where the associated perturbation kinematic relations are

$$\dot{\theta} = q + \frac{V}{r}\cos\gamma \tag{1.31}$$

$$\dot{r} = V \sin\gamma \tag{1.32}$$

and

$$\theta = \gamma + \alpha_0 + \alpha \tag{1.33}$$

with α, as the perturbation variable.

In order to derive a unified equation that describes the variations of the space shuttle angle-of-attack for all possible reentries, as suggested by Laitone in [12], we can use the following universal time transformation

$$\xi(t) = \frac{1}{L}\int_0^t V(t)dt \tag{1.34}$$

or equivalently

$$L\dot{\xi}(t) = V(t) \tag{1.35}$$

that replaces the real time t by the non-dimensional variable ξ which represents the number of reference lengths L, traveled by the space shuttle center of mass along the trajectory. The following relationships hold accordingly

$$\frac{d}{dt}[] = (\frac{V}{L})\frac{d}{d\xi}[] \tag{1.36}$$

$$\frac{d^2}{dt^2}[] = (\frac{V}{L})^2\frac{d^2}{d\xi^2}[] + (\frac{VV'}{L^2})\frac{d}{d\xi}[] \tag{1.37}$$

Henceforth, to show differentiation with respect to ξ, we will use the following notation that is more convenient

$$[]' = \frac{d}{d\xi}[]$$

The elimination of θ and q from the equations of motion as well as the kinematic relations, and change of the independent variable from t to ξ, leads to the following non-dimensional second-order nonlinear inhomogeneous differential equation with variable coefficients that describes the variations in the space shuttle angle-of-attack once perturbed from its nominal trajectory values.

$$\alpha'' + \omega_1(\xi)\alpha' + \omega_0(\xi)\alpha = f(\xi) - \mu(\xi)\delta_e(\xi) \tag{1.38}$$

The corresponding coefficients are

$$\omega_1(\xi) = \delta[C_{L_\alpha} - \beta\sigma(C_{m_{\dot{\alpha}}} + C_{m_q})] + \frac{V'}{V} \tag{1.39}$$

$$\omega_0(\xi) = -\delta(\beta\sigma C_{m_\alpha} + \frac{gL}{V^2}C_{D_\alpha}\cos\gamma + \frac{L}{H}C_{L_\alpha}\sin\gamma) - \delta^2[C_{L_\alpha}(\beta\sigma C_{m_q} + C_{D_0}) + C_{L_0}C_{D_\alpha}] + \frac{3L}{r}(\frac{gL}{V^2})\nu\cos 2(\gamma + \alpha_0) \tag{1.40}$$

$$f(\xi)=\delta(\frac{gL}{V^2})[C_{D_0}-\beta\sigma C_{m_q}(1-\frac{V^2}{gr})]\cos\gamma+\delta(\frac{L}{H}C_{L_0}\sin\gamma+\sigma C_{m_0})+\delta^2 C_{L_0}(\beta\sigma C_{m_q}+C_{D_0})$$
$$-(\frac{gL}{V^2})[(\frac{3L}{r}-\frac{gL}{V^2})\sin 2\gamma+\frac{3L}{2r}\nu\sin 2(\gamma+\alpha_0)] \quad (1.41)$$

and

$$\mu(\xi)=-\beta\sigma\delta(\xi)C_{m_{\delta_e}}(\xi) \quad (1.42)$$

Equation (1.38) is called "the unified angle-of-attack equation". Henceforth, we will call $\omega_1(\xi)$, $\omega_0(\xi)$, and $\mu(\xi)$, as the damping coefficient, the stiffness coefficient, and the control coefficient, respectively. The term $f(\xi)$ will be referred to as the disturbance term. In order to simplify the derivations and the resulting expressions of the unified equation, the following non-dimensional parameters have also been introduced.

$$\beta=\frac{\bar{c}}{L} \quad (1.43)$$

$$\delta=\frac{\rho SL}{2m} \quad (1.44)$$

$$\nu=\frac{I_x-I_z}{I_y} \quad (1.45)$$

$$\sigma=\frac{mL^2}{I_y} \quad (1.46)$$

where β serves as the matching parameter between the generic hypersonic-aircraft aerodynamic model and the trajectory model for the actual space shuttle, δ is the varying non-dimensional air density, ν is the ratio of the moments of inertia of the space shuttle in the stability axes, and considered to be invariant, and σ is a constant that can be regarded as the inverse non-dimensional pitching moment of inertia of the space shuttle.

It should be reminded that the unified equation (1.38) is nonlinear due to its inhomogeneity that stems from the presence of the inherently-induced forcing term, $f(\xi)$, on the right-hand side. Physically speaking, considering the equation (1.38) as the representation of a dynamical system, we can see that the relationship between the input, i.e. the elevator angle, and the output, i.e. the angle-of-attack, is not linear.

It is also notable that the parameters ω_1, ω_0, f, and μ, are solely functions of the aerodynamic coefficients and the nominal trajectory variables where they can be evaluated explicitly, if the trajectory flown by the center of mass of the shuttle vehicle is known. This assumes the so-called "limited problem" hypothesis that is the angle-of-attack perturbations have negligible effect on the trajectory.

The gravitational acceleration gradient, $g'(\xi)$, and the non-dimensional air density gradient, $\delta'(\xi)$, have also been used in the derivation of (1.38), where they are determined as follows. For the gravity gradient, we begin with (1.3)

$$g = g_s \frac{R_e^{\,2}}{r^2}$$

and differentiate with respect to ξ, to get

$$g' = \frac{dg}{d\xi} = g_s R_e^{\,2}\left(\frac{-2r'}{r^3}\right) = -2\left(\frac{r'}{r}\right) g_s \frac{R_e^{\,2}}{r^2} = -2\left(\frac{r'}{r}\right) g \tag{1.47}$$

However, by applying (1.36) to (1.32) we get

$$r' = \frac{L}{V}\dot{r} = L\sin\gamma \tag{1.48}$$

Substituting (1.48) into (1.47), we obtain the gravity gradient as

$$g' = -2g\left(\frac{L}{r}\right)\sin\gamma \tag{1.49}$$

For the non-dimensional air density gradient, by differentiating (1.44) we get

$$\delta' = \frac{\rho' SL}{2m}$$

and from (1.4), we can write

$$\rho' = -\frac{h'}{H}\rho \tag{1.50}$$

However, since the Earth radius is constant, we have

$$h' = r' \tag{1.51}$$

Using (1.51) and substituting (1.48) into (1.50), we can write

$$\rho' = -\frac{L}{H}\rho\sin\gamma$$

and consequently

$$\delta' = -\delta\frac{L}{H}\sin\gamma \tag{1.52}$$

The angular range, ϕ, can be computed as is described below. Breaking the velocity vector of the shuttle into the radial and tangential (or orbital) components, we can write

$$\vec{V} = V_r\hat{e}_r + V_\phi\hat{e}_\phi$$

where

$$V_r = \dot{r} = V \sin\gamma \tag{1.53}$$

$$V_\phi = r\dot{\phi} = V \cos\gamma \tag{1.54}$$

Considering the orbital component, by rearranging (1.54), we get

$$\dot{\phi} = \frac{V}{r}\cos\gamma$$

and using (1.36), we can write

$$\phi' = \frac{L}{r}\cos\gamma \tag{1.55}$$

Finally, integrating (1.55) along the trajectory with respect to ξ, yields

$$\phi(\xi) = L\int_0^{\xi} \frac{\cos\gamma}{r} d\xi \tag{1.56}$$

where γ and r are both functions of ξ.

The elapsed time for the shuttle traveling along the trajectory, can be computed at each position by inverting the transformation (1.35) to get

$$t(\xi) = L\int_0^{\xi} \frac{1}{V(\xi)} d\xi \tag{1.57}$$

1.8 Elevator Control Torque

The aerodynamic pitching torque exerted on the space shuttle due to the elevator actuation, i.e. the elevator control torque, can be determined as described below. Using Eqs. (1.10) and (1.26), we can write

$$M_{\delta_e}(\xi) = C_{m_{\delta_e}}(\xi)\delta_e(\xi)\overline{q}(\xi)S\overline{c} \tag{1.58}$$

Implementing the non-dimensional parameters introduced in Sec. 1.7, we arrive at the following relation for the elevator control torque

$$M_{\delta_e}(\xi) = \beta\sigma\delta(\xi)C_{m_{\delta_e}}(\xi)\delta_e(\xi)I_y(\frac{V}{L})^2 \tag{1.59}$$

or simply

$$M_{\delta_e}(\xi) = -\mu(\xi)\delta_e(\xi)I_y(\frac{V}{L})^2 \tag{1.60}$$

CHAPTER 2

DYNAMIC RESPONSE

The dynamic response of the space shuttle to the angle-of-attack perturbations, while traveling along the prescribed optimal reentry trajectory, is discussed in this chapter. In order to simulate the space shuttle aerodynamic characteristics, a realistic generic hypersonic-aircraft computer-simulation aerodynamic model was used for all the simulations in this thesis. The model is a geometrically-simplified hypersonic delta-wing aircraft that has similar aerodynamic characteristics to those of the space shuttle. The trajectory model that was used in the simulations is an optimal reentry trajectory, designed to minimize the weight of the thermal-protection system (TPS) of the space shuttle SSV 049 [4]. The simulation results in this chapter, for the dynamic response of the shuttle vehicle using the generic aerodynamic model, show good agreement with those of the actual space shuttle model reported in [9].

2.1 MODEL GEOMETRY

The space shuttle actual geometry, taken from [1], is shown below. Note that the scale length is in inches. It should be mentioned that the overall length of the shuttle (L = 107.75 ft. or 1293 in.) was still used as the reference length for deriving the unified equation of the angle-of-attack oscillations, Eq. (1.38), because the available trajectory data to be used for simulations are based on the actual model.

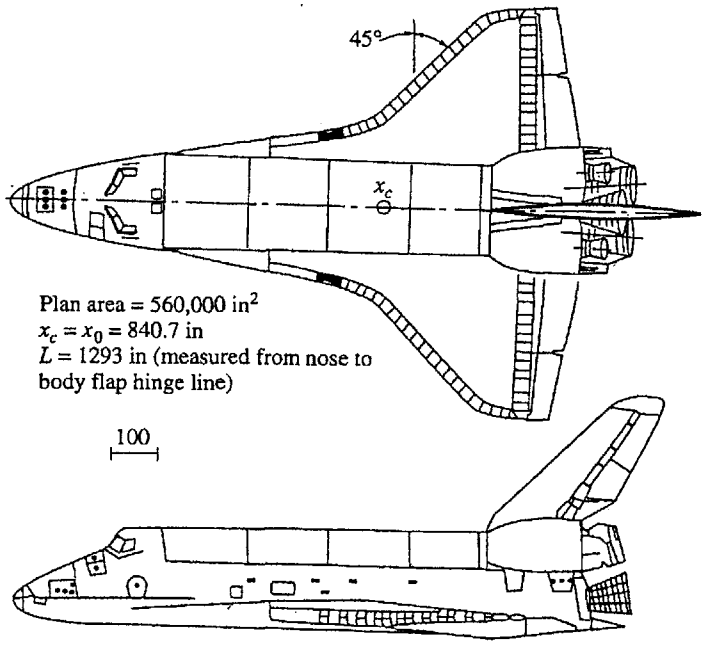

Fig. 2.1 The space shuttle geometry, taken from [1]

A sketch of the generic hypersonic aircraft model used for the simulations in this study is illustrated in Fig. 2.2.

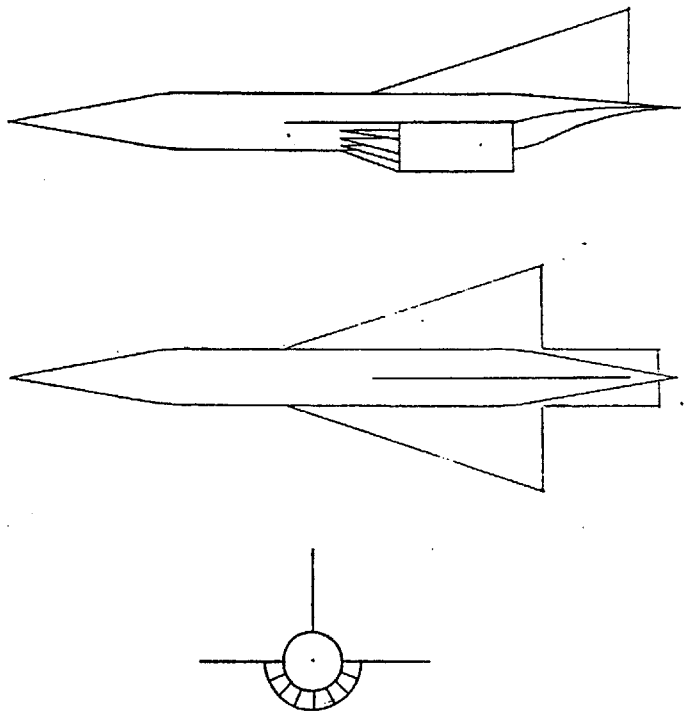

Fig. 2.2 Geometry of the generic hypersonic computer simulation aerodynamic model, taken from [3]

The model geometry is built up of simple geometric shapes in order to simplify the analysis required to estimate the mass properties [3]. The primary structure is modeled as a cylinder 20 ft. in diameter and 120 ft. long. This comprises the volume required for tankage of the liquid hydrogen. Onto this cylinder is attached a pair of 10-degree cones to form the vehicle nose and boattail. This assembly completes the fuselage.

The wings and vertical tail are modeled as thin triangular plates. The mid-wing configuration has been chosen and no dihedral has been added to the wings. The engine module is wrapped around the lower surface of the fuselage and strakes have been extended behind the wings to form the end plates of the half nozzle formed by the lower half of the boattail.

The geometric aerodynamic reference parameters are as follows

Plan Area, $S = 6000\,ft^2$
Mean Aerodynamic Chord, $\bar{c} = 75\,ft$
Span, $b = 80\,ft$
Overall Length, $L_{total} = 233.4\,ft$

2.2 MASS PROPERTIES

The mass properties of this class of hypersonic vehicles are assumed to be of the same order of magnitude as current supersonic cruise aircraft. The estimate contained in this model has been derived from the XB-70. The take off gross weight is estimated to be in the neighborhood of 300,000 pounds. Of this the fuel (liquid hydrogen) is assumed to comprise 60% (180,000 pounds), and hence the fuel-burnout gliding reentry mass can be approximated by the remaining 40% (120,000 pounds) divided by the acceleration due to gravity at sea level. Therefore

Reentry Mass, $m = 3{,}725 \;\; slugs$

Rolling Moment of Inertia, $I_x = 0.87 \times 10^6 \;\; slug - ft^2$

Pitching Moment of Inertia, $I_y = 14.2 \times 10^6 \;\; slug - ft^2$

Yawing Moment of Inertia, $I_z = 14.9 \times 10^6 \;\; slug - ft^2$

Yaw-Roll Product of Inertia, $I_{xz} = 0.28 \times 10^6 \;\; slug - ft^2$

The mass moments of inertia have been estimated from simple geometric solids and shells which approximated the configuration of the model.

2.3 REENTRY TRAJECTORY MODEL

The trajectory model and data used for simulations is an optimal reentry trajectory designed to minimize the thermal-protection system (TPS) weight for the space shuttle SSV 049 [4]. The trajectory characteristics are shown in Fig. 2.3. As can be realized from the flight-path angle history, this reentry model can be classified as a shallow glide entry. The altitude ranges from 400,000 ft at the fringe of atmosphere down to the 100,000 ft where accordingly, the atmospheric density increases about 5 orders of magnitude over the altitude range. The shuttle velocity ranges from Mach 24 in the hypersonic regime down to about Mach 2 in the supersonic range. The total entry time is about 35 minutes and the total distance traveled by the space shuttle along the trajectory is around 6000 miles. The reentry starts with very high angles-of-attack of about 53° in order to maximize the drag and ends at much lower values of around 20°.

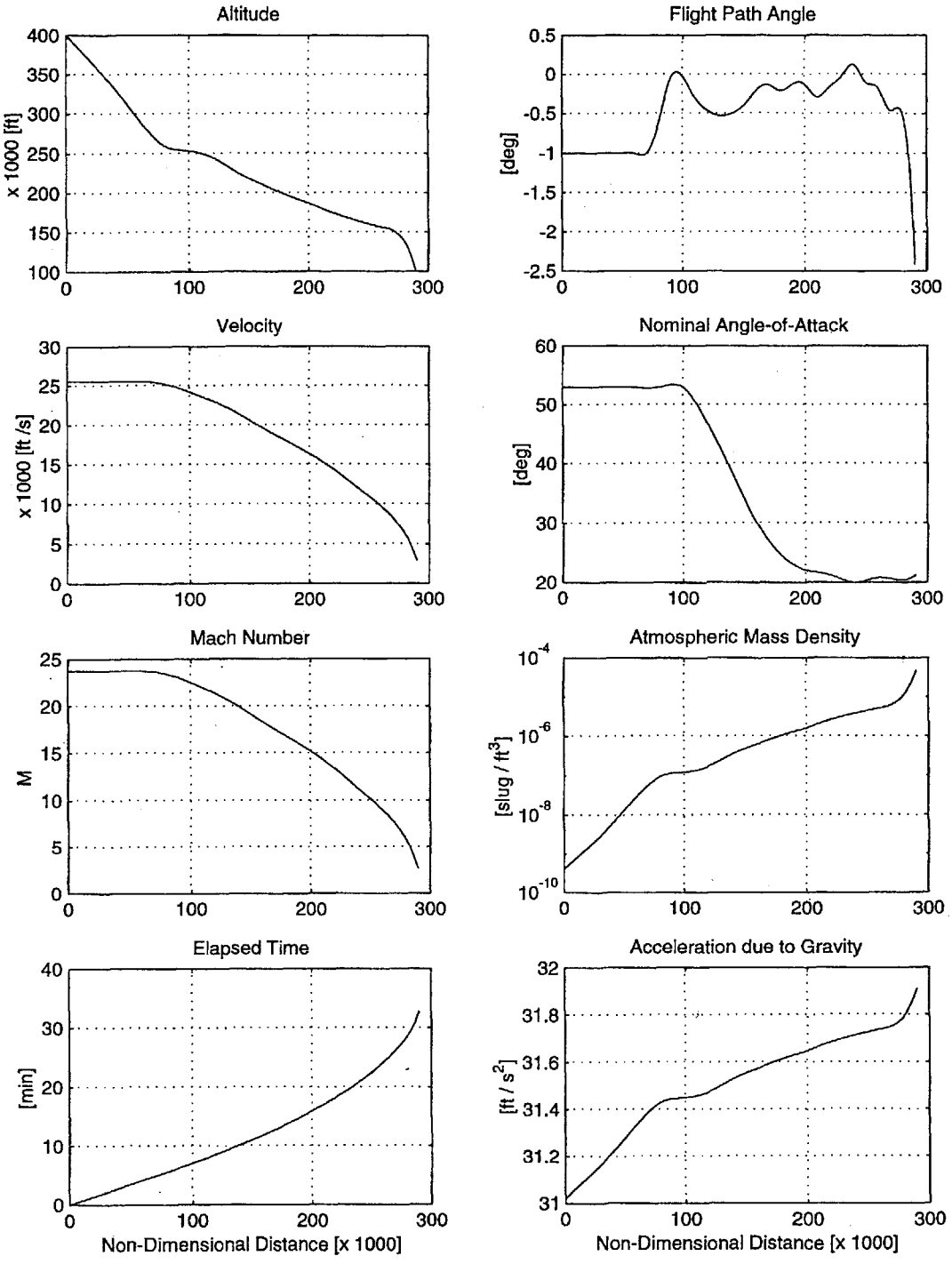

Fig. 2.3 The space shuttle prescribed reentry trajectory characteristics

2.3.1 NOMINAL AERODYNAMIC COEFFICIENTS ALONG THE TRAJECTORY

As mentioned before, the unified equation is the governing equation for the angle-of-attack perturbations from the nominal conditions along the prescribed trajectory. Therefore, to analyze and control the angle-of-attack oscillations, we need to know the characteristics of the trajectory flown by the space shuttle. These characteristics include the history of variations of the nominal drag, lift, and pitching moment coefficients along the trajectory, as well as altitude, velocity, flight path angle, and angle-of-attack. For this thesis, since only the latter four variables were available from [9] for the trajectory of interest (Fig. 2.3), the first three variables had to be found by other means.

The nominal drag and lift coefficients can be readily found from the following well-known hypersonic aerodynamic relations as functions of the nominal angle-of-attack [1]

$$C_{D_0} = 2\sin^3\alpha_0 \tag{2.1}$$

$$C_{L_0} = 2\sin^2\alpha_0\cos\alpha_0 \tag{2.2}$$

and lift-to-drag ratio is

$$\frac{Lift}{Drag} = \frac{C_{L_0}}{C_{D_0}} = \cot\alpha_0 \tag{2.3}$$

The nominal pitching moment coefficient, however, should be extracted from the equations of motion and the kinematical relations. The procedure is as the following.

Consider the original unperturbed pitching moment equation with the embedded pitching moment coefficient at its nominal value, along with the kinematic relations below

$$\dot{q} = \frac{\rho S C_{m_0} V^2}{2I_y} - \frac{3g}{2r}\left(\frac{I_x - I_z}{I_y}\right)\sin 2\theta_0 \tag{2.4}$$

$$\dot{\theta}_0 = q + \frac{V}{r}\cos\gamma \tag{2.5}$$

$$\dot{r} = V\sin\gamma \tag{2.6}$$

$$\theta_0 = \gamma + \alpha_0 \tag{2.7}$$

Applying the time transformation of (1.35) and using the previously-introduced non-dimensional parameters, we get

$$q' = \delta\sigma\left(\frac{V}{L}\right)C_{m_0} - \frac{3g}{2r}\left(\frac{L}{V}\right)\nu\sin 2\theta_0 \tag{2.8}$$

$$\frac{V}{L}\theta_0' = q + \frac{V}{r}\cos\gamma \tag{2.9}$$

$$\theta_0' = \gamma' + \alpha_0' \tag{2.10}$$

$$r' = L\sin\gamma \tag{2.11}$$

Solving (2.8) for C_{m_0}, we obtain

$$C_{m_0} = \frac{1}{\delta\sigma}\left(\frac{L}{V}\right)\left[q' + \frac{3g}{2r}\left(\frac{L}{V}\right)\nu\sin 2\theta_0\right] \tag{2.12}$$

As can be seen, the expression for C_{m_0} has the term q' that should be expressed in terms of the other available trajectory variables. To this effect, let us solve the first kinematical relation for q and substitute for θ_0' from (2.10) to get

$$q = \frac{V}{L}(\gamma' + \alpha_0') - \frac{V}{r}\cos\gamma$$

Differentiating with respect to ξ and substituting for r' from (2.11), yields

$$q' = \frac{V}{L}(\gamma'' + \alpha_0'') + \frac{V'}{L}(\gamma' + \alpha_0') - \frac{V'}{r}\cos\gamma + \left(\frac{L}{r}\cos\gamma + \gamma'\right)\frac{V}{r}\sin\gamma \tag{2.13}$$

Finally, substitution for q' from (2.13) into (2.12), results in

$$C_{m_0} = \frac{1}{\delta\sigma}\left[(\gamma'' + \alpha_0'') + \frac{LV'}{V^2}(\gamma' + \alpha_0') - \left(\frac{L}{V}\right)^2\frac{V'}{r}\cos\gamma + \left(\frac{L}{r}\cos\gamma + \gamma'\right)\frac{L^2}{rV}\sin\gamma + \frac{3g}{2r}\left(\frac{L}{V}\right)^2\nu\sin 2\theta_0\right] \tag{2.14}$$

where all the variables on the right-hand side are available or computable from the trajectory information in hand. However, note that V', γ' and α_0' as well as γ'' and α_0'' must be computed by applying a numerical differentiation scheme once and/or twice to the velocity, flight path angle, and angle-of-attack data of the trajectory. Fig. 2.4 shows the computed results.

It should be noted that in general, airspeeds above Mach 5 are considered hypersonic, and as can be seen from the nominal Mach number history, most part of the reentry trajectory under consideration falls into the hypersonic regime where the formulas for the drag and lift coefficients, Eqs. (2.1) and (2.2), are valid.

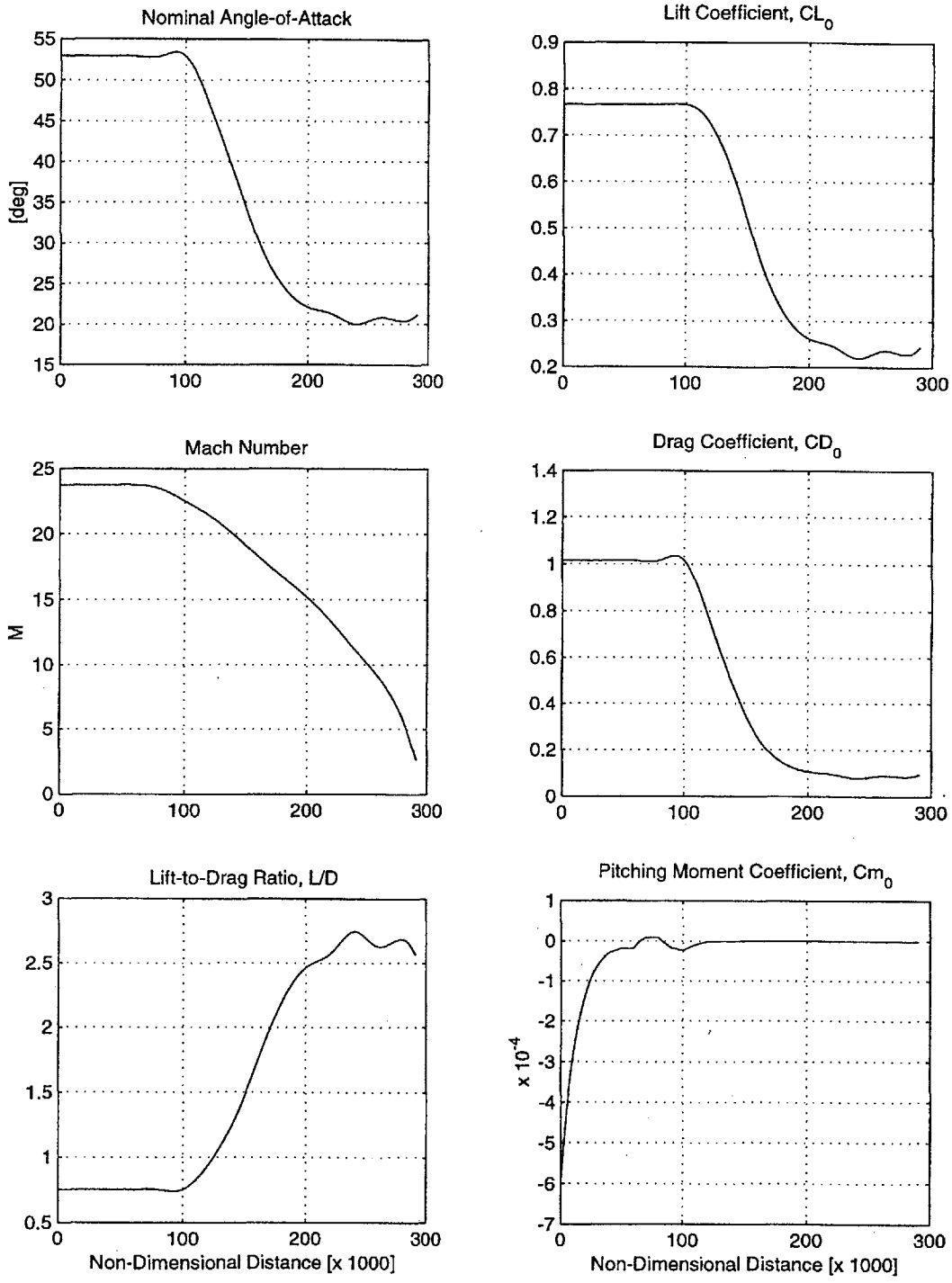

Figure 2.4 Nominal aerodynamic coefficients and lift-to-drag ratio during the space shuttle reentry

2.4 MODEL AERODYNAMICS

The model aerodynamic characteristics needed for this study consist of only the longitudinal stability and control derivatives. The stability and control derivatives along the trajectory are functions of the nominal angle-of-attack and Mach number. The following plots that show their variations have been generated by providing the angle-of-attack and Mach number information from the trajectory model presented in [3], in turn taken from [4], as inputs to the corresponding aerodynamic data tables of the generic model taken from [3] and using two-dimensional linear interpolation.

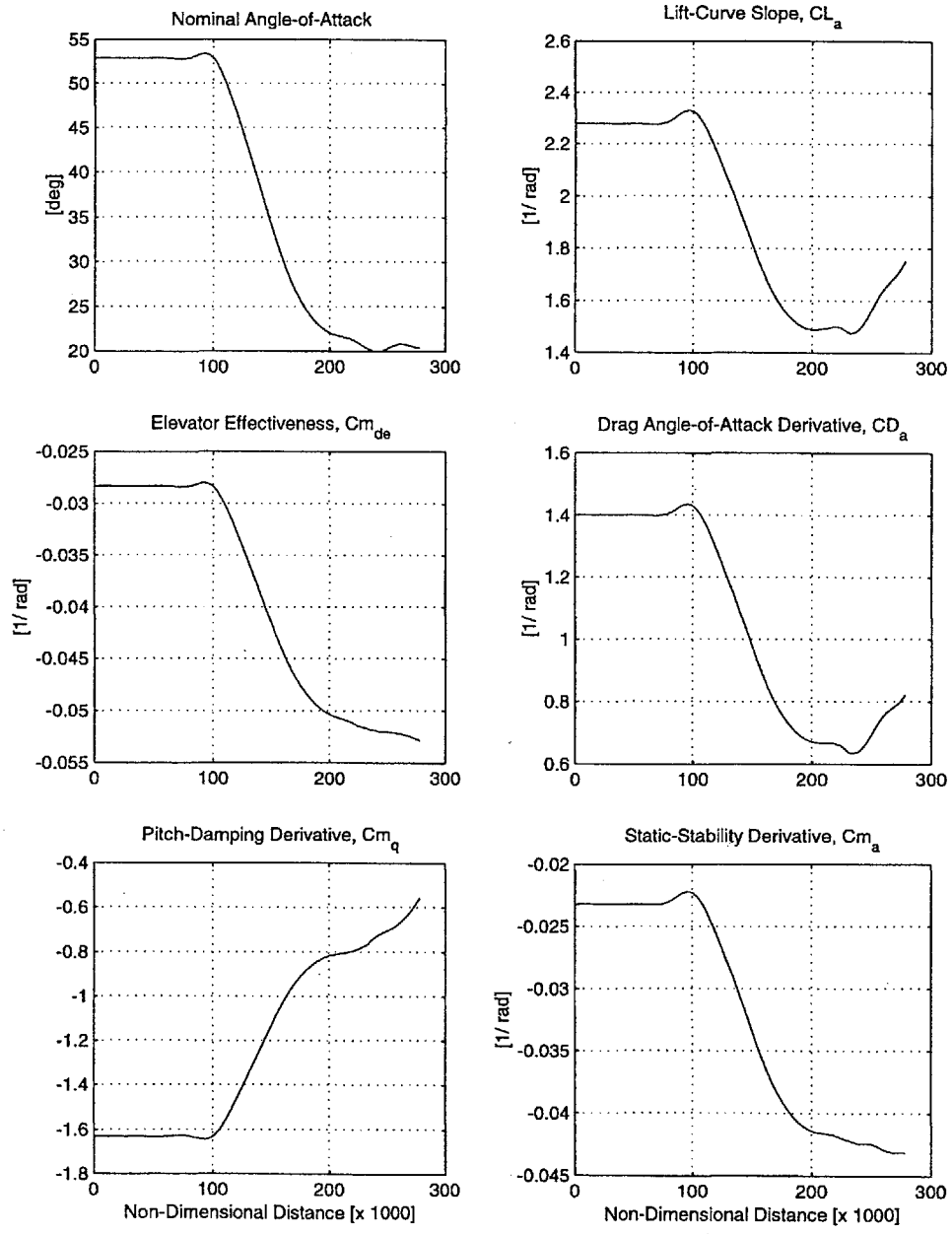

Fig. 2.5 Aerodynamic stability and control derivatives along the reentry trajectory of the space shuttle

2.5 DYNAMIC RESPONSE TO ANGLE-OF-ATTACK PERTURBATIONS

As derived in the previous chapter, the coefficients of the unified angle-of-attack equation (1.38) vary as functions of the trajectory variables. These variations are slow compared to the uncontrolled natural dynamic response of the shuttle once the angle-of-attack is perturbed from its nominal prescribed values. However, as will be discussed in the next chapter, for long-term control periods that are unavoidable due to the very low air density at the upper portion of the reentry trajectory, the variations of the trajectory variables are comparable to that of the controlled response. These variations are shown in the figure below.

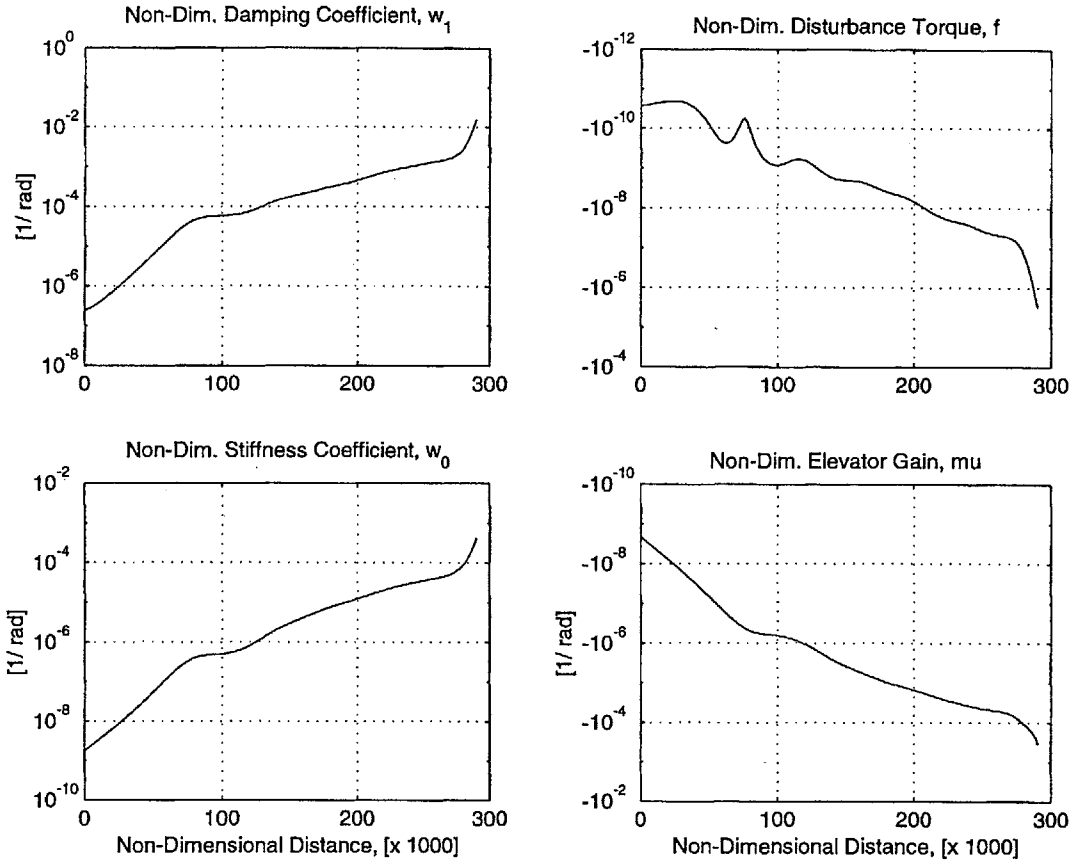

Fig. 2.6 Variations of the coefficients of the unified angle-of-attack equation

It can be seen that the damping and stiffness coefficients are almost monotonically increasing and favorably positive throughout the trajectory which is a necessary condition for longitudinal dynamic stability of the shuttle. Not surprisingly, as the space shuttle travels deeper into the atmosphere, the damping and stiffness coefficients grow almost exponentially, which is due to the exponentially-increasing air density. This phenomenon results in higher dynamic stability and faster dynamic response. Note that the magnitudes of the non-dimensional perturbation-induced disturbance torque and the elevator control coefficient, also follow nearly-exponential trends, again due to the dominant air density factor that they carry. As plotted in Fig. 2.6, the

disturbance torque appears to be negative over the entire trajectory, and as will be seen in Sec. 2.6.1, tends to nose down the space shuttle. The negative sign of the non-dimensional elevator gain is simply because $C_{m_{\delta_e}}$ is always negative due to sign convention for the control surface deflections.

2.5.1 Simulation Results and Discussion

The uncontrolled dynamic responses to the angle-of-attack perturbation at two different altitudes of 400,000 ft and 150,000 ft, corresponding to the upper and lower portions of the trajectory, are shown in Figs. 2.7 and 2.8 respectively. The initial conditions are $\alpha(\xi_0) = 5°$ and $\alpha'(\xi_0) = 0$.

As demonstrated in Figs. 2.7 and 2.8, the dynamic responses are stable, but highly oscillatory with increasing frequency ($f = 1/2\pi\sqrt{(1-\zeta^2)\omega_0}$ with the damping ratio of $\zeta = \omega_1/2\sqrt{\omega_0}$) as the shuttle travels deeper into the atmosphere of increasing density. Also, the settling time in both cases is relatively large (about 15 min. and 2 min., respectively) which is not desirable. As can be seen, the die-out time is much larger for the upper portion of the trajectory compared to that of the lower part. This is due to the smaller equivalent damping ratio, ζ, associated with the unified angle-of-attack equation (1.38), as a result of the much lower air density in the upper atmosphere (Fig. 2.3). The increasing frequency is especially visible for the case of upper trajectory as it takes much longer for the oscillations to die out. The highly-oscillatory response, with increasing frequency and long die-out periods, readily justifies the need for providing the space shuttle orbiter with an artificial angle-of-attack controller.

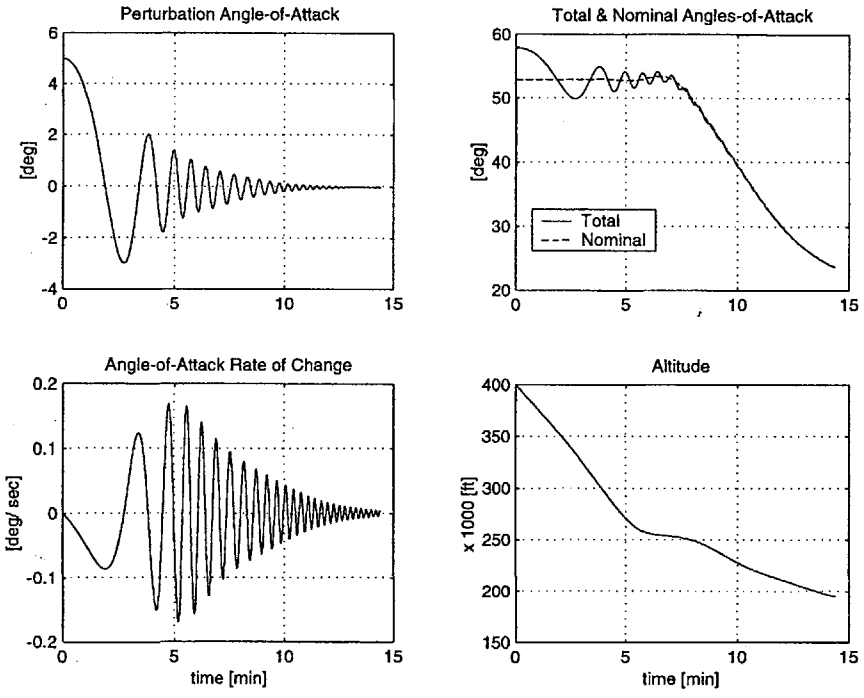

Fig. 2.7 Perturbation response for 400,000 ft initial altitude

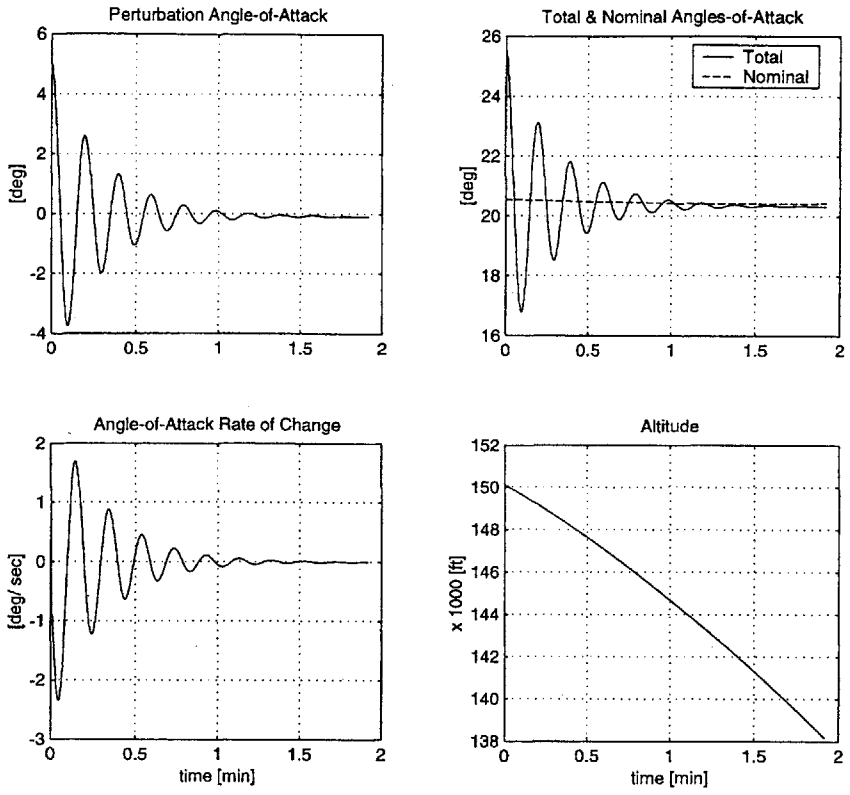

Fig. 2.8 Perturbation response for 150,000 ft initial altitude

2.6 FEED-FORWARD DISTURBANCE CONTROL

The non-dimensional perturbation-induced disturbance torque, $f(\xi)$, as will be shown in this section, has unnoticeable effect on the dynamic response of the shuttle to the angle-of-attack perturbations. Using the unified equation of (1.38), we can determine the amount of the elevator deflection needed to eliminate the disturbance effect. This will leave the perturbations to vanish naturally, as a result of the stable longitudinal dynamics of the space shuttle aerodynamic design, without following the additional forcing disturbance. From Eq. (1.38) we have

$$\alpha'' + \omega_1(\xi)\alpha' + \omega_0(\xi)\alpha = f(\xi) - \mu(\xi)\delta_e(\xi) \tag{2.15}$$

Putting the right-hand side equal to zero and solving for the elevator deflection yields

$$\tilde{\delta}_e(\xi) = \frac{f(\xi)}{\mu(\xi)} \tag{2.16}$$

where $\tilde{\delta}_e(\xi)$ denotes the required feed-forward disturbance-control deflection of the elevator. Using (1.60), the corresponding elevator control torque will be

$$\tilde{M}_{\delta_e}(\xi) = -\mu(\xi)\tilde{\delta}_e(\xi) I_y \left(\frac{V}{L}\right)^2 \tag{2.17}$$

2.6.1 SIMULATION RESULTS AND DISCUSSION

The disturbance-controlled dynamic response to the angle-of-attack perturbations at the same altitudes and with the same initial conditions as those of Sec. 2.5.1 are shown in Figs. 2.9 and 2.10. As can be seen, the effect of the perturbation-induced disturbance torque, appearing as the inhomogeneous forcing term in the unified equation, is hardly noticeable. Accordingly, the maximum required elevator deflection is seen to be less than one degree for the 400,000-ft altitude, and less than 0.1 degree for 150,000-ft altitude.

The results of the feedforward disturbance control presented in this section will be used as a reference for evaluating as well as validating the performance of the other control techniques discussed in the subsequent chapters of this document. The reason for choosing the disturbance control output as reference is that firstly, the disturbance controller does not change or compensate the aerodynamic damping and stiffness properties of the shuttle so that the controlled response is in fact the transient dynamic response of the vehicle, and secondly, the outcome of the application of other control strategies must asymptotically tend to that of the disturbance control scheme. This is due to the fact that other controllers must also cancel out the induced disturbance while suppressing the angle-of-attack oscillations, and clearly the disturbance remains in effect once the transient angle-of-attack oscillations are canceled out.

As mentioned earlier in Sec. 2.5, the induced disturbance torque always tends to nose down the shuttle which can be verified by noticing the required negative elevator control angles and correspondingly, positive control torques shown in Figs. 2.9 and 2.10.

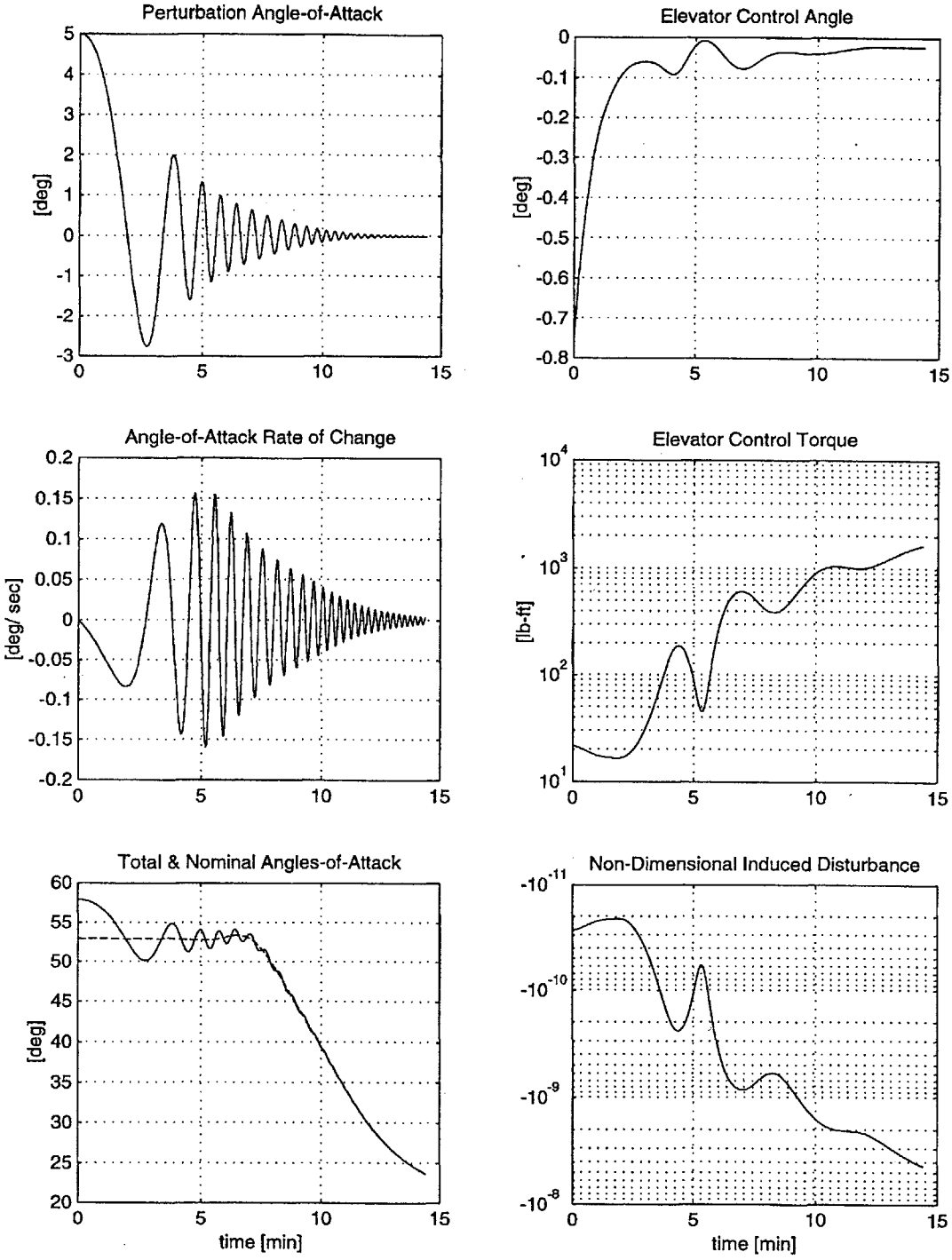

Fig. 2.9 Feedforward disturbance control results for 400,000 ft initial altitude

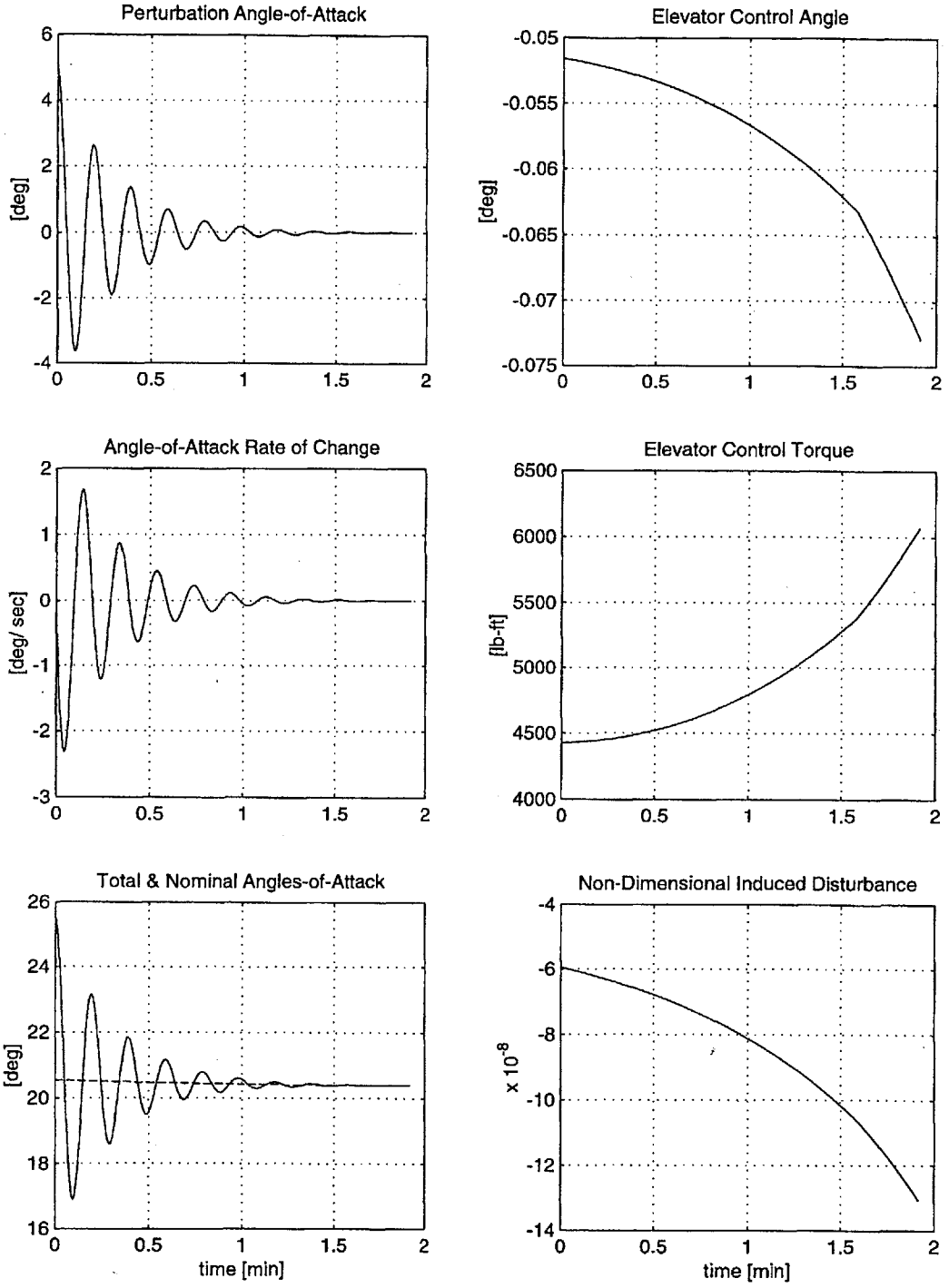

Fig. 2.10 Feedforward disturbance control results for 150,000 ft initial altitude

CHAPTER 3

NONLINEAR CONTROL

In this chapter, in order to suppress the undesired angle-of-attack oscillations, the nonlinear control method of feedback linearization is implemented. Because of its simplicity, the feedback linearization is used to characterize the controlled response of the shuttle to the angle-of-attack perturbations. The feedback-linearization nonlinear controller, subject to the maximum available elevator-angle constraint, offers realistic estimations for the duration and the corresponding rate of decay of the controlled response that will be helpful to design the controllers discussed in the subsequent chapters. The feedback linearization is easy to implement since as will be seen, we only needed to specify the desired time for control action and check if the maximum demanded elevator angle is available.

Feedback linearization is in general, a nonlinear control design methodology that algebraically transforms a nonlinear system dynamics into a fully or partly linear one with constant parameters. In its simplest form, feedback linearization amounts to canceling the nonlinearities in a nonlinear system so that the closed-loop dynamics is in a simple linear form. The technique assumes that the dynamic model of the system is known exactly, and uses it for the controller design. The resulting closed-loop dynamics is exponentially stable.

However, since in this problem, by simply introducing the right-hand side of the unified equation (1.38) as the control variable, the system dynamics becomes linear, the notion of linearization will not be essentially true. Nevertheless, the technique is applied in a similar fashion to transform the linear time-varying (LTV) model to a time-invariant one (LTI). The transformed model dynamic response is enforced to have the desired characteristics, by choosing a proper characteristic value.

3.1 FEEDBACK LINEARIZATION

Recall the unified equation (1.39) as

$$\alpha'' + \omega_1(\xi)\alpha' + \omega_0(\xi)\alpha = f(\xi) - \mu(\xi)\delta_e(\xi) \tag{3.1}$$

with the initial conditions of $\alpha(\xi_0) = \alpha_0$ and $\alpha'(\xi_0) = \alpha_0'$. Let us assume

$$\alpha'' + \omega_1(\xi)\alpha' + \omega_0(\xi)\alpha = u(\xi) \tag{3.2}$$

where $u(\xi)$ is the non-dimensional control variable and we have

$$u(\xi) = f(\xi) - \mu(\xi)\delta_e(\xi) \tag{3.3}$$

Once the control law is determined, from (3.3) the corresponding elevator control deflection will be

$$\delta_e(\xi) = \frac{f(\xi) - u(\xi)}{\mu(\xi)} \tag{3.4}$$

Now, let the control law be as the following

$$u(\xi) = \omega_1(\xi)\alpha' + \omega_0(\xi)\alpha - (2\lambda\alpha' + \lambda^2\alpha) \tag{3.5}$$

where λ is an arbitrary characteristic value and must be positive ($\lambda > 0$). Rearranging gives

$$u(\xi) = [\omega_1(\xi) - 2\lambda]\alpha' + [\omega_0(\xi) - \lambda^2]\alpha \tag{3.6}$$

Substituting (3.6) into (3.4) and collecting terms, we obtain the corresponding elevator control command as

$$\delta_e(\xi) = [\frac{2\lambda - \omega_1(\xi)}{\mu(\xi)}]\alpha' + [\frac{\lambda^2 - \omega_0(\xi)}{\mu(\xi)}]\alpha + [\frac{f(\xi)}{\mu(\xi)}] \tag{3.7}$$

Note that the feedback gains and the feedforward term vary along the trajectory. The control law of (3.5), forces the perturbation angle-of-attack dynamics to be

$$\alpha''(\xi) + 2\lambda\alpha'(\xi) + \lambda^2\alpha(\xi) = 0 \tag{3.8}$$

where the coefficients are now constant. The solution to this differential equation with repeated characteristic roots, is simply known to be of the form

$$\alpha(\xi) = (A + B\xi)e^{-\lambda\xi} \tag{3.9}$$

Applying the initial conditions, we obtain the response as

$$\alpha(\xi) = [\alpha_0 + (\alpha_0' + \lambda\alpha_0)(\xi - \xi_0)]e^{-\lambda(\xi - \xi_0)} \tag{3.10}$$

that is an exponentially-decaying behavior.

In case, the final position, ξ_f, is specified, we can use the following formula to achieve the desired accuracy in canceling out the oscillations

$$\lambda = \frac{n}{\xi_f - \xi_0} \tag{3.11}$$

where the suppressed angle-of-attack perturbation at the end of the control action will be

$$\alpha(\xi_f) = O(e^{-n}\alpha_0) \tag{3.12}$$

3.1.1 Simulation Results and Discussion

The feedback linearization control results for the same set of initial altitudes and initial conditions as those in Sec. 2.5.1, are demonstrated in Figs. 3.1 and 3.2. The characteristic values listed below were used in the simulations where they proved to give the fastest response while keeping the required elevator deflection within the available range of $\pm 25^{\circ}$.

400,000 ft Initial Altitude: $\lambda = 1.11 \times 10^{-4}$
150,000 ft Initial Altitude: $\lambda = 1.92 \times 10^{-2}$

As can be seen, the time needed for the oscillations to die out has been reduced considerably as compared to that of the disturbance control or the transient response which uses the natural or inherent damping and stiffness characteristics of the shuttle aerodynamic design.

Inspecting the results, we can see that the feedback linearization is an effective and yet very simple control strategy. In addition to its simple methodology, the feedback linearization is also easy to implement in the sense that we only need to specify the desired time period for control action in Eq. (3.11), which is intuitive and easy to choose, and the desired level of suppression by applying the rule of Eq. (3.12).

However, it should be reminded that the feedback linearization technique requires the exact knowledge of the dynamical-system parameters. For our problem, as can be seen in (3.5), the parameters include the trajectory characteristics and the aerodynamic data of the shuttle orbiter.

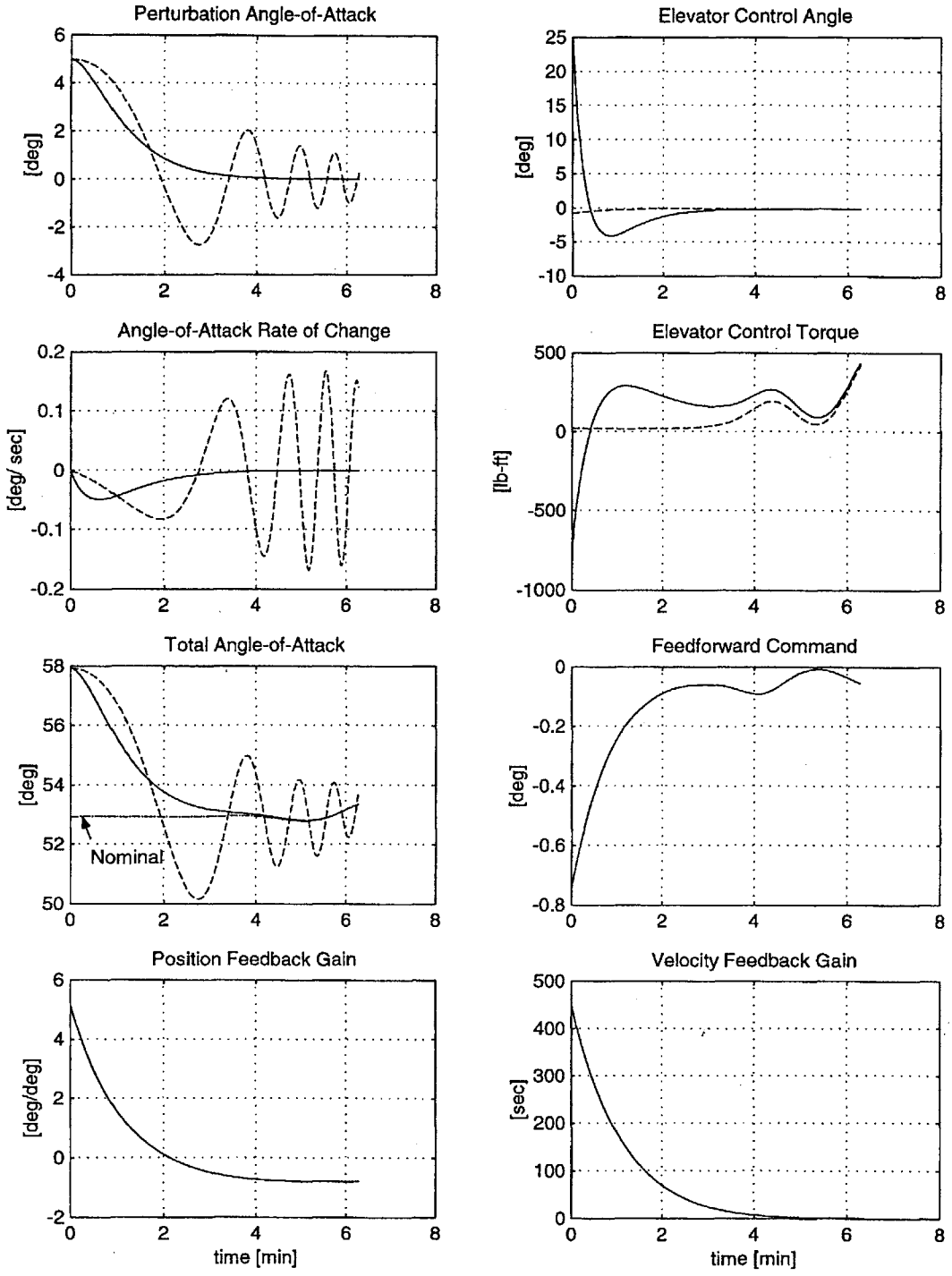

Fig. 3.1 Feedback linearization results for 400,000 ft initial altitude

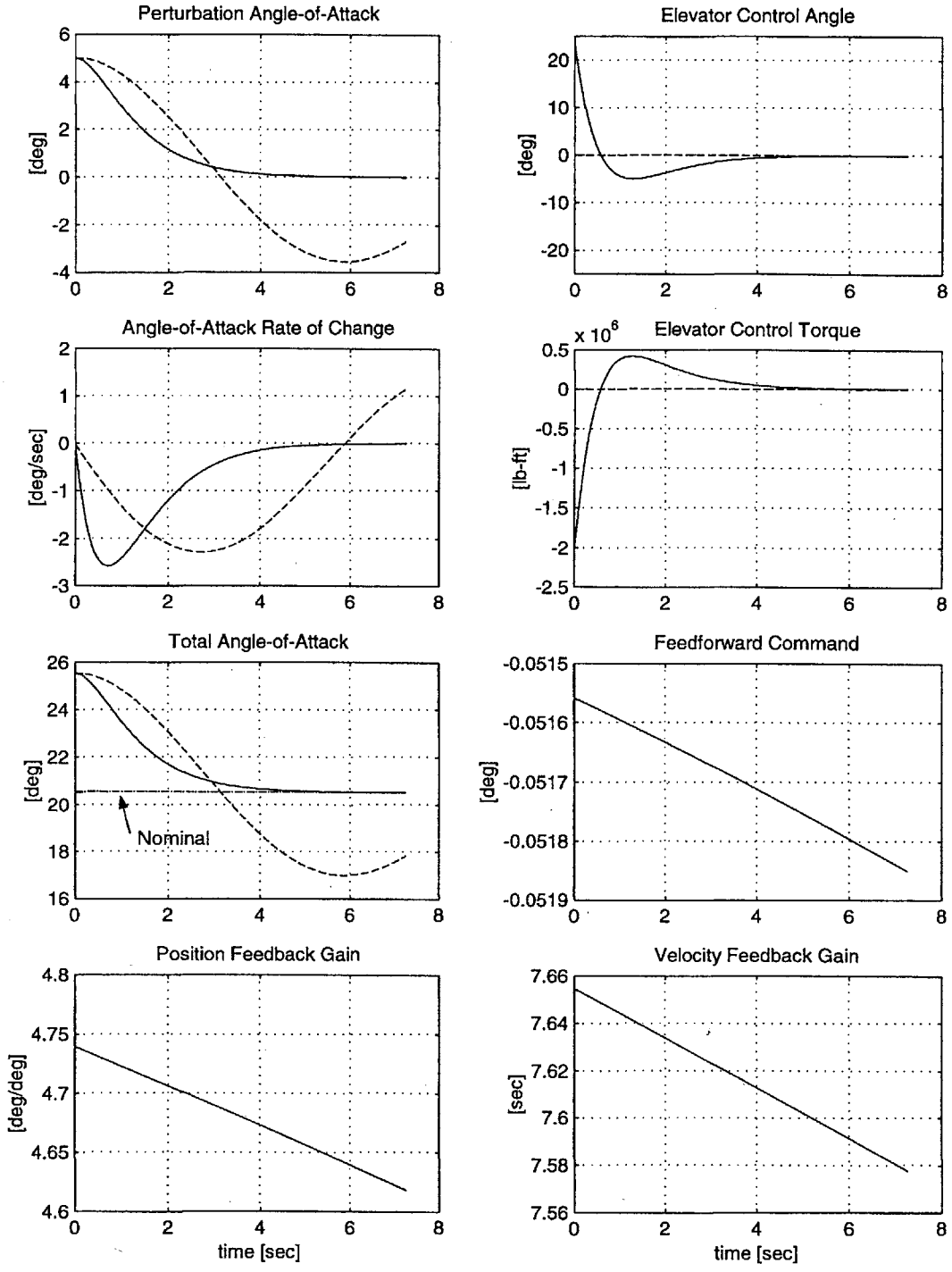

Fig. 3.2 Feedback linearization results for 150,000 ft initial altitude

CHAPTER 4

OPTIMAL CONTROL

In this chapter, in order to control the perturbations of the space shuttle angle-of-attack during reentry, an optimal control approach is applied to the state space representation of the unified equation. The underlying scheme is the linear quadratic regulator (LQR) formulation [6] that forms a boundary value problem with the specified initial and final conditions for the state vector. Due to the zero final conditions for the state vector as a special case, the formulation and the corresponding Riccati equation derived in Sec. 4.1 are different from those of the conventional linear regulator methodology. The Riccati equation for this special case is called the Riccati equation of the Lyapunov type [5]. Henceforth, for convenience we will call it simply as the Riccati matrix.

In the first part, the completely numerical solution to the optimal control problem, that is considered to be exact, is presented. In the first step, the Riccati equation which is a nonlinear first-order ordinary differential equation in matrix form with the boundary condition known at the final time is solved using backward numerical integration. The numerical solution gives the initial condition for the Riccati matrix as well as its variation history during the course of control action. In the second step, having the Riccati matrix in hand, the co-state differential equation which is a linear first-order differential equation in matrix form is solved by using forward numerical integration. Finally, using the Riccati matrix and the co-state vector time-histories, the optimal control law and the associated state vector history are readily obtained. The numerical solution is considered to be exact.

In the second part, a completely analytical, but approximate, solution to the optimal control problem is developed. In other words, the abovementioned backward and forward numerical integrations are eliminated from the optimal control solution. Approximate analytical solutions offer better physical and mathematical understanding of the problems compared to the numerical solutions, and they can also reduce the computation time. This is due to the fact that while numerical integration schemes require small stepsize to give acceptable results, the accuracy of analytical solutions is not affected by the evaluation stepsize. Of course, in the case of approximate analytical solutions, there must be a balance between the accuracy of the method and the computation time.

To develop an analytical solution, as suggested by Ramnath, the Riccati matrix equation is linearized by using a mathematical matrix transformation lemma, and subsequently, an asymptotic approximate solution describing the variations of the linearized Riccati matrix is derived by breaking down the matrix equation to the composing scalar differential equations. The asymptotic solution is developed by using the multiple time-scales technique. The analytical solutions to the components of the linearized Riccati matrix appear to be a combination of simple harmonic and hyperbolic functions. In the third step, the co-state first-order matrix differential equation is solved analytically, by using a novel mathematical transformation. Eventually, the optimal control law and the corresponding state-vector history are determined by using the solutions for the linearized Riccati matrix and the co-state vector.

The performance of the presented asymptotic method is evaluated by comparing the corresponding simulation results and computation time to those of the numerical exact solution. The developed asymptotic solution is shown to perform well for the lower portion of the trajectory.

4.1 LINEAR REGULATOR FORMULATION

The state space representation of the unified equation (1.38) is as the following

$$X'(\xi) = A(\xi)X(\xi) + Bu(\xi) \tag{4.1}$$

where the state vector is

$$X = \begin{bmatrix} \alpha \\ \alpha' \end{bmatrix} \tag{4.2}$$

and the coefficient matrices are

$$A(\xi) = \begin{bmatrix} 0 & 1 \\ -\omega_0(\xi) & -\omega_1(\xi) \end{bmatrix} \tag{4.3}$$

$$B = \begin{bmatrix} 0 \\ 1 \end{bmatrix} \tag{4.4}$$

The non-dimensional scalar control variable is the same as that in (3.3), i.e.

$$u(\xi) = f(\xi) - \mu(\xi)\delta_e(\xi) \tag{4.5}$$

The optimal control problem here is in fact a linear regulator problem with time-varying coefficients. The initial states, i.e. the initially-induced perturbation angle-of-attack, $\alpha(\xi_0)$, and its rate of change, $\alpha'(\xi_0)$ are known once the controller is triggered on. The final states must clearly be zero, because our goal is having the angle-of-attack and its rate-of-change back to their nominal value. Mathematically

$$X(\xi_f) = \begin{bmatrix} \alpha(\xi_f) \\ \alpha'(\xi_f) \end{bmatrix} = \begin{bmatrix} 0 \\ 0 \end{bmatrix} \tag{4.6}$$

The final position, i.e. the final non-dimensional distance, must also be specified. This is due to the fact that the space shuttle is longitudinally stable over the most part of the reentry trajectory, and hence the angle-of-attack oscillations are already asymptotically stable. As such, our goal here can be defined as canceling out the oscillations in the shortest period of time with the available elevator deflection.

Since the final states are zero, the quadratic final-state penalty term vanishes and the quadratic performance measure to be minimized is therefore

$$J = \frac{1}{2}\int_{\xi_0}^{\xi_f} [X^T Q X + R u^2] d\xi \tag{4.7}$$

where Q and R are the penalty gain factors for the state and control variables respectively. In general, Q is a real symmetric positive semi-definite time-varying matrix, and R is a real positive time-varying scalar. Mathematically

$$Q = \begin{bmatrix} q_{11}(\xi) & q_{12}(\xi) \\ q_{12}(\xi) & q_{22}(\xi) \end{bmatrix} \geq 0$$
$$R = R(\xi) > 0 \tag{4.8}$$

Once the control law is determined, the corresponding elevator control deflection can be readily obtained by using (4.5), as the following

$$\delta_e(\xi) = \frac{f(\xi) - u(\xi)}{\mu(\xi)} \tag{4.9}$$

The Hamiltonian is [6]

$$H = \frac{1}{2} X^T Q X + \frac{1}{2} R u^2 + P^T X' \tag{4.10}$$

where the co-state vector is

$$P = \begin{bmatrix} p_1(\xi) \\ p_2(\xi) \end{bmatrix} \tag{4.11}$$

Substituting (4.1) into (4.10) yields

$$H = \frac{1}{2} X^T Q X + \frac{1}{2} R u^2 + P^T A X + P^T B u \tag{4.12}$$

The necessary conditions for optimal control, assuming the admissible control is not bounded, are as the following

$$X'^* = \frac{\partial H}{\partial P}$$
$$P'^* = -\frac{\partial H}{\partial X} \tag{4.13a-c}$$
$$0 = \frac{\partial H}{\partial u}$$

Of course, the assumption of bounded control is not true in reality for the elevator deflection, however the maximum optimal deflection can be checked a posteriori and in the case of

violation, the penalty factors can be readjusted accordingly. The case with bounded control will be attempted in later work.
The optimality conditions of (4.13a-c), translate to

$$X'^{*} = AX^{*} + Bu^{*} \tag{4.14}$$

$$P'^{*} = -QX^{*} - A^{T}P^{*} \tag{4.15}$$

$$0 = Ru^{*} + B^{T}P^{*} \tag{4.16}$$

Eq. (4.16) can be solved for $u^{*}(\xi)$ to give

$$u^{*}(\xi) = -R(\xi)^{-1}B^{T}P^{*}(\xi) \tag{4.17}$$

The existence of R^{-1} is assured since R is a non-zero positive scalar. Substituting (4.17) into (4.1) yields

$$X'^{*}(\xi) = A(\xi)X^{*}(\xi) - BR(\xi)^{-1}B^{T}P^{*}(\xi) \tag{4.18}$$

Thus, we have the set of four linear homogeneous state and co-state differential equations as below

$$\begin{bmatrix} X'^{*}(\xi) \\ P'^{*}(\xi) \end{bmatrix} = \begin{bmatrix} A(\xi) & -BR^{-1}(\xi)B^{T} \\ -Q(\xi) & -A^{T}(\xi) \end{bmatrix} \begin{bmatrix} X^{*}(\xi) \\ P^{*}(\xi) \end{bmatrix} \tag{4.19}$$

It is noteworthy that the above set of four coupled first-order differential equations, constitute a boundary-value problem where the initial and final states are specified but the co-state boundary conditions are not known. The solution to these equations has the form

$$\begin{bmatrix} X^{*}(\xi_f) \\ P^{*}(\xi_f) \end{bmatrix} = \Phi(\xi_f, \xi) \begin{bmatrix} X^{*}(\xi) \\ P^{*}(\xi) \end{bmatrix} \tag{4.20}$$

where ξ_f denotes the final non-dimensional distance and Φ is the 4×4 transition matrix of the system. Partitioning the transition matrix in (4.20), we can write

$$\begin{bmatrix} X^{*}(\xi_f) \\ P^{*}(\xi_f) \end{bmatrix} = \begin{bmatrix} \varphi_{11}(\xi_f, \xi) & \varphi_{12}(\xi_f, \xi) \\ \varphi_{21}(\xi_f, \xi) & \varphi_{22}(\xi_f, \xi) \end{bmatrix} \begin{bmatrix} X^{*}(\xi) \\ P^{*}(\xi) \end{bmatrix} \tag{4.21}$$

where the components of Φ are themselves 2×2 matrices. Obviously at ξ_f, we have

$$\Phi(\xi_f, \xi_f) = \begin{bmatrix} I & 0 \\ 0 & I \end{bmatrix} \tag{4.22}$$

Due to the final condition for the state vector, from (4.21) we have

$$\begin{bmatrix} 0 \\ P^*(\xi_f) \end{bmatrix} = \begin{bmatrix} \varphi_{11}(\xi_f,\xi) & \varphi_{12}(\xi_f,\xi) \\ \varphi_{21}(\xi_f,\xi) & \varphi_{22}(\xi_f,\xi) \end{bmatrix} \begin{bmatrix} X^*(\xi) \\ P^*(\xi) \end{bmatrix} \tag{4.23}$$

Expanding the first row of the matrix equation (4.23), gives

$$\varphi_{11}(\xi_f,\xi)X^*(\xi) + \varphi_{12}(\xi_f,\xi)P^*(\xi) = 0 \tag{4.24}$$

Solving (4.24) for the state vector, yields

$$X^*(\xi) = -\varphi_{11}{}^{-1}(\xi_f,\xi)\varphi_{12}(\xi_f,\xi)P^*(\xi) \tag{4.25}$$

which means that the states and co-states of the system are linearly related as motion evolves. It is noticeable that writing the state vector in terms of the co-state vector is particular to the regulator problems with final states fixed at the origin. This lemma is applied because $\varphi_{11}{}^{-1}(\xi_f,\xi)$ at the final time exists and is equal to the identity matrix, whereas $\varphi_{12}(\xi_f,\xi)$ vanishes at ξ_f and is not invertible. The above equation can be written as

$$X^*(\xi) = K(\xi)P^*(\xi) \tag{4.26}$$

where it can be shown that $K(\xi)$ is a symmetric positive definite matrix and it satisfies the nonlinear first-order matrix differential equation below, called the Riccati equation of the Lyapunov type

$$K' = KQK + KA^T + AK - BR^{-1}B^T \tag{4.27}$$

with the boundary condition $K(\xi_f) = 0$. The Riccati equation (4.27) is derived by first differentiating (4.26) with respect to ξ following by the substitution of Eqs.(4.14) and (4.15) into the resulting equation, then using (4.26) to write the entire equation only in terms of $P^*(\xi)$, and finally crossing out $P^*(\xi)$ from both sides of the equation. Henceforth, we will call K as "the Riccati matrix". The boundary condition can be justified by considering that from (4.26) at the final time we have

$$X^*(\xi_f) = 0 = K(\xi_f)P^*(\xi_f) \tag{4.28}$$

and since in general

$$P^*(\xi_f) \neq 0$$

it is deduced that

$$K(\xi_f) = 0 \tag{4.29}$$

In the numerical solution scheme, the Riccati matrix equation (4.27) is integrated numerically, starting at $\xi = \xi_f$ and proceeding backwards in ξ to eventually obtain the value of $K(\xi)$ at ξ_0. At the end of each integration step, the value of the matrix $K(\xi)$ is stored so that it can be used later in the forward integration procedure to evaluate the state vector, $X(\xi)$. In the asymptotic

approach, the Riccati equation (4.27) is first linearized by using a mathematical matrix transformation and then integrated analytically by the asymptotic method of multiple time-scales. Having the solution to the Riccati matrix over the course of control action, writing (4.26) at the initial position we get

$$X^*(\xi_0) = K(\xi_0)P^*(\xi_0) \tag{4.30}$$

that yields the initial condition for the co-states as follows

$$P^*(\xi_0) = K^{-1}(\xi_0)X^*(\xi_0) \tag{4.31}$$

Finally, substitution of (4.26) into the co-state differential equation (4.15), leads to

$$P'^* = -(QK + A^T)P^* \tag{4.32}$$

which is the differential equation for the evolution of the co-states with the initial conditions of (4.31). Solving (4.32) by forward integration, either numerically or analytically, the co-state vector history, $P^*(\xi)$, is obtained and accordingly applied to the equations (4.26) and (4.17) to get the optimal states, $X^*(\xi)$, and the optimal control law, $u^*(\xi)$, respectively. Having the optimal control law in hand, the time history of the optimal elevator deflection is computed by using (4.9).

4.2 NUMERICAL EXACT SOLUTION

The simulation results for the numerical exact solution by implementing backward numerical integration of the Riccati equation (4.27), and forward numerical integration of the co-state equation (4.32) for the same two altitudes of 400,000 ft and 150,000 ft as in Sec. 2.5.1, corresponding to the upper and lower portions of the reentry trajectory, are presented. The numerical integration scheme used is the Euler's method where the corresponding derivatives in (4.27) and (4.32) are considered constant within each integration step. Although the Euler's method is simple as compared to other techniques such as Runge-Kutta method, it proves to be efficient and robust for our application since we are only dealing with first order differential equations. The initial conditions for the perturbation angle-of-attack and its rate of change are also the same as those in Sec. 2.5.1, i.e. $\alpha(\xi_0) = 5°$ and $\alpha'(\xi_0) = 0$. The initial altitudes and initial perturbation angle-of-attack and its rate of change are kept the same for the purpose of comparison with the results of the simple disturbance control (or the transient response) in Sec. 2.6.1, as the reference output.

Figs. 4.1 and 4.2 show the output of practical interest such as the controlled variations angle-of-attack and its rate-of-change, about their nominal values as well as the corresponding required elevator control deflection and torque for 400,000-ft and 150,000-ft altitudes, respectively. Figures 4.3 and 4.4 show the variations of the elements of the Riccati matrix during the course of control action. The importance of checking the solution to the Riccati matrix can be justified by the following facts. Firstly, the solution to the optimal control problem builds up on the solution to the Riccati matrix equation, therefore the accuracy of the final results depends on how well

and accurate the Riccati equation is being solved. Secondly, the Riccati matrix must come out symmetric, therefore checking the symmetry is an appropriate accuracy test for the solution.

Note that in the simulation results of the subsequent section where the asymptotic analytical solution is developed, the exact numerical solution will serve as a reference solution. The following control and state penalty gains were used in the simulations where they proved to give the fastest response while keeping the required elevator deflection within the available range of $\pm 25^{\circ}$.

400,000-ft Initial Altitude: $R = 6.55\times10^{15}$, $Q = I$
150,000-ft Iinitial Altitude: $R = 6.55\times10^{6}$, $Q = I$

It should be remarked that in terms of the time required for the control task to be achieved, the maximum available deflection of the elevator is the major constraint on the performance of the optimal controller as well as the controllers discussed in the subsequent chapters.

Comparing the results in Figs. 4.1 and 4.2, we can see that the elevator control torque for the case of 150,000 ft initial altitude is higher than that of the 400,000 ft by more than 3 orders of magnitude. Referring to the expression (1.59) for the elevator control torque and the variation history of the atmospheric density in Fig. (2.3), it becomes clear that the atmospheric density has the dominant effect on the required control effort.

As can be seen, the time needed for the oscillations to die out has been reduced considerably for both altitudes compared to that of the disturbance control (or the transient response) which employs the inherent damping and stiffness characteristics of the space shuttle aerodynamic design. The die-out time reduction is about 3 times for 400,000 ft initial altitude and 6 times for 150,000 ft initial altitude.

However, it should be reminded that the optimal controller needs the variation history of the system parameters as online input data. For this application, the parameters include the trajectory variables and the aerodynamic characteristics of the shuttle orbiter.

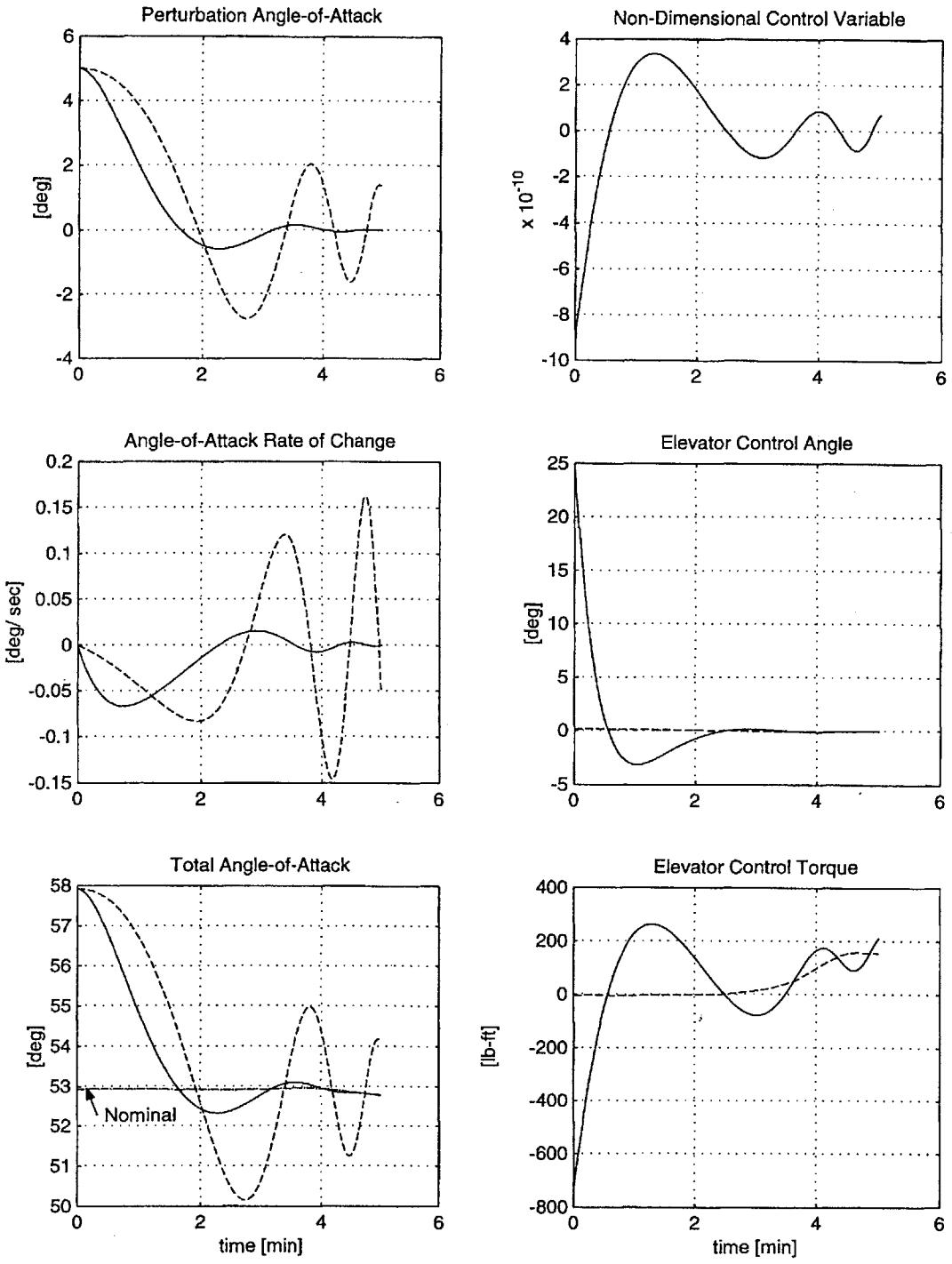

Fig. 4.1 Optimal control results for 400,000 ft initial altitude using numerical solution

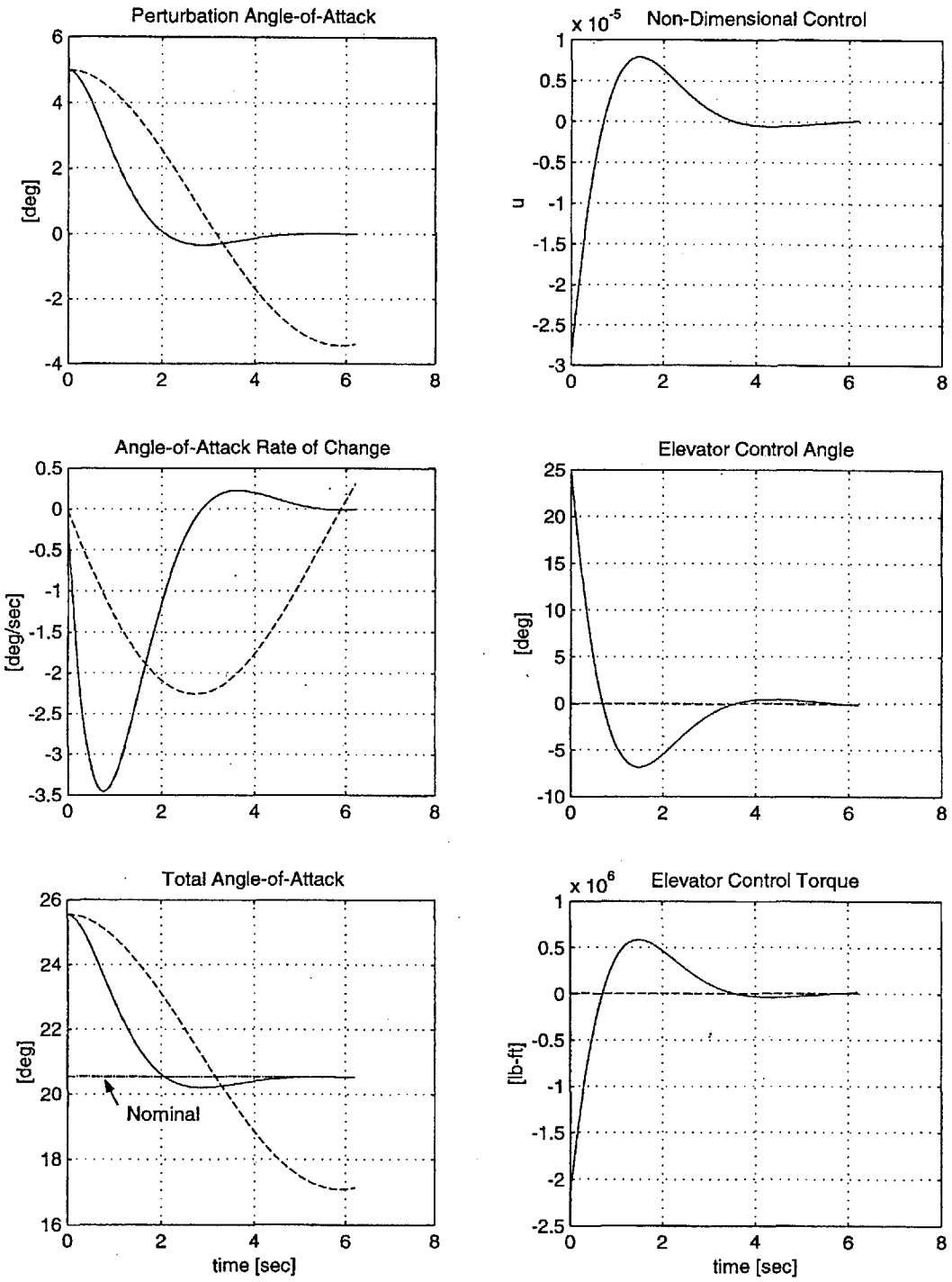

Fig. 4.2 Optimal control results for 150,000 ft initial altitude using numerical solution

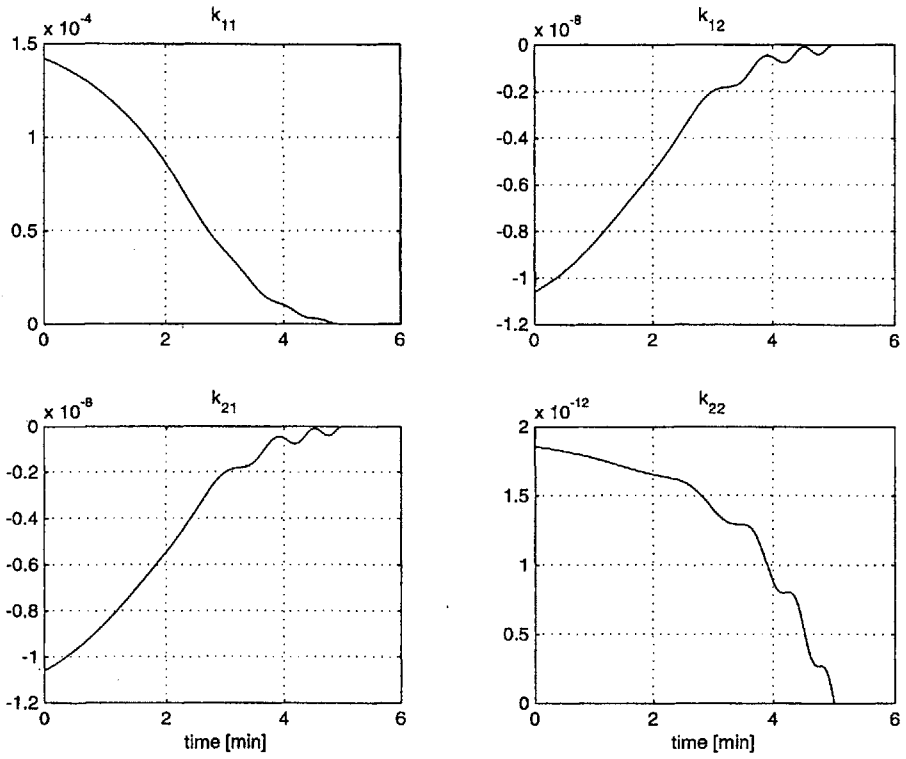

Fig. 4.3 Variations of the Riccati matrix components for 400,000 ft initial altitude

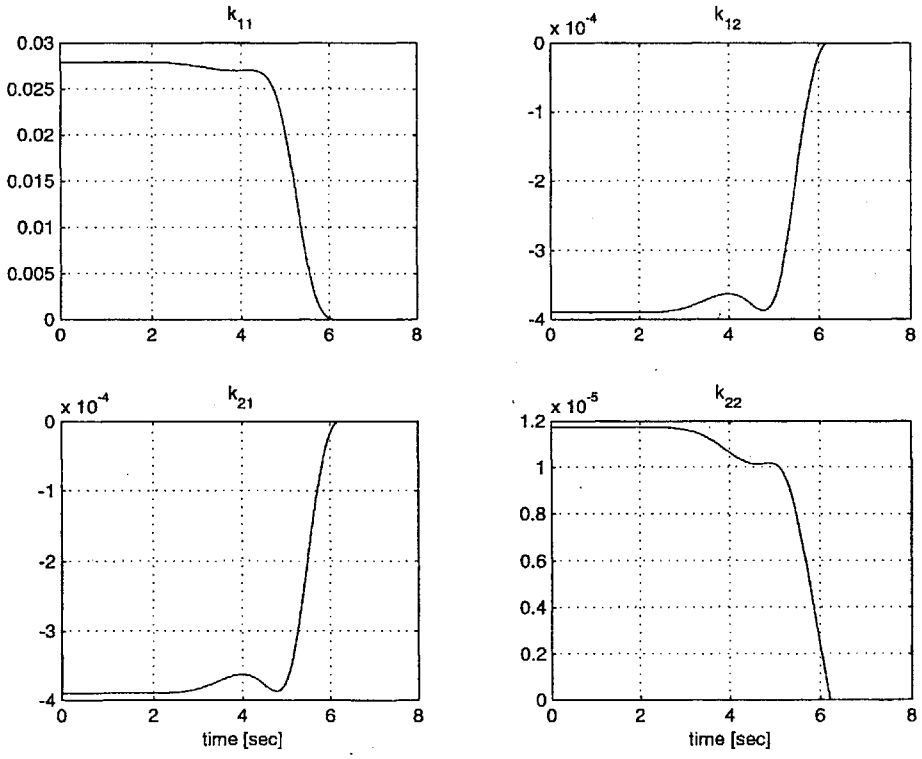

Fig. 4.4 Variations of the Riccati matrix components for 150,000 ft initial altitude

4.3 ASYMPTOTIC APPROXIMATE SOLUTION

4.3.1 LINEARIZATION OF THE RICCATI EQUATION

We have the Lyapunov-type Riccati equation (4.27) as

$$K' = KQK + KA^T + AK - BR^{-1}B^T$$

where K is a symmetric positive definite matrix with the boundary condition of (4.29) as

$$K(\xi_f) = 0$$

The Riccati matrix equation above can be linearized through the following variable transformations.

Step 1

Let

$$QK = M \tag{4.33}$$

Hence

$$K = Q^{-1}M \tag{4.34}$$

where Q must be chosen to be invertible, i.e. $|Q| \neq 0$. Differentiating (4.33) with respect to ξ gives

$$Q'K + QK' = M'$$

Multiply by Q^{-1} from left to get

$$Q^{-1}Q'K + K' = Q^{-1}M'$$

where rearranging gives

$$K' = Q^{-1}M' - Q^{-1}Q'K$$

Substituting for K on the right-hand side yields

$$K' = Q^{-1}M' - Q^{-1}Q'Q^{-1}M \tag{4.35}$$

and substitution of K' from (4.35) and K (4.34) into the Riccati equation (4.27) results in

$$Q^{-1}M' - Q^{-1}Q'Q^{-1}M = (Q^{-1}M)Q(Q^{-1}M) + (Q^{-1}M)A^T + A(Q^{-1}M) - BR^{-1}B^T$$

which leads to

$$Q^{-1}M' - Q^{-1}Q'Q^{-1}M = Q^{-1}M^2 + Q^{-1}MA^T + AQ^{-1}M - BR^{-1}B^T$$

Multiply by Q from left to get

$$M' - Q'Q^{-1}M = M^2 + MA^T + QAQ^{-1}M - QBR^{-1}B^T$$

and rearrange to obtain

$$M' - M^2 - MA^T - (Q'Q^{-1} + QAQ^{-1})M + QBR^{-1}B^T = 0$$

or

$$M' - (M^2 + MA^T) - (Q'Q^{-1} + QAQ^{-1})M + QBR^{-1}B^T = 0 \tag{4.36}$$

However, we can write

$$M^2 + MA^T = (M + A^T)^2 - A^T M - (A^T)^2 \tag{4.37}$$

Substituting into the above equation to get

$$M' - (M + A^T)^2 + A^T M + (A^T)^2 - (Q'Q^{-1} + QAQ^{-1})M + QBR^{-1}B^T = 0 \tag{4.38}$$

Step 2

Now let

$$M + A^T = N \tag{4.39}$$

Therefore

$$M = N - A^T \tag{3.40}$$

Differentiate (3.40) to get

$$M' = N' - (A^T)'$$

and substitute for M' and M in (4.38) to obtain

$$[N' - (A^T)'] - N^2 + A^T(N - A^T) + (A^T)^2 - (Q'Q^{-1} + QAQ^{-1})(N - A^T) + QBR^{-1}B^T = 0$$

where rearranging and collecting terms yield

$$N' - N^2 + (A^T - Q'Q^{-1} - QAQ^{-1})N + (Q'Q^{-1} + QAQ^{-1})A^T - (A^T)' + QBR^{-1}B^T = 0 \tag{4.41}$$

Step 3

Eventually let

$$N = -\Lambda'\Lambda^{-1} \tag{4.42}$$

that gives

$$N\Lambda = -\Lambda'$$

Differentiate

$$N'\Lambda + N\Lambda' = -\Lambda''$$

and multiply by Λ^{-1} from the right to get

$$N' + N\Lambda'\Lambda^{-1} = -\Lambda''\Lambda^{-1}$$

or

$$N' - N(-\Lambda'\Lambda^{-1}) = -\Lambda''\Lambda^{-1} \tag{4.43}$$

Substituting from the transformation relation (4.42) into (4.43) yields

$$N' - N^2 = -\Lambda''\Lambda^{-1} \tag{4.44}$$

Using (4.44) and substituting for N from (4.42) into (4.41) , results in

$$-\Lambda''\Lambda^{-1} - (A^T - Q'Q^{-1} - QAQ^{-1})\Lambda'\Lambda^{-1} + [(Q'Q^{-1} + QAQ^{-1})A^T - (A^T)' + QBR^{-1}B^T] = 0$$

Multiplying by $-\Lambda$ from the right, finally leads to the following 2^{nd}-order linear differential equation with time-varying coefficients, which we will call it the linearized Riccati equation.

$$\Lambda'' + (A^T - Q'Q^{-1} - QAQ^{-1})\Lambda' + [(A^T)' - (Q'Q^{-1} + QAQ^{-1})A^T - QBR^{-1}B^T]\Lambda = 0 \tag{4.45}$$

Eq. (4.45) can also be written as

$$\Lambda'' + \Omega_1(\xi)\Lambda' + \Omega_0(\xi)\Lambda = 0 \tag{4.46}$$

where the 2×2 coefficient matrices are

$$\Omega_1 = A^T - Q'Q^{-1} - QAQ^{-1} \tag{4.47}$$

and

$$\Omega_0 = (A^T)' - (Q'Q^{-1} + QAQ^{-1})A^T - QBR^{-1}B^T \tag{4.48}$$

Writing Eq. (4.33) at the final position, we get

$$M(\xi_f) = Q(\xi_f)K(\xi_f) \tag{4.49}$$

However, since $K(\xi_f) = 0$, we get

$$M(\xi_f) = 0 \tag{4.50}$$

Now, from (4.39) at the final position, we have

$$N(\xi_f) = M(\xi_f) + A^T(\xi_f) \tag{4.51}$$

that according to (4.50), leads to

$$N(\xi_f) = A^T(\xi_f) \tag{4.52}$$

And finally, substitution of (4.42) into (4.52) yields

$$\Lambda'(\xi_f)\Lambda^{-1}(\xi_f) = -A^T(\xi_f) \tag{4.53}$$

Note that since we have added one order to the original Riccati equation, which is a 1st-order differential equation, by the variable transformation (4.42), in fact we have the freedom to apply an arbitrary and convenient boundary condition such as

$$\Lambda(\xi_f) = I \tag{4.54}$$

where I is the 2×2 identity matrix, and accordingly we get

$$\Lambda'(\xi_f) = -A^T(\xi_f) \tag{4.55}$$

The obtained 2nd-order linearized Riccati equation must be integrated backwards with the boundary conditions at the final position, or its equivalent non-dimensional distance ξ_f, that is a specified parameter. The combined transformation relation is

$$K = -Q^{-1}[A^T + \Lambda'\Lambda^{-1}] \tag{4.56}$$

4.3.2 Approximate Analytical Solution of the Linearized Riccati Equation using the Asymptotic Multiple Time-Scales Method

Experience with the entry trajectory of the space shuttle suggests that the coefficients of the unified angle-of-attack equation (1.38) can be realistically considered to be slowly varying compared to the uncontrolled dynamic response of the space shuttle to the angle-of-attack perturbations, as discussed by Ramnath and Sinha in [9]. In traversing the earth's atmosphere during reentry, variations in the coefficients of the unified equation are due to changes in air density, velocity of the vehicle, flight path angle, nominal angle-of-attack, and the aerodynamic force and moment parameters along the trajectory. The dominant effect however, is due to the atmospheric density variation, which can be easily verified by inspecting the Figs. 2.3 and 2.6.

For the case of controlled response however, the assumption of slow variation is valid as long as the duration of the control action is small compared to the total reentry time. This is due to the fact that the controlled response is an over-damped non-oscillatory response. As will be seen in the simulation results in Sec. 4.3.4, only for the low-altitude portion of the reentry trajectory, the assumption of slow variations of trajectory parameters and the space shuttle aerodynamic characteristics is valid since the control period is adequately short.

Nevertheless, throughout this section, we proceed with the assumption of slow variations of parameters and at the end we will verify the assumption by inspecting the results. The linearized Riccati equation (4.46) can be rewritten as

$$\frac{d^2}{d\xi^2}\Lambda + \Omega_1(\xi)\frac{d}{d\xi}\Lambda + \Omega_0(\xi)\Lambda = 0 \tag{4.57}$$

where the primary boundary condition was chosen arbitrarily to be

$$\Lambda(\xi_f) = I \tag{4.58}$$

and accordingly, the secondary boundary condition became

$$\frac{d\Lambda}{d\xi}(\xi_f) = -A^T(\xi_f) \tag{4.59}$$

For the case of constant R, and a constant matrix Q with zero off-diagonal weight factors as

$$Q = \begin{bmatrix} q_{11} & 0 \\ 0 & q_{22} \end{bmatrix} \tag{4.60}$$

the coefficient matrices in (4.46) or (4.57) using (4.47) and (4.48), turn out to be

$$\Omega_1(\xi) = \begin{bmatrix} 0 & -\frac{q_{11}}{q_{22}} - \omega_0(\xi) \\ 1 + \frac{q_{22}}{q_{11}}\omega_0(\xi) & 0 \end{bmatrix} \tag{4.61}$$

and

$$\Omega_0(\xi) = \begin{bmatrix} -\frac{q_{11}}{q_{22}} & \frac{q_{11}}{q_{22}}\omega_1 - \omega_0' \\ \omega_1 & -(\omega_1' + \frac{q_{22}}{q_{11}}\omega_1^{\,2} + \omega_0^{\,2} + \frac{q_{22}}{R}) \end{bmatrix} \tag{4.62}$$

where the expressions for ω_1 and ω_0 can be determined from (1.39) and (1.40) respectively. Notice that since we have chosen the control penalty gain R and the states penalty matrix Q to be constant which is convenient and practical, the coefficient matrices Ω_1 and Ω_0 are also slowly-varying as they are functions of ω_1, ω_0, and their derivatives only.

It should be reminded that, as opposed to the coefficients, the components of $\Lambda(\xi)$ are fast-varying. This is due to the fact that they determine the variation history of the control variable and the associated controlled response within the specified time frame corresponding to $\xi_f - \xi_0$.

Mathematically, it is equivalent to saying that ω_1 and ω_0 vary on a new slow variable $\eta = \varepsilon\xi$, as first introduced by Ramnath [8,9], where ε is a small positive parameter being a measure of the ratio of the time constants of the oscillatory transient response of the space shuttle and the coefficient variations. Therefore, we can write

$$\frac{d}{d\xi}[] = \frac{d}{d\eta}[]\frac{d\eta}{d\xi} = \varepsilon\frac{d}{d\eta}[] \tag{4.63}$$

and similarly

$$\frac{d^2}{d\xi^2}[] = \varepsilon^2\frac{d^2}{d\eta^2}[] \tag{4.64}$$

Substituting into the linearized Riccati equation (4.46) gives

$$\varepsilon^2 \frac{d^2}{d\eta^2}\Lambda + \varepsilon\Omega_1(\eta)\frac{d}{d\eta}\Lambda + \Omega_0(\eta)\Lambda = 0 \tag{4.65}$$

In order to develop an asymptotic solution to the equation (4.65), we will invoke the concept of multiple time scales as developed by Ramnath [8]. To do so, first we "extend" the independent variable η as $\eta \rightarrow \{\tau_0, \tau_1\}$

$$\tau_0 = \eta = \varepsilon\xi \tag{4.66a}$$

$$\tau_1 = \frac{\eta}{\varepsilon} = \xi \tag{4.66b}$$

where τ_0 and τ_1 are the slow and fast time scales, respectively. Referring to [8], it should be reminded that Eqs. (4.66) represent an "extension" from one-dimensional space to the two-dimensional space which is essentially a mapping operation and not a variable transformation. In other words, the variations of the dependent variable Λ are measured by two different clocks, namely a fast-scale and a slow-scale clock. In accordance with (4.66), we can write

$$\frac{d}{d\eta}[] = \frac{\partial}{\partial\tau_0}[]\frac{d\tau_0}{d\eta} + \frac{\partial}{\partial\tau_1}[]\frac{d\tau_1}{d\eta}$$

and hence

$$\frac{d}{d\eta}[] = \frac{\partial}{\partial\tau_0}[] + \frac{1}{\varepsilon}\frac{\partial}{\partial\tau_1}[] \tag{4.67}$$

Similarly

$$\frac{d^2}{d\eta^2}[] = \frac{\partial^2}{\partial\tau_0^{\,2}}[] + (\frac{2}{\varepsilon})\frac{\partial^2}{\partial\tau_0\partial\tau_1}[] + (\frac{1}{\varepsilon^2})\frac{\partial^2}{\partial\tau_1^{\,2}}[] \tag{4.68}$$

Applying (4.67) and (4.68) to Eq. (4.65), and rearranging in terms of powers of ε, yield

$$[\frac{\partial^2}{\partial\tau_1^{\,2}}\Lambda + \Omega_1(\tau_0)\frac{\partial}{\partial\tau_1}\Lambda + \Omega_0(\tau_0)\Lambda] + \varepsilon[2\frac{\partial^2}{\partial\tau_0\partial\tau_1}\Lambda + \Omega_1(\tau_0)\frac{\partial}{\partial\tau_0}\Lambda] + \varepsilon^2[\frac{\partial^2}{\partial\tau_0^{\,2}}\Lambda] = 0$$

Using the multiple scales theory, the zeroth-, first-, and second-order extended perturbation equations are the following, respectively

$$\frac{\partial^2}{\partial\tau_1^{\,2}}\Lambda + \Omega_1(\tau_0)\frac{\partial}{\partial\tau_1}\Lambda + \Omega_0(\tau_0)\Lambda = 0 \tag{4.69}$$

$$2\frac{\partial^2}{\partial\tau_0\partial\tau_1}\Lambda + \Omega_1(\tau_0)\frac{\partial}{\partial\tau_0}\Lambda = 0 \tag{4.70}$$

$$\frac{\partial^2}{\partial\tau_0^{\,2}}\Lambda = 0 \tag{4.71}$$

where $\Lambda = \Lambda(\tau_0, \tau_1)$. It should be mentioned that Eqs. (4.69-71) are valid in the general case of the scalar differential equations with slowly-varying coefficients as developed by Ramnath and Sinha in [9]. For our problem however, due to the matrix form of (4.65) as a special case, the first- and second-order perturbation equations in (4.70) and (4.71) can not be used to obtain better approximations. Nevertheless, the asymptotic approximation to the dominant order, i.e. the zeroth order, using (4.69) works well for our application as will be seen in the results in Sec. 4.3.4. In the following steps, the solution to the dominant-order perturbation Eq. (4.69) will be developed. Since the second boundary condition of the linearized Riccati equation is for the derivative of Λ with respect to ξ, using the extension relations we can write

$$\frac{d\Lambda}{d\xi} = \varepsilon \frac{d\Lambda}{d\eta} \rightarrow \varepsilon \frac{\partial \Lambda}{\partial \tau_0} + \frac{\partial \Lambda}{\partial \tau_1}$$

For the dominant-order solution, we can consider

$$\frac{d\Lambda}{d\xi}(\xi_f) \approx \frac{\partial \Lambda}{\partial \tau_1}(\xi_f) = -A^T(\xi_f)$$

Now let assume

$$\Lambda(\tau_0, \tau_1) = \begin{bmatrix} \lambda_{11}(\tau_0, \tau_1) & \lambda_{12}(\tau_0, \tau_1) \\ \lambda_{21}(\tau_0, \tau_1) & \lambda_{22}(\tau_0, \tau_1) \end{bmatrix} \tag{4.72}$$

where the components, λ_{ij}, will be called the characteristic functions. Also let

$$\Omega_1(\tau_0) = \begin{bmatrix} a_{11}(\tau_0) & a_{12}(\tau_0) \\ a_{21}(\tau_0) & a_{22}(\tau_0) \end{bmatrix} \tag{4.73}$$

and

$$\Omega_0(\tau_0) = \begin{bmatrix} b_{11}(\tau_0) & b_{12}(\tau_0) \\ b_{21}(\tau_0) & b_{22}(\tau_0) \end{bmatrix} \tag{4.74}$$

Upon substitution of (4.72) through (4.74) into (4.69), we get

$$\frac{\partial^2}{\partial \tau_1^2}\begin{bmatrix} \lambda_{11} & \lambda_{12} \\ \lambda_{21} & \lambda_{22} \end{bmatrix} + \begin{bmatrix} a_{11}(\tau_0) & a_{12}(\tau_0) \\ a_{21}(\tau_0) & a_{22}(\tau_0) \end{bmatrix} \frac{\partial}{\partial \tau_1}\begin{bmatrix} \lambda_{11} & \lambda_{12} \\ \lambda_{21} & \lambda_{22} \end{bmatrix} + \begin{bmatrix} b_{11}(\tau_0) & b_{12}(\tau_0) \\ b_{21}(\tau_0) & b_{22}(\tau_0) \end{bmatrix}\begin{bmatrix} \lambda_{11} & \lambda_{12} \\ \lambda_{21} & \lambda_{22} \end{bmatrix} = \begin{bmatrix} 0 & 0 \\ 0 & 0 \end{bmatrix}$$

For simplicity, let

$$\frac{\partial}{\partial \tau_1}[\,] = [\,]'$$

and

$$\frac{\partial^2}{\partial \tau_1^2}[\,] = [\,]''$$

Rewriting, we have

$$\begin{bmatrix} \lambda''_{11} & \lambda''_{12} \\ \lambda''_{21} & \lambda''_{22} \end{bmatrix} + \begin{bmatrix} a_{11}(\tau_0) & a_{12}(\tau_0) \\ a_{21}(\tau_0) & a_{22}(\tau_0) \end{bmatrix} \begin{bmatrix} \lambda'_{11} & \lambda'_{12} \\ \lambda'_{21} & \lambda'_{22} \end{bmatrix} + \begin{bmatrix} b_{11}(\tau_0) & b_{12}(\tau_0) \\ b_{21}(\tau_0) & b_{22}(\tau_0) \end{bmatrix} \begin{bmatrix} \lambda_{11} & \lambda_{12} \\ \lambda_{21} & \lambda_{22} \end{bmatrix} = \begin{bmatrix} 0 & 0 \\ 0 & 0 \end{bmatrix} \tag{4.75}$$

with the boundary conditions of

$$\begin{bmatrix} \lambda_{11}(\xi_f) & \lambda_{12}(\xi_f) \\ \lambda_{21}(\xi_f) & \lambda_{22}(\xi_f) \end{bmatrix} = I = \begin{bmatrix} 1 & 0 \\ 0 & 1 \end{bmatrix} \tag{4.76}$$

and

$$\begin{bmatrix} \lambda'_{11}(\xi_f) & \lambda'_{12}(\xi_f) \\ \lambda'_{21}(\xi_f) & \lambda'_{22}(\xi_f) \end{bmatrix} = -A^T(\xi_f) = \begin{bmatrix} 0 & \omega_0(\xi_f) \\ -1 & \omega_1(\xi_f) \end{bmatrix} \tag{4.77}$$

Upon expanding (4.75), we obtain the following four 2nd-order homogeneous differential equations

$$\begin{aligned}
&[\lambda''_{11} + a_{11}(\tau_0)\lambda'_{11} + b_{11}(\tau_0)\lambda_{11}] + [a_{12}(\tau_0)\lambda'_{21} + b_{12}(\tau_0)\lambda_{21}] = 0 \\
&[\lambda''_{21} + a_{22}(\tau_0)\lambda'_{21} + b_{22}(\tau_0)\lambda_{21}] + [a_{21}(\tau_0)\lambda'_{11} + b_{21}(\tau_0)\lambda_{11}] = 0 \\
&[\lambda''_{12} + a_{11}(\tau_0)\lambda'_{12} + b_{11}(\tau_0)\lambda_{12}] + [a_{12}(\tau_0)\lambda'_{22} + b_{12}(\tau_0)\lambda_{22}] = 0 \\
&[\lambda''_{22} + a_{22}(\tau_0)\lambda'_{22} + b_{22}(\tau_0)\lambda_{22}] + [a_{21}(\tau_0)\lambda'_{12} + b_{21}(\tau_0)\lambda_{12}] = 0
\end{aligned} \tag{4.78a-d}$$

where the first two (4.78a-b) are coupled and so are the second two (4.78c-d). Note that the coefficients are functions of τ_0 whereas the differentiations are with respect to τ_1. This means that for integration purposes, we can regard the coefficients as constants, that is an advantage of the multiple scales method. The general case of the linear systems with slowly-varying coefficients has been solved by Ramnath [8] and as a special case of this general approach which is somewhat easier to implement, for the first and the second pair of equations in (4.78) respectively, we seek the solutions in the form

$$\lambda_{ij}(\tau_0, \tau_1) = C_{ij}(\tau_0) e^{s(\tau_0)\tau_1} \tag{4.79a-b}$$

$$\lambda_{ij}(\tau_0, \tau_1) = C_{ij}(\tau_0) e^{z(\tau_0)\tau_1} \tag{4.79c-d}$$

where $s(\tau_0)$ and $z(\tau_0)$ are the corresponding slowly-varying characteristic roots and $i, j = 1,2$ accordingly. Henceforth, the C_{ij} will be called the characteristic coefficients. Substituting Eqs.

(4.79) into Eqs. (4.78) accordingly, results in the following set of 2nd-order homogeneous algebraic equations

$$[s^2 + a_{11}(\tau_0)s + b_{11}(\tau_0)]C_{11} + [a_{12}(\tau_0)s + b_{12}(\tau_0)]C_{21} = 0$$
$$[a_{21}(\tau_0)s + b_{21}(\tau_0)]C_{11} + [s^2 + a_{22}(\tau_0)s + b_{22}(\tau_0)]C_{21} = 0 \quad \text{(4.80a-b)}$$

$$[z^2 + a_{11}(\tau_0)z + b_{11}(\tau_0)]C_{12} + [a_{12}(\tau_0)z + b_{12}(\tau_0)]C_{22} = 0$$
$$[a_{21}(\tau_0)z + b_{21}(\tau_0)]C_{12} + [z^2 + a_{22}(\tau_0)z + b_{22}(\tau_0)]C_{22} = 0 \quad \text{(4.80c-d)}$$

As expected, Eqs. (4.80a-b) share C_{11} and C_{21} as their unknowns whereas Eqs. (4.80c-d) share C_{12} and C_{22}. In order for the above algebraic equations to have nontrivial solutions, the following 4th-order determinant expansion equations must hold

$$[s^2 + a_{11}(\tau_0)s + b_{11}(\tau_0)][s^2 + a_{22}(\tau_0)s + b_{22}(\tau_0)] - [a_{12}(\tau_0)s + b_{12}(\tau_0)][a_{21}(\tau_0)s + b_{21}(\tau_0)] = 0 \quad \text{(4.81a-b)}$$

$$[z^2 + a_{11}(\tau_0)z + b_{11}(\tau_0)][z^2 + a_{22}(\tau_0)z + b_{22}(\tau_0)] - [a_{12}(\tau_0)z + b_{12}(\tau_0)][a_{21}(\tau_0)z + b_{21}(\tau_0)] = 0$$

We can see that both equations have identical coefficients, which means they have the same set of roots. Therefore, we will treat them as a single characteristic equation in terms of the parameter s. Upon expanding and factoring the first equation, we arrive at the following full-order quartic characteristic equation

$$s^4 + P_3 s^3 + P_2 s^2 + P_1 s + P_0 = 0 \quad \text{(4.82)}$$

where

$$P_3 = a_{11} + a_{22}$$
$$P_2 = a_{11}a_{22} - a_{12}a_{21} + b_{11} + b_{22}$$
$$P_1 = a_{11}b_{22} + a_{22}b_{11} - a_{12}b_{21} - a_{21}b_{12} \quad \text{(4.83a-d)}$$
$$P_0 = b_{11}b_{22} - b_{12}b_{21}$$

For the case of constant R and constant matrix Q with zero off-diagonal weight factors, the quartic equation of (4.82) turns into

$$s^4 + (2\omega_0 - \omega_1^2 - \frac{q_{22}}{R} - \omega'_1)s^2 + \omega'_0(1 + \frac{q_{22}}{q_{11}}\omega_0)s + (\omega_0^2 + \frac{q_{11}}{R} + \omega_1\omega'_0 + \frac{q_{11}}{q_{22}}\omega'_1) = 0 \quad \text{(4.84)}$$

that contains no cubic term. In fact, the linear term is also negligible. This is due to the fact that for short control periods, ω_0 and ω_1 vary slowly so that their derivatives are rather small as well and can be neglected. Elimination of the derivative terms from the coefficient expressions results in the following biquadratic equation the roots of which can be readily found.

$$s^4 + (2\omega_0 - \omega_1{}^2 - \frac{q_{22}}{R})s^2 + (\omega_0{}^2 + \frac{q_{11}}{R}) = 0 \tag{4.85}$$

It should be mentioned that although in the simulations, for the sake of accuracy, the characteristic roots are found using (4.82), the roots appear to be two pairs of complex conjugates which are negative of each other. This is clearly the peculiarity of the roots of biquadratic equations such as (4.85).

After finding the slowly-varying roots as functions of ξ, we only need to evaluate them at the particular points of interest. For instance, in order to find the unknown coefficients of λ_{ij}, the final position, ξ_f, is the point under consideration that will be discussed subsequently. The other point of interest is ξ_0 or the initial position which is of particular importance in that it determines the initial condition for the co-state vector, i.e. $P^*(\xi_0)$. Since there are four roots, we can consider the complete solution for the components of the matrix Λ as the following

$$\lambda_{ij}(\tau_0,\tau_1) = C_{ij1}(\tau_0)e^{s_1(\tau_0)\tau_1} + C_{ij2}(\tau_0)e^{s_2(\tau_0)\tau_1} + C_{ij3}(\tau_0)e^{s_3(\tau_0)\tau_1} + C_{ij4}(\tau_0)e^{s_4(\tau_0)\tau_1}$$

Or in the short form

$$\lambda_{ij}(\tau_0,\tau_1) = \sum_{k=1}^{4} C_{ijk}(\tau_0)e^{s_k(\tau_0)\tau_1} \tag{4.86}$$

where $i, j = 1,2$. Having found the four characteristic roots of (4.82), from (4.80a) and (4.80c) we obtain the following linear-dependence relations for the characteristic coefficients

$$C_{21k} = F(s_k)C_{11k} \tag{4.87a}$$

$$C_{22k} = F(s_k)C_{12k} \tag{4.87b}$$

where the dependence factor is

$$F(s_k) = -\frac{s_k{}^2 + a_{11}s_k + b_{11}}{a_{12}s_k + b_{12}} \tag{4.88}$$

Having the root functions known, we can determine the characteristic coefficients at the final position by applying the available boundary conditions. At the final position, we can write

$$\lambda_{ij}(\xi_f) = \sum_{k=1}^{4} C_{ijk}(\xi_f)e^{s_k(\xi_f)\xi_f} \tag{4.89}$$

where the left-hand side is known and the four coefficients are the only unknowns on the right-hand side. Differentiating the solution expressions for $\lambda_{ij}(\tau_0,\tau_1)$ in (4.79a-b) with respect to τ_1, and evaluating them at the final position, lead to the following relations, respectively

$$\lambda'_{ij}(\xi_f)=\sum_{k=1}^{4} s_k(\xi_f)C_{ijk}(\xi_f)e^{s_k(\xi_f)\xi_f} \tag{4.90}$$

To simplify the algebra, let us use the following substitutions

$$D_{11k}=C_{11k}(\xi_f)e^{s_k(\xi_f)\xi_f} \tag{4.91a}$$

$$D_{12k}=C_{12k}(\xi_f)e^{s_k(\xi_f)\xi_f} \tag{4.91b}$$

Therefore, using Eqs. (4.91) we can expand (4.89) as the following

$$\begin{aligned} \lambda_{11}(\xi_f)&=\sum_{k=1}^{4} D_{11k} & \lambda_{12}(\xi_f)&=\sum_{k=1}^{4} D_{12k} \\ \lambda_{21}(\xi_f)&=\sum_{k=1}^{4} F(s_k(\xi_f))D_{11k} & \lambda_{22}(\xi_f)&=\sum_{k=1}^{4} F(s_k(\xi_f))D_{12k} \end{aligned} \tag{4.92}$$

Accordingly, Eq. (4.90) can be expanded as follows

$$\begin{aligned} \lambda'_{11}(\xi_f)&=\sum_{k=1}^{4} s_k(\xi_f)D_{11k} & \lambda'_{12}(\xi_f)&=\sum_{k=1}^{4} s_k(\xi_f)D_{12k} \\ \lambda'_{21}(\xi_f)&=\sum_{k=1}^{4} s_k(\xi_f)F(s_k(\xi_f))D_{11k} & \lambda'_{22}(\xi_f)&=\sum_{k=1}^{4} s_k(\xi_f)F(s_k(\xi_f))D_{12k} \end{aligned} \tag{4.93}$$

Applying the final-position boundary conditions of (4.76) and (4.77) to (4.92) and (4.93), we get the following two sets of four linear algebraic equations

$$\begin{bmatrix} 1 & 1 & 1 & 1 \\ F(s_1) & F(s_2) & F(s_3) & F(s_4) \\ s_1 & s_2 & s_3 & s_4 \\ s_1F(s_1) & s_2F(s_2) & s_3F(s_3) & s_4F(s_4) \end{bmatrix}\begin{Bmatrix} D_{111} \\ D_{112} \\ D_{113} \\ D_{114} \end{Bmatrix}=\begin{Bmatrix} \lambda_{11} \\ \lambda_{21} \\ \lambda'_{11} \\ \lambda'_{21} \end{Bmatrix}=\begin{Bmatrix} 1 \\ 0 \\ 0 \\ -1 \end{Bmatrix} \tag{4.94}$$

$$\begin{bmatrix} 1 & 1 & 1 & 1 \\ F(s_1) & F(s_2) & F(s_3) & F(s_4) \\ s_1 & s_2 & s_3 & s_4 \\ s_1F(s_1) & s_2F(s_2) & s_3F(s_3) & s_4F(s_4) \end{bmatrix}\begin{Bmatrix} D_{121} \\ D_{122} \\ D_{123} \\ D_{124} \end{Bmatrix}=\begin{Bmatrix} \lambda_{12} \\ \lambda_{22} \\ \lambda'_{12} \\ \lambda'_{22} \end{Bmatrix}=\begin{Bmatrix} 0 \\ 1 \\ \omega_0 \\ \omega_1 \end{Bmatrix} \tag{4.95}$$

Upon solving the matrix-form sets of algebraic equations, i.e. (4.94) and (4.95), for D_{ij}'s by using the Cramer's rule, Eqs. (4.91) give the characteristic coefficients, $C_{ij}(\xi_f)$, as

$$C_{11k}(\xi_f) = D_{11k} e^{-s_k(\xi_f)\xi_f} \tag{4.96a}$$

$$C_{12k}(\xi_f) = D_{12k} e^{-s_k(\xi_f)\xi_f} \tag{4.96b}$$

Note that the obtained values for the characteristic coefficients at the final position, will be used to evaluate the corresponding characteristic functions in (4.86) during the course of control action. This means that the slow variations of the characteristic coefficients will be ignored as opposed to the variations of the characteristic roots that are kept in effect. Of course this introduces some error to the solution, however this is a trade off for keeping the computation time short. As can be seen, the algebra needed for finding the characteristic coefficients is quite involved and time-consuming for the computation purposes.

Upon finding the characteristic roots and the corresponding characteristic coefficients, the resulting analytical solution for the characteristic functions turn out to be a combination of harmonic and hyperbolic functions as the following

$$\begin{aligned}\lambda_{ij}(\xi) = {} & 2\cos(s_{1_{\text{Im}}}\xi)\{[C_{ij1_{\text{Re}}} + C_{ij3_{\text{Re}}}]\cosh(s_{1_{\text{Re}}}\xi) + [C_{ij1_{\text{Re}}} - C_{ij3_{\text{Re}}}]\sinh(s_{1_{\text{Re}}}\xi)\} \\ & - 2\sin(s_{1_{\text{Im}}}\xi)\{[C_{ij1_{\text{Im}}} + C_{ij3_{\text{Im}}}]\cosh(s_{1_{\text{Re}}}\xi) + [C_{ij1_{\text{Im}}} - C_{ij3_{\text{Im}}}]\sinh(s_{1_{\text{Re}}}\xi)\}\end{aligned} \tag{4.97}$$

4.3.3 Closed-Form Solution of the Optimal Control Problem using the Linearized Riccati Equation

Having the asymptotic solution for $\Lambda(\xi)$ and using the combined transformation relation (4.56), we arrive at the solution for the Riccati matrix $K(\xi)$ as the following

$$K(\xi) = -Q^{-1}[A^T(\xi) + \Lambda'(\xi)\Lambda^{-1}(\xi)] \tag{4.98}$$

Accordingly, at the initial position we will have

$$K(\xi_0) = -Q^{-1}[A^T(\xi_0) + \Lambda'(\xi_0)\Lambda^{-1}(\xi_0)] \tag{4.99}$$

The next task is finding the time history of the states and the control law by using the relations of section 4.1. Substituting for K from (4.98) into (4.32), gives

$$P'^* = -\{Q[-Q^{-1}(A^T + \Lambda'\Lambda^{-1})] + A^T\}P^*$$

that leads to the following differential equation for the co-states

$$P'^* = \Lambda'\Lambda^{-1}P^* \tag{4.100}$$

Now, let assume

$$P^* = \Lambda\Gamma \tag{4.101}$$

where Γ is an unknown 2×1 column vector. Differentiation of (4.101) with respect to ξ, yields

$$P'^* = \Lambda'\Gamma + \Lambda\Gamma' \tag{4.102}$$

Substituting (4.102) into the new co-state equation (4.100), results in

$$\Lambda'\Gamma + \Lambda\Gamma' = \Lambda'\Lambda^{-1}(\Lambda\Gamma) = \Lambda'\Gamma$$

and hence

$$\Lambda\Gamma' = 0 \tag{4.103}$$

However, since in general $\Lambda(\xi) \neq [0]$ and also $|\Lambda(\xi)| \neq 0$, therefore

$$\Gamma' = \frac{d\Gamma}{d\xi} = 0 \tag{4.104}$$

which means that Γ is a constant vector, or

$$\Gamma = const. \tag{4.105}$$

Therefore, by writing (4.101) at the initial position and solving for Γ, we get

$$\Gamma = \Lambda^{-1}(\xi_0)P^*(\xi_0) \tag{4.106}$$

where $\Lambda^{-1}(\xi_0)$ is known and $P^*(\xi_0)$ is obtained from (4.31). Note that since $\Lambda(\xi_f) = I$, also we have

$$\Gamma = \Lambda^{-1}(\xi_f)P^*(\xi_f) = P^*(\xi_f) \tag{4.107}$$

However, we do not have information about the co-state vector at the final position yet. Writing the relation for Γ in terms of the initial state vector, gives

$$\Gamma = \Lambda^{-1}(\xi_0)K^{-1}(\xi_0)X^*(\xi_0) \tag{4.108}$$

Therefore

$$P^*(\xi) = \Lambda(\xi)[\Lambda^{-1}(\xi_0)K^{-1}(\xi_0)X^*(\xi_0)] \tag{4.109}$$

Substituting (4.98) and (4.109) into (4.26), we arrive at the following expression for the optimal state vector, that gives the time history of the angle-of-attack perturbations being suppressed by the optimal controller.

$$X^*(\xi) = -Q^{-1}[A^T(\xi)\Lambda(\xi) + \Lambda'(\xi)][\Lambda^{-1}(\xi_0)K^{-1}(\xi_0)X^*(\xi_0)] \tag{4.110}$$

And finally, substitution of (4.109) into (4.17), yields the optimal control law as

$$u^*(\xi) = -R^{-1}B^T\Lambda(\xi)[\Lambda^{-1}(\xi_0)K^{-1}(\xi_0)X^*(\xi_0)] \tag{4.111}$$

The corresponding elevator control angle is obtained from Eq. (4.9).

4.3.4 Simulation Results and Discussion

The optimal control results using the asymptotic solution for the linearized Riccati equation, for 150,000 ft initial altitude with the same initial conditions as those in Sec. 2.5.1, are presented in Figs. 4.5 through 4.8. For comparison purposes, the results of the corresponding numerical solution in Sec. 4.2 are also plotted on the same graphs. Also, the root variations for the 400,000 ft initial altitude are shown in Fig. 4.9. The optimal state and control penalty gains used are the same as those for the numerical solution in Sec. 4.2.

Using the same computer, the computation time for the simulation of the asymptotic solution was about 1/10 of that of the numerical solution for the same level of smoothness of the output, and the corresponding evaluation stepsize for the asymptotic solution was 4 times bigger than the integration stepsize of the numerical solution.

As can be seen in Fig. 4.5, the asymptotic approximation favorably overestimates the required elevator angle and the corresponding control torque. The approximated variations for the angle-of-attack and its rate of change are sufficiently close to the exact variations. From Fig. 4.5, the maximum approximation error for the perturbation angle-of-attack and its rate-of-change appear to be less than 0.2 degree and 0.2 degree per second, respectively.

As expected, the asymptotic prediction for the components of the Riccati equation deteriorates while it proceeds backwards (Fig. 4.6). This is due to the fact that the approximation starts at the final position of the controlled travel where the boundary conditions are known exactly and further on the approximation error begins to accumulate.

For the 150,000 ft initial altitude, the sets of four characteristic coefficients corresponding to each of the four characteristic functions are listed below. Note that since the characteristic functions must be real, and the four characteristic roots, s_k, are pairs of complex conjugates as Eq. (4.85) also suggests, the characteristic coefficients have to be pairs of complex conjugates as well. From Figs. 4.8 and 4.9, we can see that

$$s_1(\xi) = \bar{s}_2(\xi) = -\bar{s}_3(\xi) = -s_4(\xi)$$

From Fig. 4.8, we can clearly justify the assumption of slow variations of the system parameters for control purposes at lower altitudes.

The characteristic coefficients for the 150,000 ft initial altitude are listed below.

$$C_{111} = 89.752 - 135.89i \qquad C_{121} = -0.9088 - 3.4323i$$
$$C_{112} = 89.752 + 135.89i = \overline{C}_{111} \qquad C_{122} = -0.9088 + 3.4323i = \overline{C}_{121}$$
$$C_{113} = (2.1339 - 3.1897i)\times 10^{-4} \qquad C_{123} = (-8.2874 + 1.1559i)\times 10^{-6}$$
$$C_{114} = (2.1339 + 3.1897i)\times 10^{-4} = \overline{C}_{113} \qquad C_{124} = (-8.2874 - 1.1559i)\times 10^{-6} = \overline{C}_{123}$$

$$C_{211} = (6.9305 - 1.4173i)\times 10^{3} \qquad C_{221} = 77.507 - 133.33i$$
$$C_{212} = (6.9305 + 1.4173i)\times 10^{3} = \overline{C}_{211} \qquad C_{222} = 77.507 + 133.33i = \overline{C}_{221}$$
$$C_{213} = (5.8 + 17.6i)\times 10^{-3} \qquad C_{223} = (2.0294 - 3.5041i)\times 10^{-4}$$
$$C_{214} = (5.8 - 17.6i)\times 10^{-3} = \overline{C}_{213} \qquad C_{224} = (2.0294 + 3.5041i)\times 10^{-4} = \overline{C}_{223}$$

Inspecting the results for the linearized Riccati matrix in Fig. 4.7 as well as the corresponding characteristic coefficients above, we can speculate that $\lambda_{11}(\xi)$ and $\lambda_{22}(\xi)$ must be equal in the absence of the approximation errors. Also, note that the off-diagonal components are different by orders of magnitude.

The variations of the characteristic roots for the 400,000 ft initial altitude are shown in Fig. 4.9. Considering the noticeable variations of the roots (about half an order of magnitude) during the required control period for the 400,000 ft initial altitude (Sec. 4.2), we can see that the assumption of slow variations for the trajectory variables and the aerodynamic characteristics of the shuttle, is not valid for the asymptotic approximation of the solution to the linearized Riccati equation (4.53). Consequently, the asymptotic method as described in Sec. 4.4.2, is not applicable to the control of the space shuttle angle-of-attack oscillations in the upper portion of the reentry trajectory.

It should be reminded that the characteristic roots, i.e. the roots of Eq. (4.82), vary as direct functions of the traveled distance along the trajectory and not the elapsed time. As can be seen in Fig. 2.3, the relationship between time and traveled distance along the trajectory is nonlinear. As a result, we see that while the control period of 5 minutes is about 1/7 of the total reentry time, the corresponding traveled distance is nearly 1/4 of the entire trajectory and it encompasses considerable variations of the trajectory variables as well as the aerodynamic coefficients of the space shuttle.

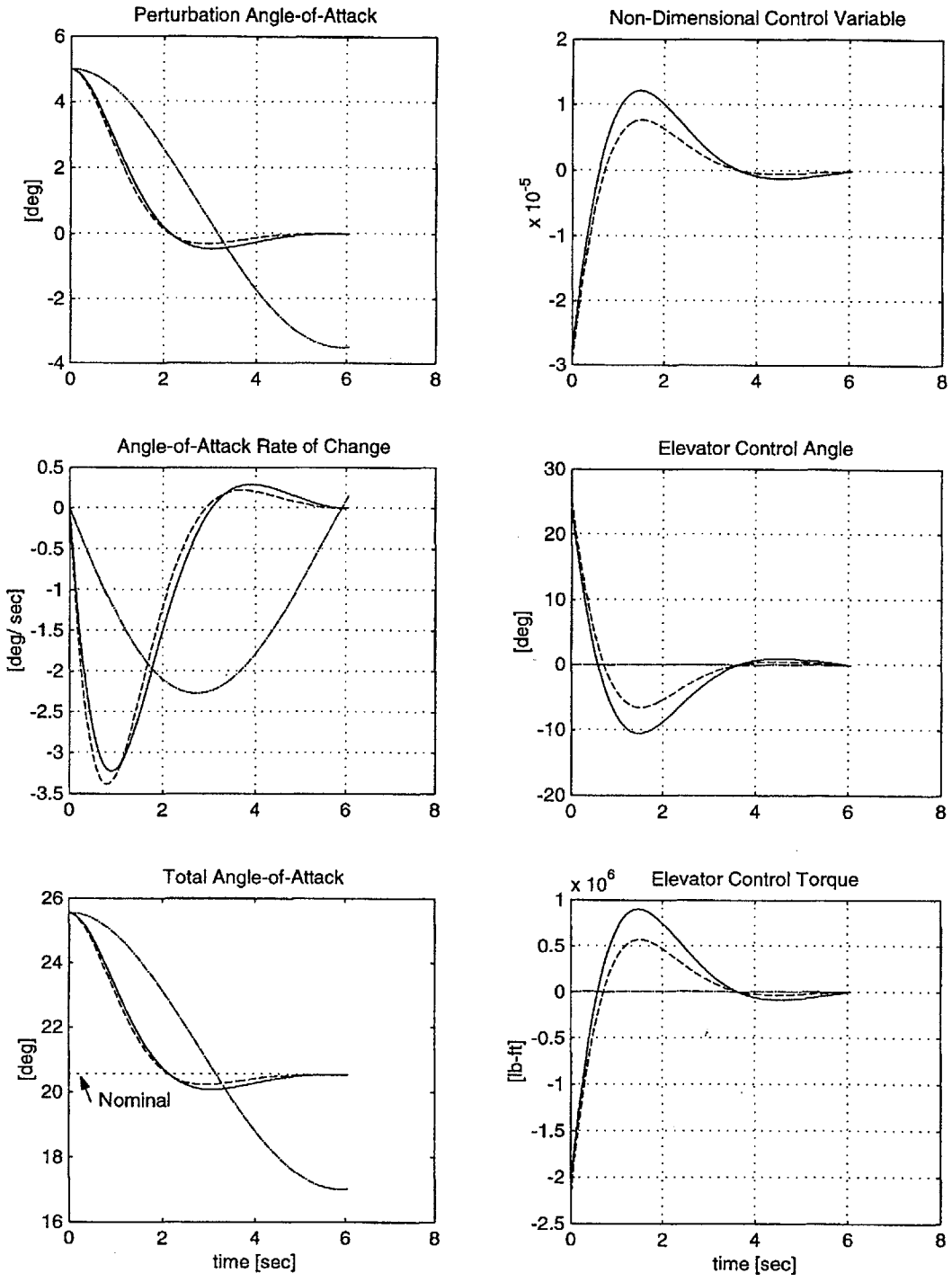

Fig. 4.5 Optimal control results for 150,000 ft initial altitude
___ Asymptotic solution ---- Numerical solution

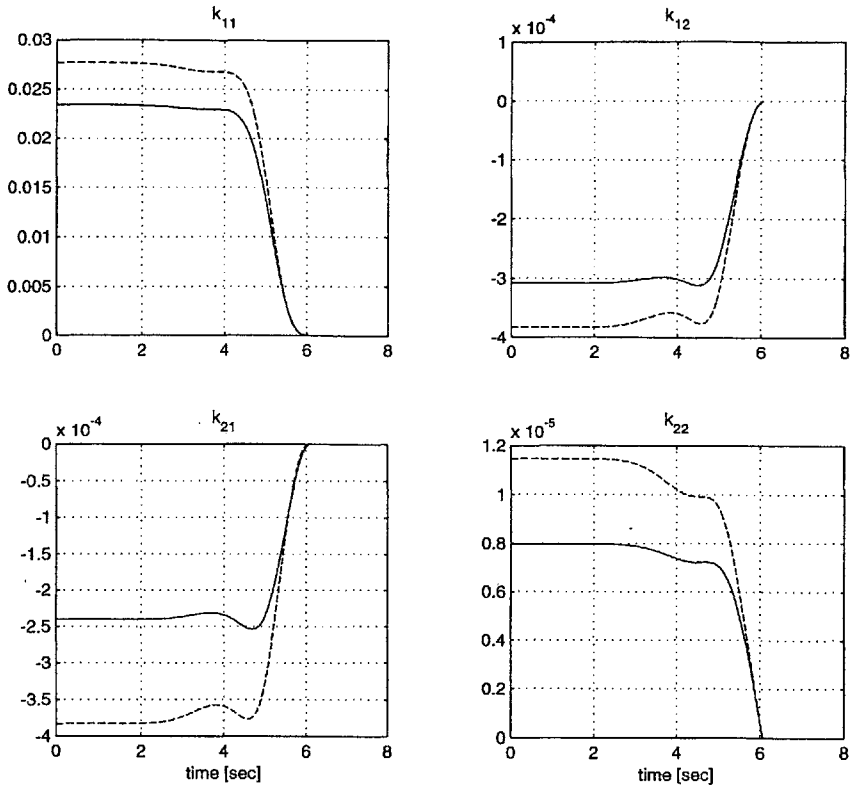

Fig. 4.6 Variations of the Riccati matrix components for 150,000 ft initial altitude
___ Asymptotic solution ---- Numerical solution

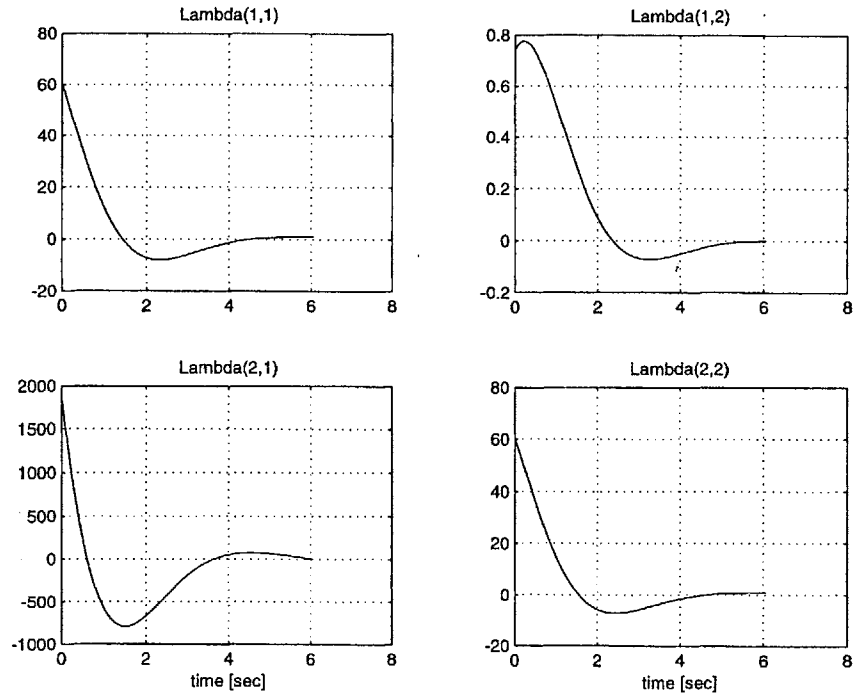

Fig. 4.7 Variations of the components of the linearized Riccati matrix, Λ, for 150,000 ft initial altitude

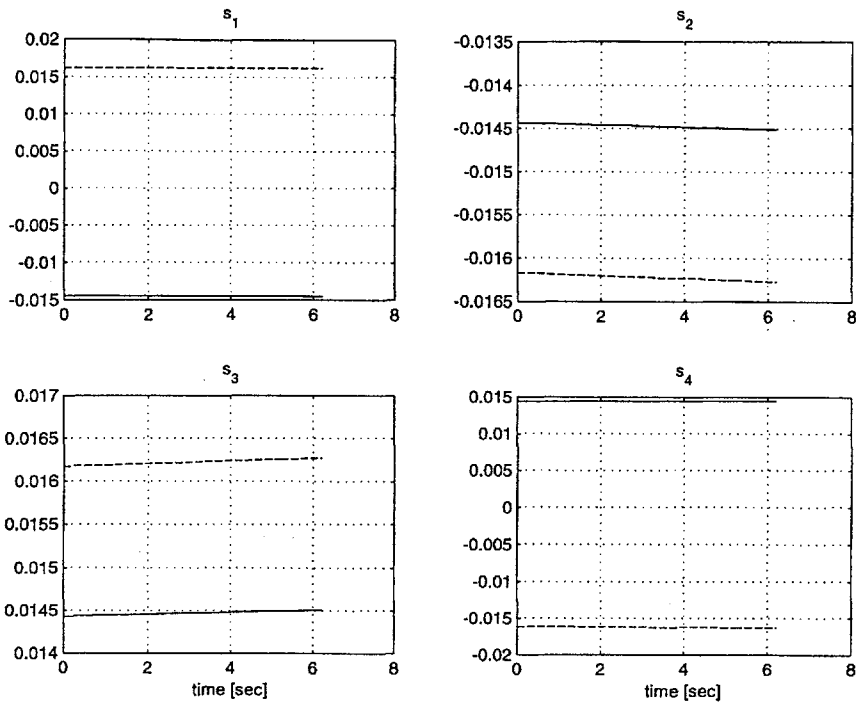

Fig. 4.8 Characteristic root variations for 150,000 ft initial altitude
___ Real part ---- Imaginary part

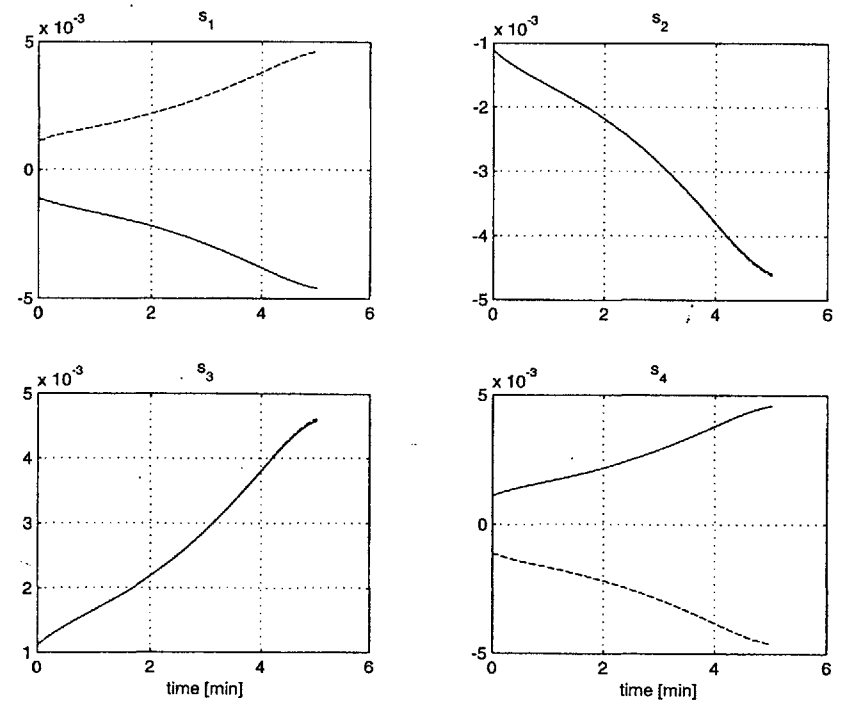

Fig. 4.9 Characteristic roots variations for 400,000 ft initial altitude
___ Real part ---- Imaginary part

CHAPTER 5

ADAPTIVE CONTROL

In this chapter, in order to suppress the undesired angle-of-attack oscillations, an adaptive control technique is applied to the unified equation, i.e. the original 2^{nd}-order nonlinear differential equation with variable coefficients for the angle-of-attack perturbations.

Adaptive control is an approach to the control of dynamic systems with constant or varying uncertain (or unknown) parameters. The basic idea in adaptive control is to maintain consistent performance of a system in the presence of uncertainty or unknown variation in plant parameters by online estimation of the uncertain parameters (or, equivalently, the corresponding controller parameters) based on the measured system signals, and using the estimated parameters in the control input computation. An adaptive control system can thus be regarded as a control system with online parameter estimation. Adaptive control systems, whether developed for linear plants or for nonlinear plants, are inherently nonlinear. The major advantage of the adaptive control systems is that they do not require a priori information about the unknown parameters. This is due to the fact that adaptive controllers feature learning behavior, which means that they start with any initial condition and then improve their performance as parameter adaptation goes on.

Research in adaptive control started in the early 1950's in connection with the design of autopilots for high-performance aircraft, which operate at a wide range of speeds and altitudes and thus experience large parameter variations [10]. Adaptive control was proposed as a way of automatically adjusting the controller parameters in the face of changing aircraft dynamics and aerodynamics. But interest in the subject soon diminished due to the lack of insights and the crash of a test flight. It is only in the last two decades that a coherent theory of adaptive control has been developed, using various tools from nonlinear control theory, such as Lyapunov functions and sliding control methodology.

Intuitively, the sliding mode control is base on the remark that it is much easier to control 1^{st}-order systems (i.e. systems described by 1^{st}-order differential equations), be they nonlinear or uncertain, than it is to control n^{th}-order systems [10]. Accordingly, a notational simplification is introduced, which in effect, allows n^{th}-order problems to be replaced by equivalent 1^{st}-order problems. It has been shown that, for the transformed problems, "perfect" performance can in principle be achieved in the presence of arbitrary parameter inaccuracies. Once a system is forced into the sliding mode, it remains there and exponentially converges (or slides) to the desired state. The rate of convergence is arbitrarily chosen by the control system designer.

The motivation for applying an adaptive controller to this problem is the fact that the parameters in the unified equation of motion for angle-of-attack oscillations are complicated functions of the shuttle aerodynamic coefficients and the prescribed trajectory variables that all need to be provided and updated for a non-adaptive controller as input data during reentry. More specifically, all the stability and control derivatives of the shuttle vary with angle-of-attack and

Mach number, and of course the air density, speed of the vehicle, flight-path angle, and nominal angle-of-attack, change along the trajectory as well.

The adaptive controller design problem here is to derive a control law for the elevator deflection, and an estimation law for the parameters without using any a priori information about them, such that the space shuttle regains its nominal trajectory angle-of-attack after being perturbed by external or internal disturbances. This means that the deviation of angle-of-attack from its nominal value and all its derivatives with respect to the independent variable or time must vanish at the end of controller action. Thence, the control problem can be categorized as a tracking problem where the desired trajectory is the origin of the state vector space at each instant, or a positioning problem in which the initial position is the disturbed state and the target position is the origin.

5.1 Modified Adaptive Control

As derived in Chapter 1, the unified equation is

$$\alpha''(\xi)+\omega_1(\xi)\alpha'(\xi)+\omega_0(\xi)\alpha(\xi)=f(\xi)-\mu(\xi)\delta_e(\xi) \tag{5.1}$$

where the coefficients $\omega_1(\xi)$, $\omega_0(\xi)$, and $\mu(\xi)$, as well as the forcing term $f(\xi)$, vary along the trajectory and during the course of control action. Taking the forcing term in (5.1) to the left-hand side and introducing the control variable, $u(\xi)$, we can write

$$\alpha''(\xi)+\omega_1(\xi)\alpha'(\xi)+\omega_0(\xi)\alpha(\xi)-f(\xi)=\mu(\xi)u(\xi) \tag{5.2}$$

where

$$u(\xi)=-\delta_e(\xi) \tag{5.3}$$

Note that since σ and $\delta(\xi)$ are positive quantities, and $C_{m_{\delta_e}}(\xi)$ is negative by convention, therefore

$$\mu(\xi)>0$$

We will need $\mu(\xi)$ to be positive later in the formulation. Dividing both sides of (5.2) by $\mu(\xi)$, yields

$$\frac{1}{\mu(\xi)}\alpha''(\xi)+\frac{\omega_1(\xi)}{\mu(\xi)}\alpha'(\xi)+\frac{\omega_0(\xi)}{\mu(\xi)}\alpha(\xi)-\frac{f(\xi)}{\mu(\xi)}=u(\xi) \tag{5.4}$$

Now let rewrite the above equation using a more convenient set of parameters as

$$m(\xi)\alpha''(\xi)+c(\xi)\alpha'(\xi)+k(\xi)\alpha(\xi)-d(\xi)=u(\xi) \tag{5.5}$$

where

$$m(\xi) = \frac{1}{\mu(\xi)}$$

$$c(\xi) = \frac{\omega_1(\xi)}{\mu(\xi)}$$

$$k(\xi) = \frac{\omega_0(\xi)}{\mu(\xi)} \qquad \text{(5.6a-d)}$$

$$d(\xi) = \frac{f(\xi)}{\mu(\xi)}$$

where m, c, k, and d are the mass, damping, stiffness, and disturbance parameters, respectively. The notation used is more descriptive because of the analogy with the conventional 2^{nd}-order mass-spring-damper system with $d(\xi)$ as a disturbance signal. The complete set of parameters to be estimated includes an additional one denoted as $n(\xi)$, which is the derivative of the mass parameter with respect to ξ, namely

$$n(\xi) = m'(\xi) = \frac{d}{d\xi}(\frac{1}{\mu}) = -\frac{\mu'(\xi)}{\mu^2(\xi)} \qquad (5.7)$$

Note that the controller will estimate this parameter as an independent one and not necessarily the derivative of the mass parameter. This is due to the fact that the adaptive control approach to be used here is control-task-oriented and does not guarantee the convergence of the estimated parameters to the true values. Being task-oriented is due to the fact that in this method, the adaptation law extracts information about the parameters from the tracking errors and not from the estimation error.

Now, let us define the vector of true parameters, P, as the following

$$P = [m, c, k, d, n]^T \qquad (5.8)$$

where the components are considered to be unknown. Also, let form the vector of parameter estimates as

$$\hat{P} = [\hat{m}, \hat{c}, \hat{k}, \hat{d}, \hat{n}]^T \qquad (5.9)$$

the components of which are to be estimated and updated by the controller. Using the above vectors, let us define the vector of parameter estimation errors as

$$\tilde{P} = \hat{P} - P = [\tilde{m}, \tilde{c}, \tilde{k}, \tilde{d}, \tilde{n}]^T \qquad (5.10)$$

with the components of

$$\tilde{m} = \hat{m} - m$$

$$\tilde{c} = \hat{c} - c$$

$$\tilde{k} = \hat{k} - k \qquad (5.11a\text{-}e)$$

$$\tilde{d} = \hat{d} - d$$

$$\tilde{n} = \hat{n} - n$$

The perturbation initial conditions are defined as before, i.e. $\alpha(\xi_0) = \alpha_0$ and $\alpha'(\xi_0) = \alpha'_0$, and the desired state for the perturbation angle-of-attack and its rate-of-change is described by

$$\alpha_d = 0 \qquad \alpha'_d = 0 \qquad (5.12)$$

Let us define the state errors as

$$\tilde{\alpha} = \alpha - \alpha_d \qquad \tilde{\alpha}' = \alpha' - \alpha'_d \qquad (5.13)$$

that lead to

$$\tilde{\alpha} = \alpha \qquad \tilde{\alpha}' = \alpha' \qquad (5.14)$$

The sliding variable is defined as the following

$$s = \tilde{\alpha}' + \lambda\tilde{\alpha} = \alpha' + \lambda\alpha \qquad (5.15)$$

where λ is a positive number that determines the rate of exponential decay of the angle-of-attack when the sliding variable tends to zero as a result of the closed-loop dynamics of the controller that will be discussed later. We can physically interpret the sliding variable as the "velocity error" measure by introducing a "reference velocity" variable, α'_r, as

$$s = \alpha' - \alpha'_r \qquad (5.16)$$

$$s' = \alpha'' - \alpha''_r \qquad (5.17)$$

where

$$\alpha'_r = \alpha'_d - \lambda\tilde{\alpha} = -\lambda\tilde{\alpha} = -\lambda\alpha \qquad (5.18)$$

and accordingly

$$\alpha''_r = -\lambda\alpha' \qquad (5.19)$$

The preceding representation of the sliding variable will also simplify the formulations as can be seen further. Now, let us consider the following Lyapunov function candidate

$$E = \frac{1}{2}ms^2 + \frac{1}{2}\tilde{P}^T\Gamma^{-1}\tilde{P} \qquad (5.20)$$

where Γ is called the adaptation gain matrix and is a constant symmetric positive definite 5×5 matrix that ensures the corresponding quadratic term remains always positive regardless of the magnitudes of the $\tilde{P}$ components. The adaptation gain matrix plays the role of a conditioning or normalizing factor that balances the contribution of the estimation errors associated with each parameter estimate to the total error, and is commonly chosen to be diagonal so that the number of weighting elements to be assigned reduces to the minimum. The first term in (5.20) is also always positive because of the choice of the parameter m to be positive earlier in the formulation. As can be seen, the Lyapunov function is a positive definite scalar function and a combined measure of the tracking and estimation errors. The decrease of the Lyapunov function indicates improvement and convergence in the tracking and parameter estimation procedures.

The next step in designing the adaptive controller is to find an adaptation law and accordingly a control law that guarantee the negative definiteness of the Lyapunov function. Mathematically, we have secured that,

$$E>0 \text{ while } s\neq 0 \text{ and/or } \tilde{P}\neq 0$$

but we further need to provide that

$$\frac{dE}{d\xi}=E'<0 \quad \text{while} \quad s\neq 0$$

Differentiating (5.20) with respect to ξ, we get

$$\frac{dE}{d\xi}=E'=\frac{1}{2}m's^2+ms's+\tilde{P}^T\Gamma^{-1}\tilde{P}' \tag{5.21}$$

Substituting for the sliding variable gradient s' from (5.17) and using the previously-introduced additional parameter n from (5.7), lead to

$$E'=\frac{1}{2}ns^2+m(\alpha''-\alpha_r'')s+\tilde{P}^T\Gamma^{-1}\tilde{P}'$$

Rearranging, we have

$$E'=(\frac{1}{2}ns+m\alpha''-m\alpha_r'')s+\tilde{P}^T\Gamma^{-1}\tilde{P}' \tag{5.22}$$

and from the unified equation, we can write

$$m\alpha''=u-c\alpha'-k\alpha+d$$

Substituting for α' from (5.16) yields

$$m\alpha''=u-c(s+\alpha_r')-k\alpha+d \tag{5.23}$$

Let take the control law as the following

$$u = (\hat{m}\alpha_r'' + \hat{c}\alpha_r' + \hat{k}\alpha - \hat{d}) + (\hat{c} - \lambda\hat{m} - \frac{1}{2}\hat{n})s \tag{5.24}$$

Substituting (5.24) into (5.23) and then putting (5.23) into (5.22), we get

$$E' = \{\frac{1}{2}ns + [\hat{m}\alpha_r'' + \hat{c}\alpha_r' + \hat{k}\alpha - \hat{d} + (\hat{c} - \lambda\hat{m} - \frac{1}{2}\hat{n})s - c(s + \alpha_r') - k\alpha + d] - m\alpha_r''\}s + \tilde{P}^T\Gamma^{-1}\tilde{P}'$$

Using Eqs. (5.11) and collecting terms as well as breaking the rightmost term, we arrive at

$$E' = s[\tilde{m}(\alpha_r'' - \lambda s) + \tilde{c}(\alpha_r' + s) + \tilde{k}\alpha - \tilde{d} - \frac{1}{2}\tilde{n}s] - \lambda m s^2 + \tilde{P}^T\Gamma^{-1}\hat{P}' - \tilde{P}^T\Gamma^{-1}P' \tag{5.25}$$

Now let us define a known vector Y_m such that the expression in the brackets in (5.25) can be written as

$$\tilde{m}(\alpha_r'' - \lambda s) + \tilde{c}(\alpha_r' + s) + \tilde{k}\alpha - \tilde{d} - \frac{1}{2}\tilde{n}s] = Y_m(\alpha, \alpha', \alpha_r', \alpha_r'')\tilde{P} \tag{5.26}$$

where

$$Y_m = [(\alpha_r'' - \lambda s), (\alpha_r' + s), \alpha, -1, -\tfrac{1}{2}s] \tag{5.27}$$

or using (5.18) and (5.19)

$$Y_m = [-\lambda(s + \alpha'), (s - \lambda\alpha), \alpha, -1, -\tfrac{1}{2}s] \tag{5.28}$$

Relation (5.26) is called linear parametrization of the control law, since by rearranging (5.24), we can write

$$u = \hat{m}(\alpha_r'' - \lambda s) + \hat{c}(\alpha_r' + s) + \hat{k}\alpha - \hat{d} - \frac{1}{2}\hat{n}s = Y_m\hat{P} \tag{5.29}$$

Note that all the components of the vector Y_m are known or computed from the output measurements of α and $\dot{\alpha}$. It must be noted that the rate measurements give the time derivative of the angle-of-attack whereas in our formulation, we need the non-dimensional derivative α' that can be found by using (1.36) as

$$\alpha' = \frac{d\alpha}{d\xi} = \frac{L}{V}\dot{\alpha}$$

Substituting (5.26) into (5.25) we get

$$E' = sY_m\tilde{P} + \tilde{P}^T\Gamma^{-1}\hat{P}' - \lambda m s^2 - \tilde{P}^T\Gamma^{-1}P' \tag{5.30}$$

Since the first term in (5.30) is a scalar, we can write

$$sY_m\tilde{P} = (sY_m\tilde{P})^T = \tilde{P}^T{Y_m}^T s$$

and hence

$$E' = \tilde{P}^T Y_m{}^T s + \tilde{P}^T \Gamma^{-1} \hat{P}' - \lambda m s^2 - \tilde{P}^T \Gamma^{-1} P'$$

or

$$E' = \tilde{P}^T (Y_m{}^T s + \Gamma^{-1} \hat{P}') - \lambda m s^2 - \tilde{P}^T \Gamma^{-1} P' \tag{5.31}$$

Finally, choosing the adaptation law as

$$\hat{P}' = -\Gamma Y_m{}^T s \tag{5.32}$$

leads to

$$E' = -\lambda m s^2 - \tilde{P}^T \Gamma^{-1} P' \tag{5.33}$$

However, since $\lambda m s^2 > 0$, as long as $\tilde{P}^T \Gamma^{-1} P' \geq -\lambda m s^2$, we have

$$E' \leq 0 \tag{5.34}$$

and since E is positive, Barbalat's lemma [10] indicates that E' does tend to zero as time elapses. This in turn results in asymptotic approaching of the sliding variable s towards zero and consequently the exponential decay of the perturbation angle-of-attack α.

Eventually, for the elevator control command, from (5.) we have

$$\delta_e = -u = -Y_m \hat{P} \tag{5.35}$$

that leads to the following control command

$$\delta_e = [2\lambda \hat{m} - \hat{c} + \tfrac{1}{2}\hat{n}]\alpha' + [\lambda^2 \hat{m} - \hat{k} - \tfrac{1}{2}\lambda \hat{n}]\alpha + \hat{d} \tag{5.36}$$

Note that the elevator control command comprises of both feedback and feedforward signals.

5.1.1 Simulation Results and Discussion

The simulation results for the adaptive controller with the same set of initial altitudes, i.e. 400,000 ft and 150,000 ft, and the same initial conditions as those in Sec. 2.5.2, are presented in this section. Figs. 5.1 and 5.5 demonstrate the results of practical interest for the two altitude ranges, and Figs. 5.2 and 5.6 show the corresponding evolutions of the parameter estimates. Accordingly, Figs. 5.3 and 5.7 depict the variations of the true parameters, and finally, the variations of the true parameters and the evolution of the parameter estimates are plotted on the same graphs for evaluating the estimation performance.

As introduced in the formulation, there are two arbitrary control parameters, i.e. λ and Γ, that must be selected for the controller based on the desired-response requirements and control availability. The characteristic value, λ, controls the speed of response such that the higher values give faster response. On the other hand, the adaptation gain matrix, Γ, controls the speed of adaptation and parameter convergence. The adaptation gain matrix also plays a conditioning

or normalizing role in the estimation process in the sense that it balances the contribution of each of the parameter estimate to the total estimation error. The characteristic value and the adaptation gain both affect the stability and functionality of the method as well as the required control effort. Larger characteristic values give more stability to the method while demanding more control effort, i.e. higher elevator deflection the associated aerodynamic torque. Similarly, higher adaptation gain offers more stability but requires more control effort. However, the adaptation gain must remain within a certain range, otherwise it causes instability. For the characteristic value, however, there is no upper bound concerning the stability. The maximum available elevator angle is a major constraint for both of the controlling parameters and consequently the performance of the adaptive controller.

The following characteristic values and adaptation gain matrices corresponding to the two initial altitudes proved to give the fastest response in each case while keeping the required elevator deflection within the available range of $\pm 25^{\circ}$. Notice that the components of the adaptation gain matrix Γ are apart by many orders of magnitude in both altitude ranges. This is due to the normalizing role of the gain matrix that is discussed in Sec. 5.1.

400,000-ft initial altitude:

$$\lambda = 1.11\times10^{-3}$$
$$\Gamma = diag\,[\ 1.0345\times10^{14},\ 6.3146,\ 3.1487\times10^{-4},\ 6.3261\times10^{-9},\ 4.5023\times10^{5}\ ]$$

150,000-ft initial altitude:

$$\lambda = 1.92\times10^{-2}$$
$$\Gamma = diag\,[\ 3.6616\times10^{10},\ 1.1163\times10^{5},\ 1.1029\times10^{2},\ 1.2975\times10^{-4},\ 6.1606\times10^{1}\ ]$$

As can be seen in Figs. 5.1 and 5.5, for both altitudes, the required time to cancel out the angle-of-attack unwanted oscillations has been reduced considerably compared to that of the disturbance control (or the transient response). The suppression time for the 400,000 ft initial altitude is about 4 minutes that is nearly one-fourth of the time that takes the transient dynamic response to die out. For the 150,000 ft initial altitude, it takes only 6 seconds for the adaptive controller to suppress the angle-of-attack oscillations compared to that of the disturbance control which is about 120 seconds.

While the elevator control angles for the two altitude ranges are at the same level, the corresponding control torques are different by nearly 3 orders of magnitude which is due to the corresponding levels of atmospheric density as discussed in Sec. 3.2.
Comparing the results in Figs. 5.4 and 5.5, we see that the estimation performance is better for the lower altitudes. Note that for the case of 150,000 ft initial altitude, the parameter estimates and the corresponding true parameters have the same orders of magnitude.

As can be justified by the presented results, we can see that the adaptive control approach, as formulated in this study, is a robust and practical technique for the control of the space shuttle angle-of-attack during reentry. It is robust in that it performs excellently in both upper and lower atmosphere regardless of the level of variations of the aerodynamic and trajectory parameters

during the course of control action. The adaptive controller is self-contained because it does not need input data corresponding to the prescribed trajectory variables and the variant aerodynamic characteristics of the space shuttle during the control process. Also, the adaptive controller is practical since the required control deflection of the elevator always starts at zero (Figs. 5.1 and 5.5), regardless of the nature of the input disturbance. This is not the case for the optimal and nonlinear controllers where they demand the maximum elevator deflection at the beginning of actuation (Figs. 3.1, 3.3, 4.1, and 4.2).

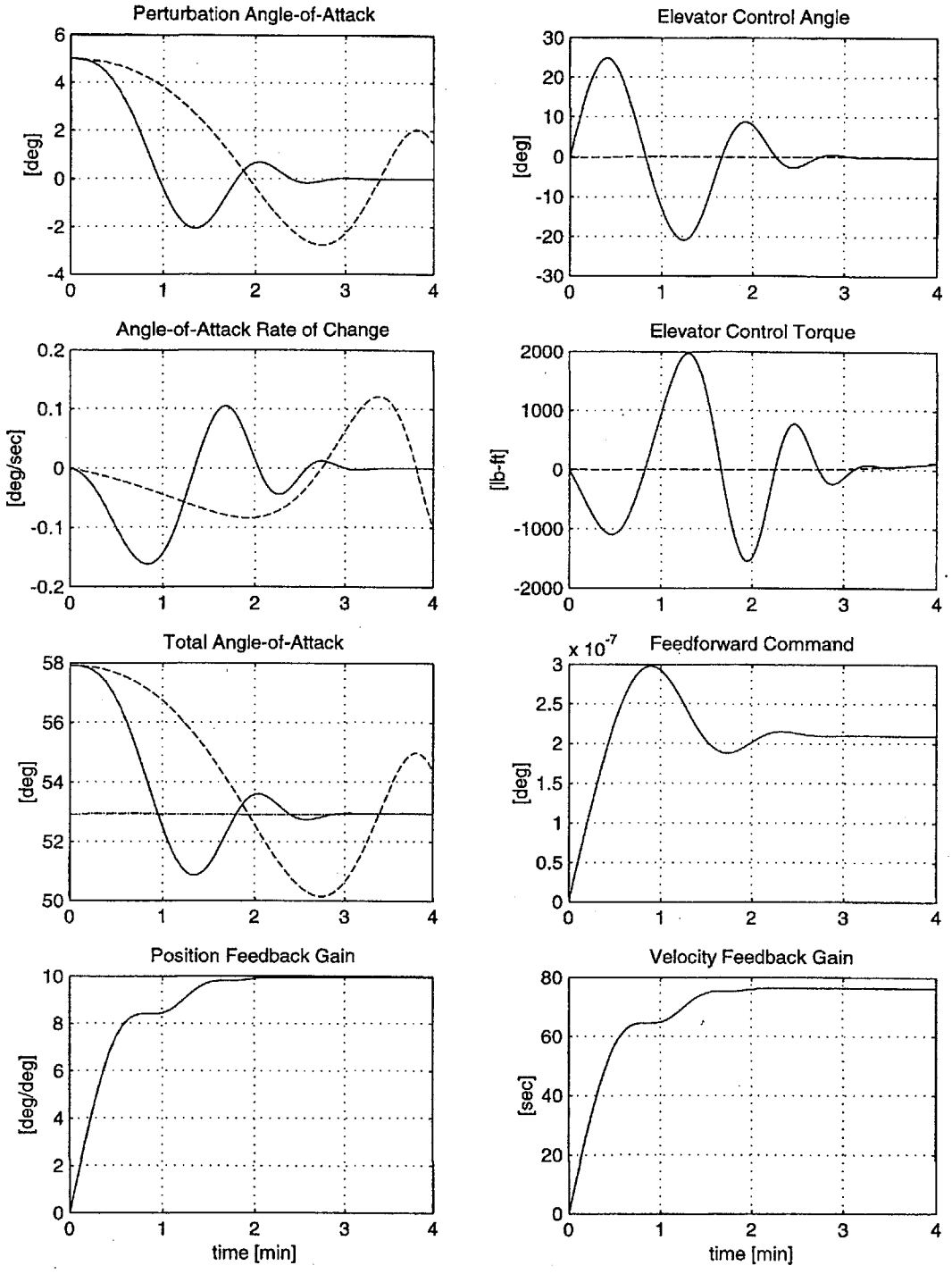

Fig. 5.1 Adaptive control results for 400,000 ft initial altitude

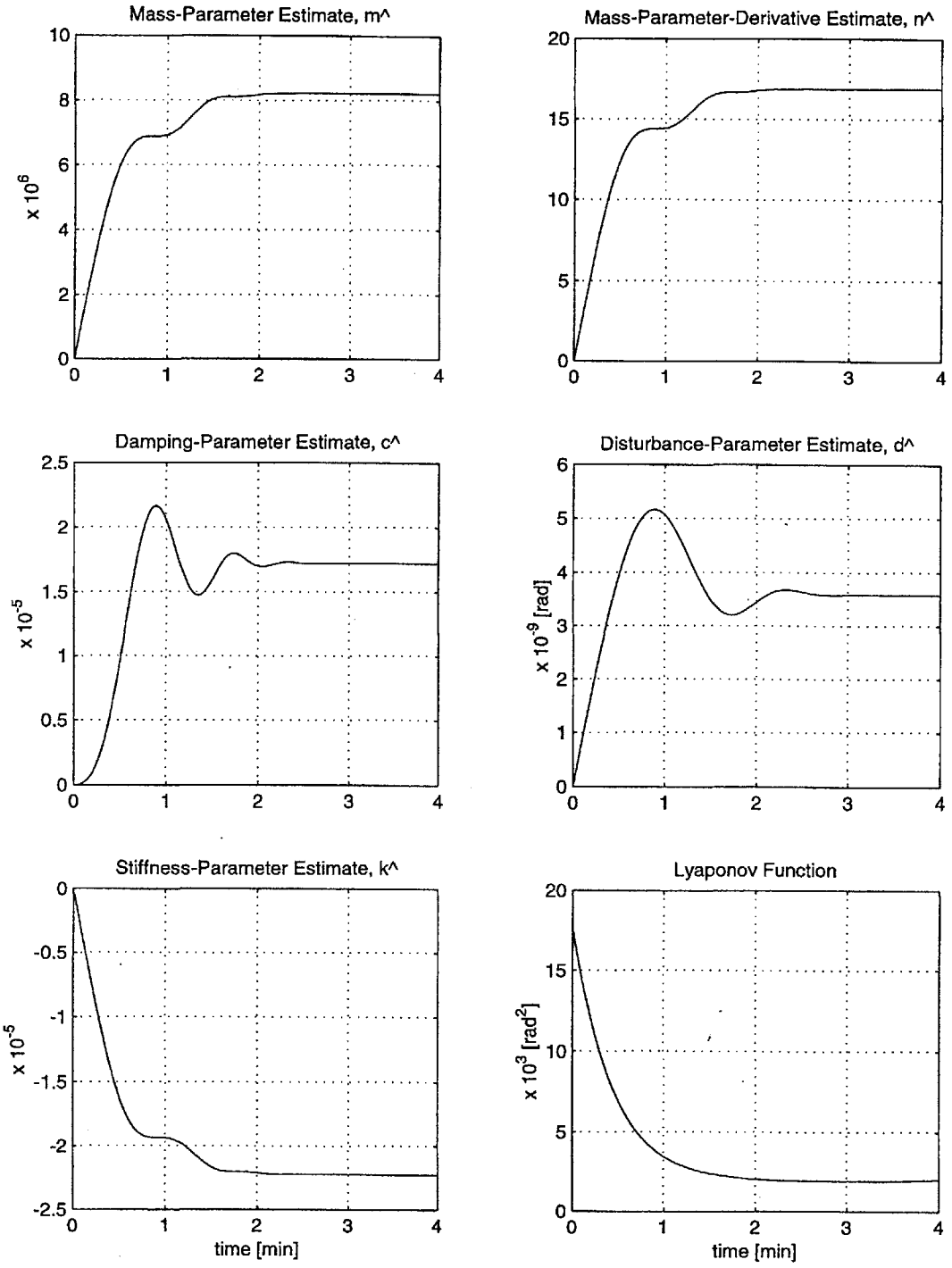

Fig. 5.2 Parameter estimates and Lyapunov function variation for 400,000 ft initial altitude

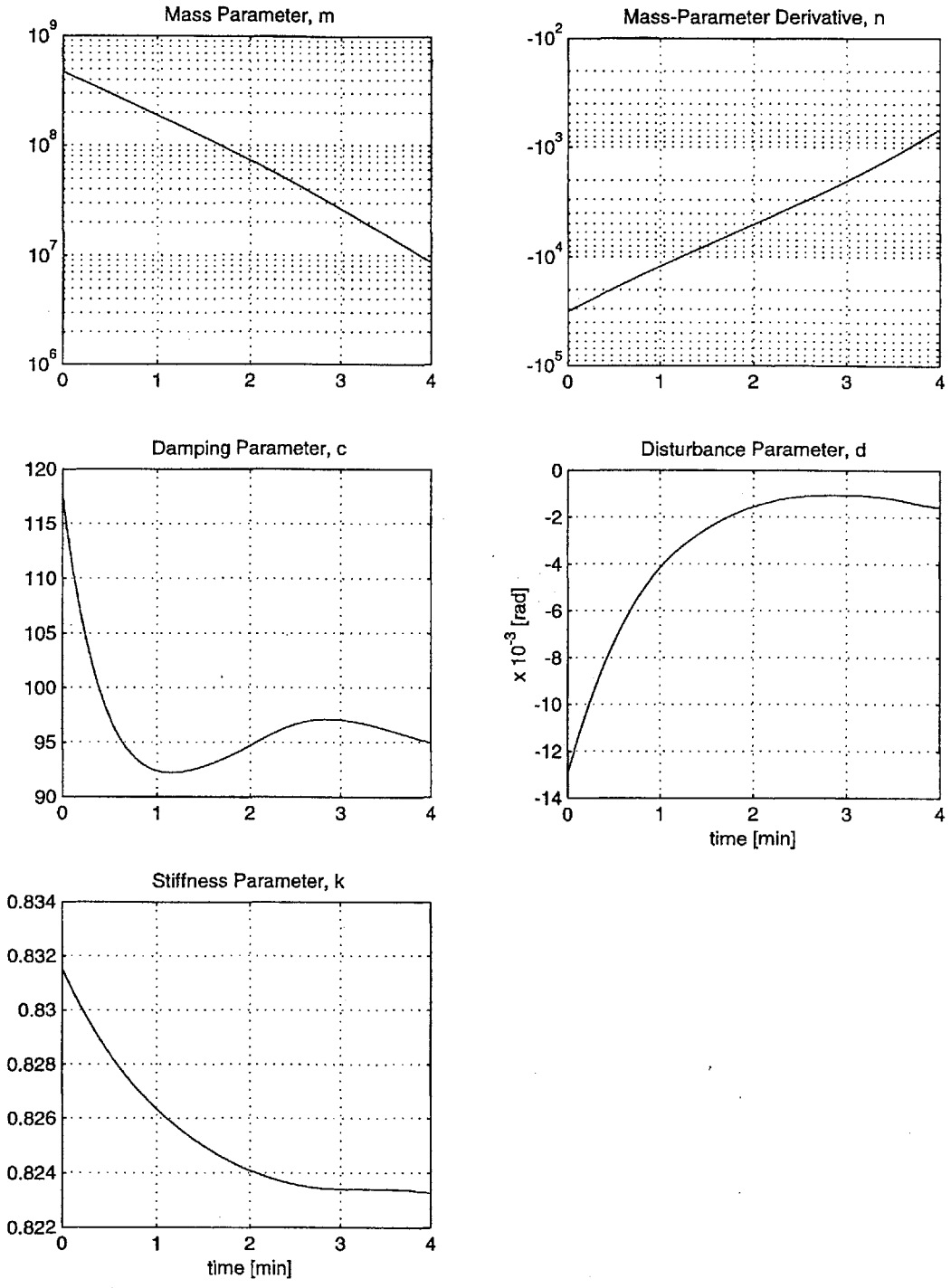

Fig. 5.3 Variations of the true parameters for 400,000 ft initial altitude

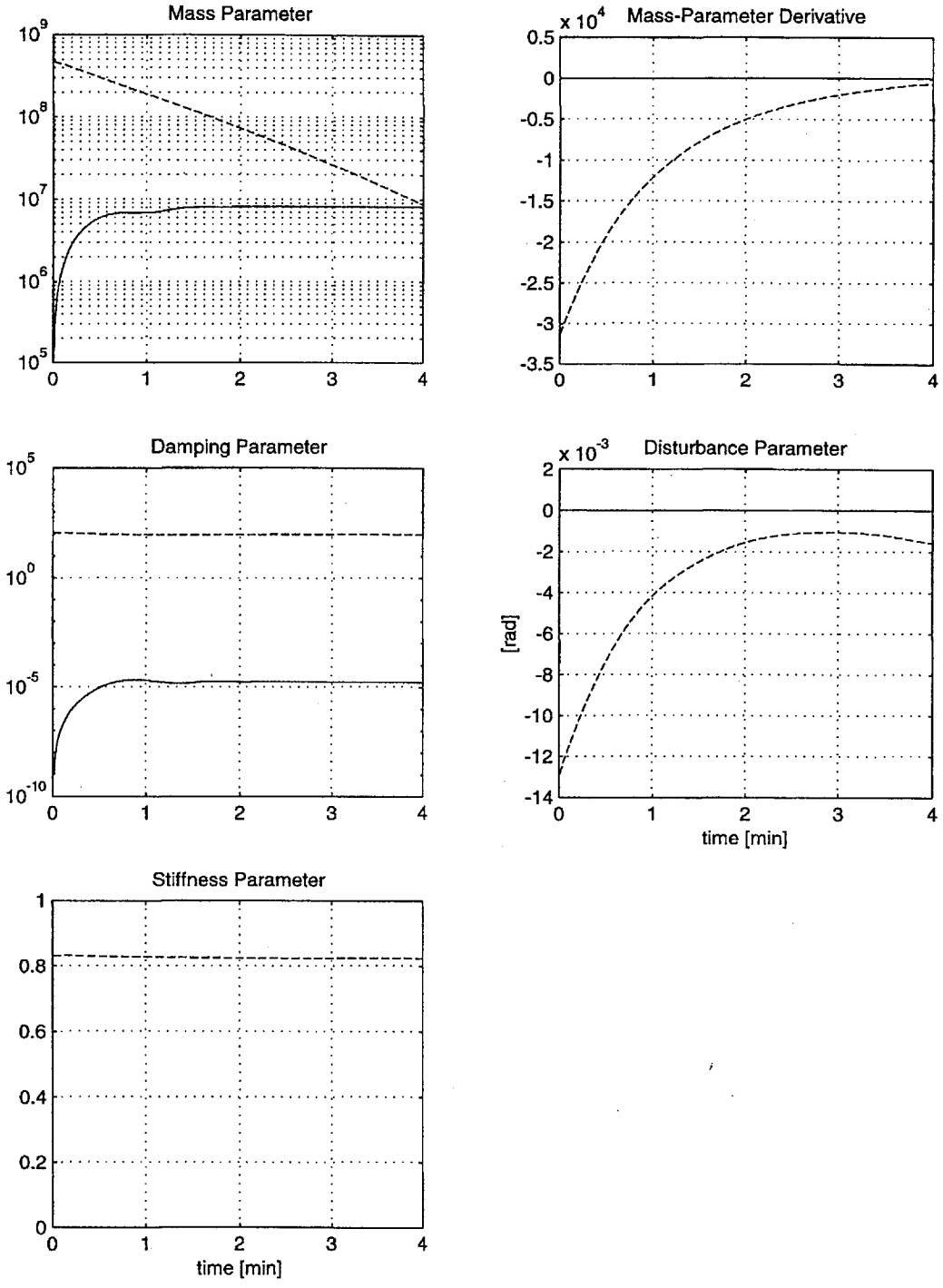

Fig. 5.4 Estimation performance for 400,000 ft initial altitude
___ Estimated parameters ---- True parameters

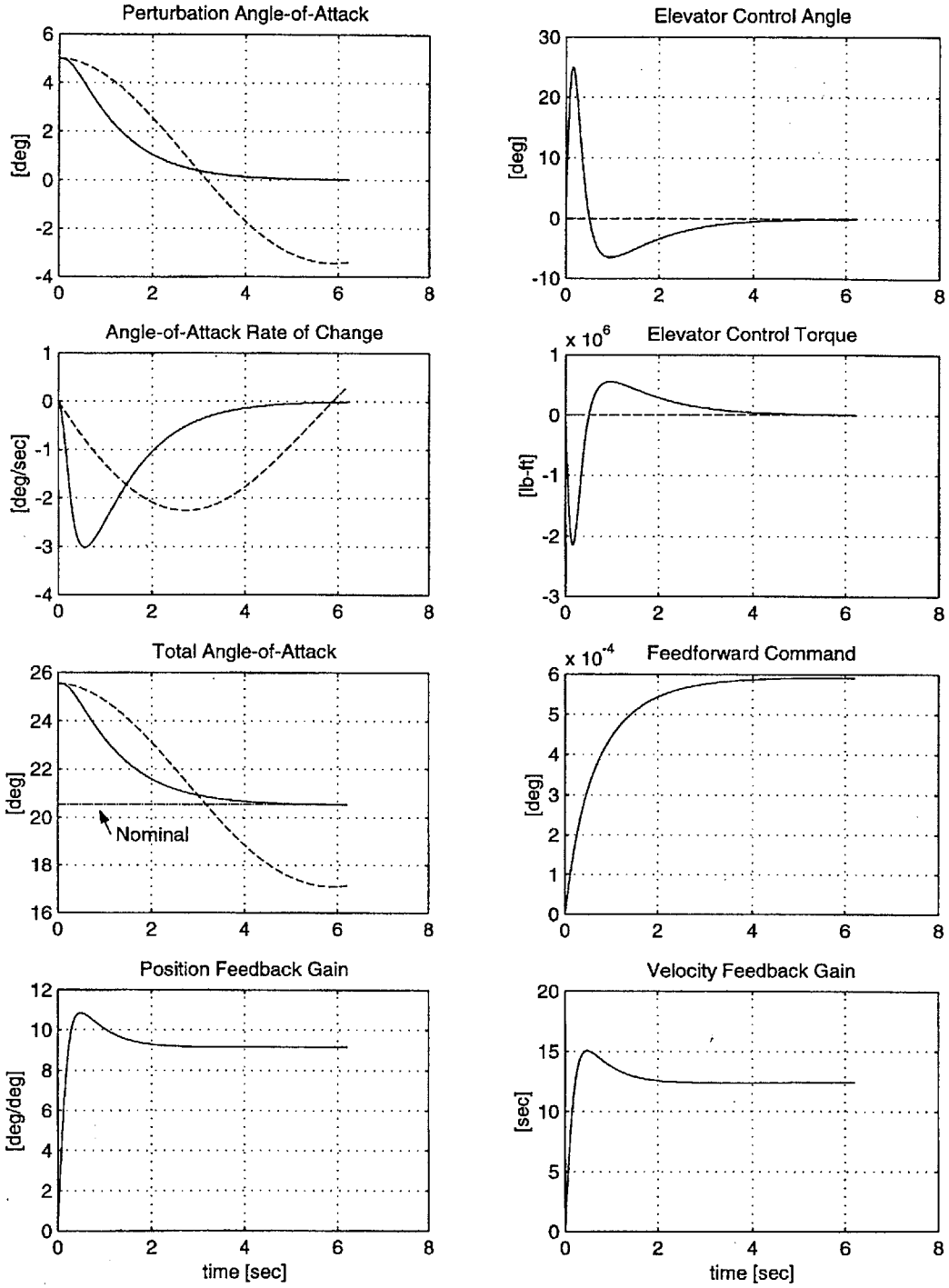

Fig. 5.5 Adaptive control results for 150,000 ft initial altitude

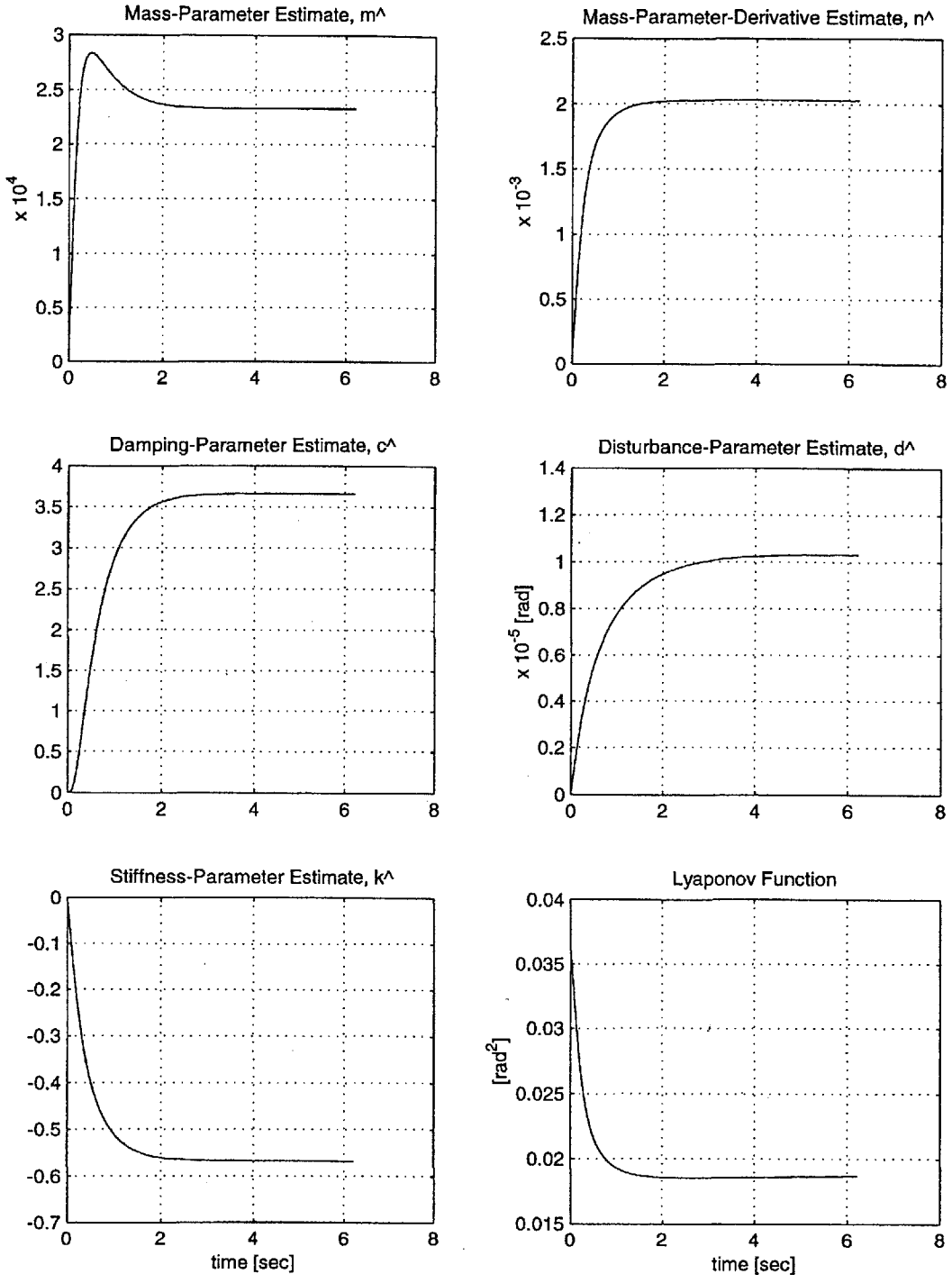

Fig. 5.6 Parameter estimates and Lyapunov function variation for 150,000 ft initial altitude

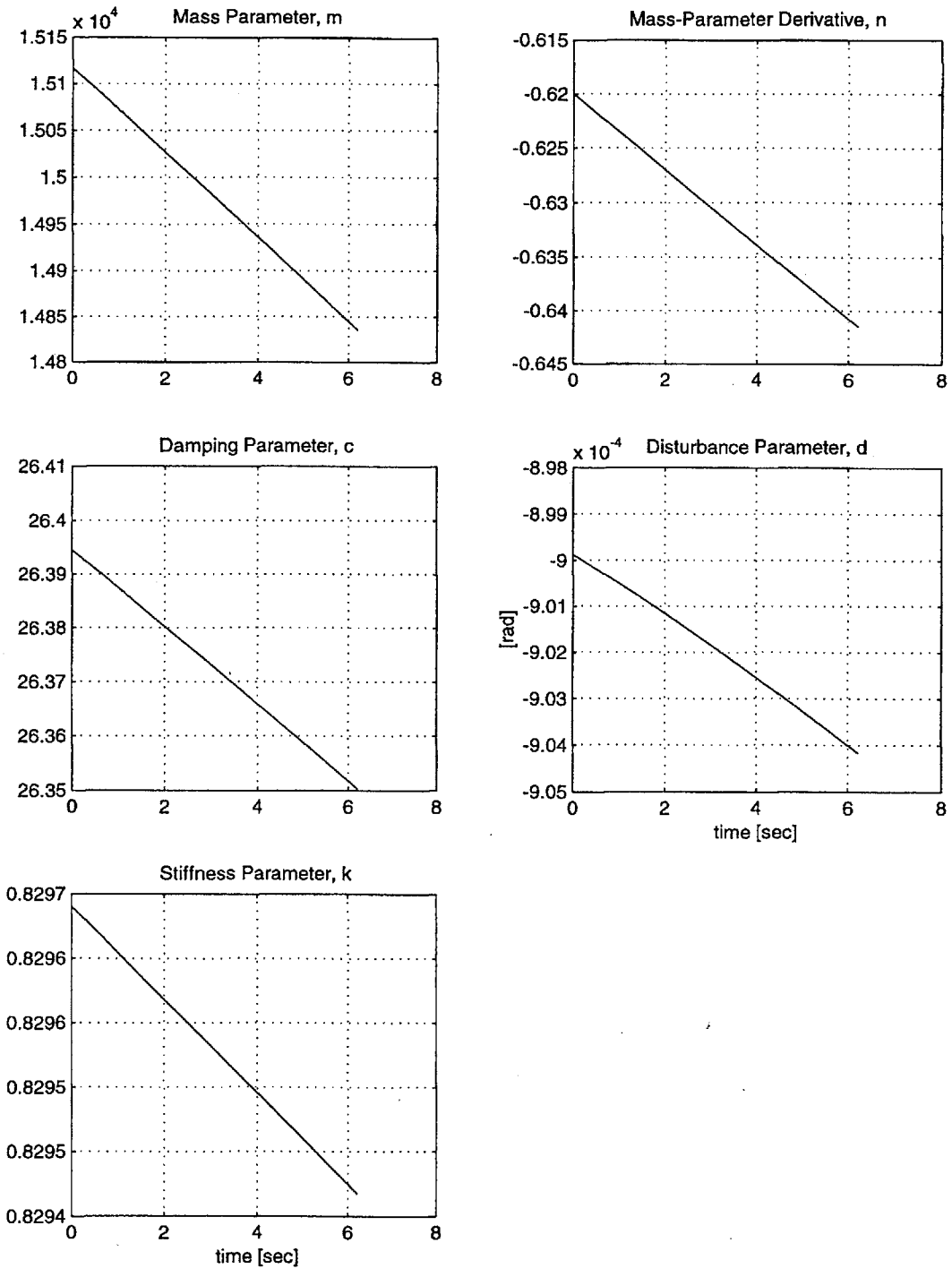

Fig. 5.7 Variations of the true parameters for 150,000 ft initial altitude

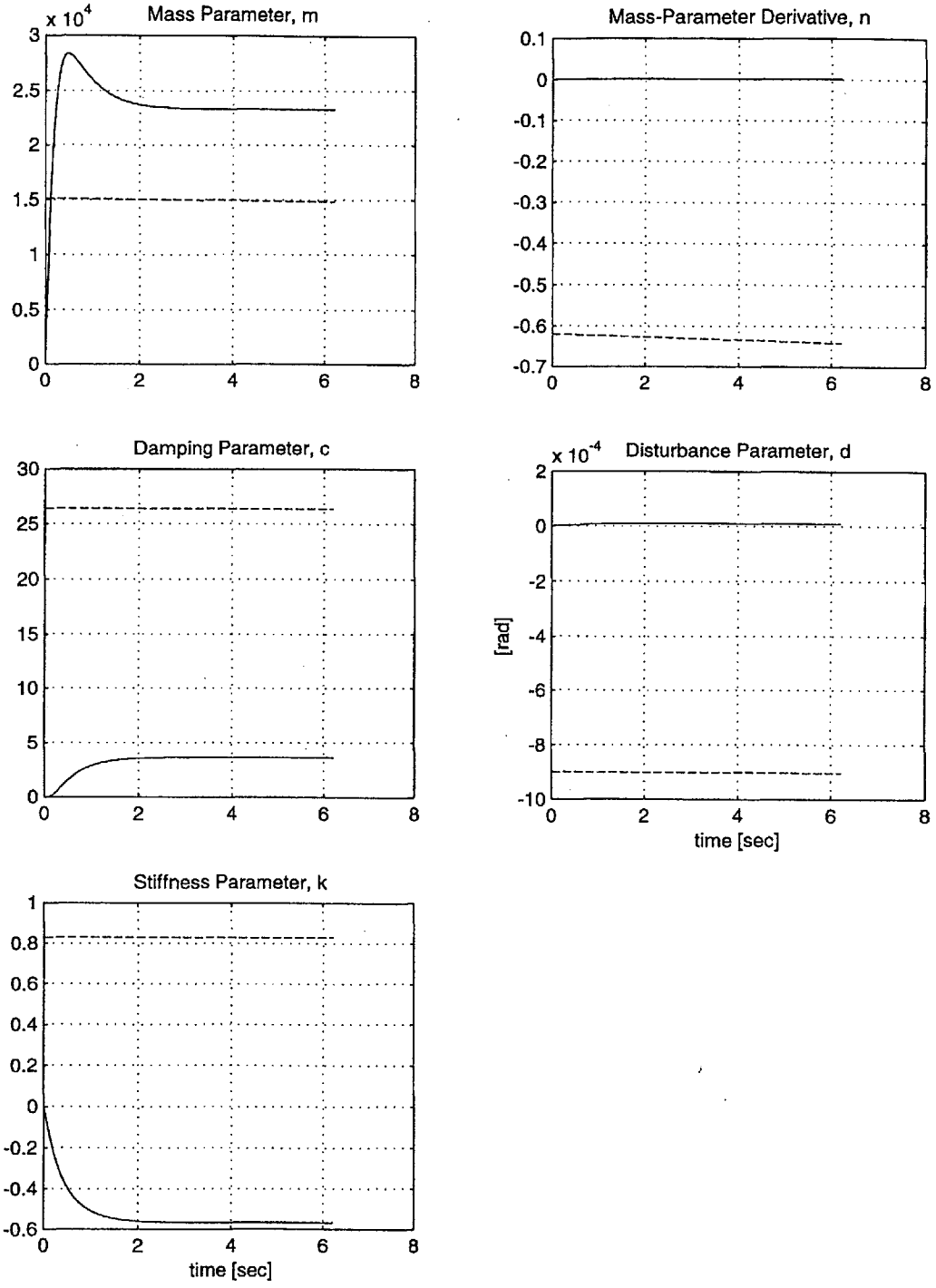

Fig. 5.8 Adaptation performance for 150,000 ft initial altitude
___ Estimated parameters ---- True parameters

CONCLUSIONS

In this study, we have presented different approaches to the control of the angle-of-attack oscillations of the space shuttle due to the atmospheric disturbances during reentry. The space shuttle glides over a prescribed reentry trajectory that is optimal in that it minimizes the weight of the thermal protection system [4]. A realistic generic hypersonic aerodynamic model taken from [3] has been used for the computer simulations in this study. The model is a geometrically-simplified hypersonic delta-wing aircraft that has similar aerodynamic characteristics to that of the space shuttle.

The oscillations of the space shuttle angle-of-attack during reentry, have been shown by Vinh and Laitone in [12] to be governed by a second-order inhomogeneous linear differential equation with variable coefficients. This so called unified equation results from the transformation of the nonlinear equations of motion by using a change of independent variable from time to a non-dimensional distance parameter along the trajectory. In this study, the original unified equation has been modified to be applicable for control purposes and using the abovementioned generic hypersonic model. In traversing the earth's atmosphere during reentry, variations in the coefficients of the unified equation are due to changes in air density, velocity of the vehicle, flight path angle, nominal angle-of-attack, and the aerodynamic characteristics of the space shuttle vehicle. The dominant parameter is shown to be the atmospheric density. However, the aerodynamic stability and control derivatives of the shuttle as a hypersonic vehicle, vary only due to variations of the nominal angle-of-attack and velocity along the prescribed trajectory. Of these two variable parameters, the nominal angle-of-attack proves to be the dominant one.

The simulation results for the dynamic response of the shuttle vehicle using the generic model show good agreement with that of the actual space shuttle model employed in [9] by Ramnath and Sinha. Also as expected, the transient response to the angle-of-attack perturbations is shown to be stable. The uncontrolled dynamic response to the angle-of-attack perturbation at two different initial altitudes of 400,000 ft and 150,000 ft, corresponding to the upper and lower portions of the trajectory, has been presented and analyzed. It is shown that the transient response in both cases is highly-oscillatory and long-lasting with increasing frequency. As such, the need for providing the space shuttle orbiter with an angle-of-attack controller is readily justified. It is shown that the die-out time is much larger for the upper atmosphere (about 15 min.) compared to that for the lower altitudes (about 2 min.). The increasing frequency is especially visible for the case of upper trajectory as it takes longer for the oscillations to vanish.

Through implementing the nonlinear, optimal, and adaptive control techniques, three different controllers have been developed and presented. Using computer simulations, the performance of the controllers has been analyzed along the upper and lower portions of the trajectory. It was observed that in reducing the time required to achieve the control tasks, the maximum available deflection of the elevator is the major constraint. Accordingly, in designing the controllers, the corresponding gains and characteristic values have been selected to give the fastest response while keeping the required elevator deflections within the available range of $\pm 25^{\circ}$. The required control time for the upper trajectory, turns out to be about 4 to 5 minutes and for the lower trajectory, less than 6 seconds. These control periods seem to be satisfactory when compared

with those of the uncontrolled response (15 min. and 2 min., respectively), and reasonable as compared to the entire reentry time which is about 35 minutes.

It is seen in the simulation results of all three controllers that, while the elevator control angles for the abovementioned altitudes remain in the same available range, the corresponding control torques are apart by nearly 3 orders of magnitude. It is shown that the level of difference is mainly due to the corresponding levels of atmospheric density.

The feedback linearization nonlinear approach proved to be a useful and very simple control strategy. Because of its simplicity, the feedback linearization method was basically employed to characterize the controlled response of the shuttle to the angle-of-attack perturbations. The feedback-linearization nonlinear controller, subject to the maximum available elevator-angle constraint, offered realistic estimations for the duration and the corresponding rate of decay of the controlled response that were helpful to calibrate the optimal and adaptive controllers. The feedback linearization is easy to implement since we only need to specify the desired time for the control action and check if the maximum demanded elevator angle is available.

In order to formulate the optimal controller model, the linear quadratic regulator (LQR) methodology was applied to the state space representation of the unified equation. Due to the zero final conditions for the state vector, as a peculiar case, the formulation and the corresponding Riccati equation are different from those of the conventional linear regulator methodology. The Riccati equation for this special case is called the Riccati equation of the Lyapunov type [5].

Subsequently, a fully numerical solution has been discussed followed by the development of a completely analytical solution for the control of the space shuttle angle-of-attack perturbations during reentry. The numerical solution, that is considered to be exact, was obtained by numerically integrating the Riccati equation backwards, and subsequently, solving the co-state differential equation using forward numerical integration. The analytical solution was developed basically to eliminate the backward and forward numerical integrations from the optimal control solution and thereby reduce the computation time. The motivation for developing an approximate analytical solution was primarily to reduce the computation time that an optimal controller needs to suppress the unwanted oscillations of the space shuttle during reentry. The fact is that while numerical integration schemes require small stepsize to give acceptable results, the accuracy of analytical solutions is not affected by the evaluation stepsize. In the case of approximate analytical solutions however, there must be a balance between the accuracy of the method versus the computation time. The other reason for developing an asymptotic solution was to gain better mathematical insight into the optimal control approach.

As suggested by Ramnath, in order to develop an asymptotic analytical solution, first the Riccati matrix equation is linearized by using a rigorous mathematical transformation, and subsequently, an asymptotic analytical solution describing the variations of the linearized Riccati matrix is derived. The asymptotic solution is developed by using the multiple time-scales technique as introduced by Ramnath [11]. The analytical solutions to the components of the linearized Riccati matrix were derived as a combination of simple harmonic and hyperbolic functions. In the third step, the co-state first-order matrix differential equation is solved analytically, by using a novel

matrix transformation. Eventually, the optimal control law and the corresponding state-vector history are determined by using the solutions for the linearized Riccati matrix and the co-state vector.

The coefficients and the forcing term in the unified equation are functions of the prescribed trajectory variables and the aerodynamic characteristics of the space shuttle during reentry. As has been discussed by Ramnath and Sinha in [9], these functions vary slowly along the trajectory as compared to the highly-oscillatory transient response of the space shuttle to angle-of-attack perturbations regardless of the duration of the response. However, it is shown that for the case of controlled response, the assumption of slow variation of these parameters is valid as long as the distance traversed during the control period is small compared to the total distance along the reentry trajectory. This is due to the fact that the controlled response is an over-damped non-oscillatory response where its fastness is inversely proportional to the duration of the control action. In fact, the time constant of the controlled response is nearly equal to the duration of control action. It is shown that for the high-altitude portion of the reentry trajectory, the assumption of slow variations is not valid since the space shuttle travels about a quarter of the entire trajectory during the optimal control period.

For the lower portion of the trajectory where the required control time and the corresponding travel are adequately short, the coefficients of the unified equation and consequently the coefficient matrices of the linearized Riccati equation appear to vary slowly compared to the variations of the angle-of-attack controlled response. Accordingly, it is shown that the optimal controller using the asymptotic solution for the Riccati equation is satisfactorily functional for lower altitudes.

The computation time for the asymptotic approximate solution is compared with that of the numerical exact solution. It is shown that using the same computer, the computation time for asymptotic solution is about 1/10 of that of the numerical solution for the same level of smoothness of the output. The appropriate evaluation stepsize for the asymptotic solution was 4 times bigger than the integration stepsize needed for the numerical solution.

It is also shown that the asymptotic approximation favorably overestimates the required elevator angle and the corresponding control torque. The approximated variations for the angle-of-attack and its rate of change are sufficiently close to the exact variations. The maximum approximation errors for the perturbation angle-of-attack and its rate-of-change are less than 0.2 degree and 0.2 degree per second, respectively.

It is seen that the asymptotic prediction for the components of the Riccati equation deteriorates as it proceeds backwards along the traveled segment of the trajectory. This is due to the fact that the approximation starts at the end point of the controlled travel where the boundary conditions are known exactly.

The disadvantage of the optimal and nonlinear controllers is that they need exact knowledge of the system time-varying parameters, however this not the case for an adaptive controller. For this application, the parameters include the trajectory variables and the aerodynamic characteristics of the shuttle orbiter.

The adaptive controller was developed and designed by using the modified adaptive control methodology. The main advantage of the adaptive controllers is that they achieve the control task without using any *a priori* information about the system parameters and their variations. This fact is of special interest in our problem where the trajectory variables and the aerodynamic characteristics of the space shuttle vary along the reentry trajectory.

Adaptive control approach as formulated in this study, proves to be a robust and practical technique for the control of the space shuttle angle-of-attack perturbations during reentry. It is robust in that it performs excellently in both upper and the lower atmosphere regardless of the level of variations of the aerodynamic and trajectory parameters during the course of control action, and it is practical since the required control deflection of the elevator always starts at zero, regardless of the nature of the input disturbance. This is not the case for the optimal and nonlinear controllers where they demand the maximum elevator deflection at the beginning of actuation.

The modified adaptive control method used in this study is essentially a task-oriented approach. This means that while the control task is achieved, the convergence of the parameter estimates to the true values is not guaranteed. This is due to the fact that the parameter adaptation is updated based on the tracking errors rather than the estimation errors or both.

Finally, according to the simulation results for the adaptive controller, the performance of parameter estimation is much better at lower altitudes. For the case of 150,000 ft initial altitude, the estimated parameters and the corresponding true parameters have the same orders of magnitude, which is quite noticeable in the context of task-oriented adaptive control.

REFERENCES

[1] Anderson, J. D., Jr., *Fundamentals of Aerodynamics*, 3rd ed., McGraw-Hill, New York, 2001.

[2] Bertin, J. J., *Hypersonic Aerothermodynamics*, A.I.A.A. Inc., Washington, DC, 1994.

[3] Bowers, A. H., A Generic Hypersonic Computer Simulation Model, N.A.S.A. Ames Research Center, Dryden Flight Research Facility, Research Engineering Division, Fluid and Flight Mechanics Branch, Edwards, California, April 21, 1987.

[4] Deyst, J., Kriegsman, B., and Marcus, F., Entry-Trajectory Design to Minimize Thermal-Protection-System Weight, Rept. E-2614, C. S. Draper Lab., MIT, Cambridge, Mass., Nov. 1971.

[5] Hocking, L. M., *Optimal Control: an introduction to the theory with applications*, Clarendon Press, Oxford, 1991.

[6] Kirk, D. E., *Optimal Control Theory*, Prentice-Hall, Englewood Cliffs, New Jersey, 1970.

[7] Ramnath, R. V., "Class Notes", MIT.

[8] Ramnath, R. V., Hedrick, J. K., and Paynter, H. J., *Nonlinear Systems Analysis and Synthesis*, ASME, 1981.

[9] Ramnath, R. V. and Sinha, P., Dynamics of the Space Shuttle during Entry into Earth's Atmosphere, *A.I.A.A. Journal*, Vol. 13, No. 3, pp. 337-342, March 1975.

[10] Slotine, J.-J. E., and Li, W., *Applied Nonlinear Control*, Prentice Hall, Englewood Cliffs, New Jersey, 1991.

[11] Vinh, N. X., Busemann, A., and Culp, R. D., *Hypersonic and Planetary Entry Flight Mechanics*, The University of Michigan Press, Ann Arbor, 1980.

[12] Vinh, N. X. and Laitone, E. V., Longitudinal Dynamic Stability of a Shuttle Vehicle, *The Journal of the Astronautical Sciences*, Vol. XIX, No. 5, pp. 337-363, Mar.-Apr., 1972.